INTERIM TECHNICAL PROGRESS REPORT

Second Semi-Annual Technical Report

April 1968 - October 1968

PROJECT THEMIS: A CENTER FOR REMOTE SENSING

Compiled by

R. D. Ellermeier, Associate Program Manager
Approved: R. K. Moore, Program Manager

October 1968

Sponsored by

ADVANCED RESEARCH PROJECTS AGENCY, DEPARTMENT OF DEFENSE
Work Order 1079

Monitored by

U.S. ARMY ENGINEER TOPOGRAPHIC LABORATORIES
GEOGRAPHIC INFORMATION SYSTEMS BRANCH
GEOGRAPHIC SYSTEM DIVISION
FT. BELVOIR, VIRGINIA

Contract No. DAAK 02-68-C-0089

CRES

THE UNIVERSITY OF KANSAS • CENTER FOR RESEARCH INC
ENGINEERING SCIENCE DIVISION • LAWRENCE, KANSAS

AD _____

INTERIM TECHNICAL PROGRESS REPORT
SECOND SEMI ANNUAL TECHNICAL REPORT, APRIL 1968 - OCTOBER 1968
PROJECT THEMIS: A CENTER FOR REMOTE SENSING

compiled by

R. D. Ellermeier, Associate Program Manager

Approved: R. K. Moore, Program Manager

October 1968

Sponsored by: Advanced Research Projects Agency, Department of Defense, Work Order 1079

Monitored by: U.S. Army Engineer Topographic Laboratories
Geographic Information Systems Branch
Geographic Sciences Division
Ft. Belvoir, Virginia

Contract No. DAAK02-68-C-0089

With: Center for Research, Inc.
The University of Kansas
Lawrence, Kansas 66044

BLANK PAGE

SUMMARY

The objective of Project THEMIS, A Center for Remote Sensing (Contract No. DAAK02-68-C-0089) at the University of Kansas is advancement in the fields of remote sensing with primary emphasis on user application of remotely sensed data of natural and cultural environments. The program includes four major areas of interest: theoretical studies, system design, data processing and display, and the data analysis and interpretation. During this report period work has been performed along the lines drawn in the study plan and is a continuation of the work reported in the previous semi-annual technical report under this contract. Theoretical investigations of the frequency dependence of ultrasonic scatter from statistically known rough surfaces and the results of the ultrasonic model studies experiment are reported. The design and construction of the one octave (4-8 GHz) broadband radar system is almost complete; it is presently in the final testing and calibration phase. Except for a few delays in delivery of equipment placed on order for the interface units between the existing analog IDECS and digital equipment, the progress in the construction of the data processing and display system is as anticipated in the study plan. As described in the data processing section of this report, studies are reported on the application of adaptive classification techniques to both spatial and measurement space clustering and on the application of Bayes' statistical decision theory to data obtained from a remotely sensed environment.

Project THEMIS at the University of Kansas is funded under ARPA-DOD Work Order 1079 and is monitored as Contract DAAK02-68-C-0089 by the U.S. Army Engineer Topographic Laboratories, the Geographic Sciences Division. Mr. Bernard B. Scheps has been the Project Engineer since contract inception; Mr. Abraham Anson has recently replaced Mr. Scheps in this capacity. The project is supported at the University of Kansas by the following personnel, some of whom are not directly funded under THEMIS, but whose work is contributory to the effort:

A. Faculty Members

Electrical Engineering	6
Geography	1
Geology	2

B. Ph.D. Candidates

Electrical Engineering	15
Geography	5
Geology	2

C. Masters Candidates

Electrical Engineering	7
Geography	5
Geology	2

In addition to the personnel listed, a number of undergraduate students are employed as technicians under the three principal disciplines. A working arrangement is being developed with faculty members of the departments of Psychology and Sociology in the field of pattern recognition and false-color perception and some experimentation was carried on during this report period. It is hoped that a formalized arrangement can be made in the future to carry this work forward in a systematic manner.

Since its inception in 1964, the Remote Sensing Laboratory at the University of Kansas has been actively engaged in a number of studies which relate directly to the work being done under Project THEMIS. Themis is of particular importance to the University of Kansas since, because of its broad objectives, it provides a focus for the work being done under the other studies. As a result, considerable cross-fertilization between projects is occuring almost automatically and the total effort of the Remote Sensing Laboratory is emerging as a cohesive entity.

The studies currently underway at the Remote Sensing Laboratory in addition to Project THEMIS are:

Name of Project	Granting Agency	No.
Theoretical and Experimental Study of the Nature of Rough-Surface Scattering	NSF	GK 1153
*Research in Radar Scatterometry and Altimetry Applied to Oceanographic Problems	USNOO	NG2306-67C-0044
Study of Waves Backscattered from Layered Rough Surfaces	NSF	GK 875
*Study the Utility of Radar and Other Remote Sensor Imagery in Thematic Land Use Mapping for Geographic Research	USGS	14-08-0001-10848
*Radar Studies Related to Orbiting Research Labs	NASA/MSC	NAS 9-7175
A Study of High Performance Antenna Systems for Deep Space Communication	NASA/MSC	NGR 17-004-013
*Multi-Image Correlation Systems Study for Military Geographic Intelligence	USAETL	DAAK02-67-C-0435
Application of Nonlinear Optimization Techniques to Obtain Network Designs having Low Multiparameter Sensitivity	NSF	GK 3657
Study of Backscattering Characteristics of Mars and Venus	Ryan Aeronautical Co.	
A Study of Optimum Interpretability of Digitized Imagery	NASA	BG17-002-053
*Project Darien	USAETL	DAAK02-68-M-6993
*Project SAND	USAETL	DAAK02-69-M-0255

*Geoscience Participation or Geoscience Project

PROPOSALS

*Research Contract to Study the Utility of Radar in Applications and Research on Crops, Natural Vegetation, and Soil Moisture	U.S. Dept. of Agric.
*A Center for Excellence in Remote Sensing	NSF
Theoretical and Experimental Study of the Nature of Rough Scattering--A Continuation	NSF

PROJECT THEMIS: A CENTER FOR REMOTE SENSING
SEMI-ANNUAL TECHNICAL REPORT (U)

I. INTRODUCTION

The purpose of this report is to describe the technical work accomplished under contract No. DAAK02-68-C-0089 during the period April 1, 1968 through October 1, 1968. It is, in effect, a continuation of the work described in the previous semi-annual technical report[1] with emphasis on the rate at which the work under the various tasks has been progressing and the technical and/or scientific significance of the results obtained to date. This report has been prepared in the form of a summary in which appropriate references are made to the technical reports and memoranda which describe the work under each subtask in detail. Some of the more significant memoranda and parts of long technical reports are appended in this text.

Except for a few delays in delivery of equipment placed on order, the range of progress of the overall project is as anticipated.

II. TECHNICAL REPORT

TASK 4.1* TARGET-SENSOR INTERACTION STUDIES

This task includes theoretical, modeling, and experimental studies of broad-spectrum radar systems. Considerable progress has been made in all of the above studies, as detailed below.

---

*Task numbers are those of the USAETL Purchase Description dated 16 September 1967.

SUBTASK 4.1.1 THEORETICAL STUDIES

Theoretical studies of broad-spectrum scattering are being performed at the University of Kansas under National Science Foundation grants.* Major work under the above heading appeared as a technical publication in the 1968 Wescon convention of the IEEE.[2] This publication is appended as Appendix A.

SUBTASK 4.1.2 ULTRASONIC MODEL STUDIES

Technical Memorandum 113-2 (March 1968), which appeared under Appendix A of the previous semi-annual technical report of Project THEMIS[1], examined the various aspects involved in the study of the frequency dependence of backscatter from statistically rough surfaces using a broad spectrum backscatter acoustic system. This included a brief discussion of the acoustic simulation technique, a detailed description of the system instrumentation and calibration problems, and the data processing and analysis involved in the scattering and image experiments. Since March 1968, the program has progressed through the final stages of data acquisition and analysis. The complete work is compiled and presented by Dr. J. W. Rouse, Jr. as his Ph.D. dissertation[3]. An interim technical report under Project THEMIS in the form of Dr. Rouse's dissertation is presently in the printing process. Appendix B is a condensed form of the results reported in the above dissertation.

SUBTASKS 4.1.3, 4.1.4, 4.1.5, 4.1.6 ELECTROMAGNETIC INSTRUMENTATION AND MEASUREMENT

These subtasks are combined into a single task description because of the close inter-relation of subtasks which prevents convenient separation.

---

*NSF Grants GK-875 and GK-1153

The one octave bandwidth system being constructed is near laboratory operation. This system was operated in the laboratory in August 1968, however, incorrect manufacturers rating led to the burn-out of the PIN diode switch used for duplexing. This malfunction required redesign of the switching system to utilize higher power rating switches. Hewlett Packard Associates is furnishing the additional replacement switches required at no cost due to the error in specification which led to the initial failure.

The replacement switches are due by November 1 and calibration and alighment of the RF portion of the system can be started with the new switching arrangement.

CRES Technical Memorandum 133-1-2, shows the latest detailed block diagram and component diagram of the system after the above mentioned change in duplexing. The GFE boom truck has been repaired and is now ready for limited range use. The original bucket has been replaced by a mounting fixture for the antenna positioner. The antenna positioner itself is the only remaining item not yet received; however, delivery is estimated by November 1. The delay in ordering the positioner was due to the time required for fund transfer to purchase the item and not to lack of definition.

The Logic Control system required to perform the gating of the pulses for subsequent integration in time or frequency is described in CRES Technical Memorandum 133-1-3. This system is now in the final construction stages. All circuits have been through initial breadboard and test and the system is being fabricated in replaceable plug-in card modules.

The GFE laboratory van and truck have been received; however, this vehicle has not yet been placed in operating condition.

CRES Technical Memoranda 133-1-2 and 133-1-3 are appended as Appendices C and D.

TASK 4.2 SENSOR AND PREPROCESSOR DEVELOPMENT

The emphasis in this task is on parameter and design considerations and development of prototype sensors and sensor systems including associated preprocessing of sensor data. As was mentioned in the previous semi-annual

technical report, due to fund limitations subtasks 4.2.2 (Cartographic radar systems) and 4.2.5 (semi-focused imaging systems) are not being attacked under this contract. Work on subtask 4.2.1 (evaluation of broad-spectrum imaging systems) is still pending until data from the system under development are available.

SUBTASK 4.2.3 STUDY OF IMAGING RADAR SYSTEMS FOR SMALL SATELLITES

At this time work is being done on defining a class of ground-mapping imaging radar systems to be flown aboard small earth orbiting satellites. This study is being performed under NASA Contract No. NAS 9-7175. Investigations made in this study which are applicable under the above subtask title will be reported both to the granting agency and to USAETL.

SUBTASK 4.2.4 A STUDY OF RADAR SCATTEROMETER SYSTEMS

Study of radar scatterometer systems is presently being implemented jointly under the auspices of the Naval Ordnance Laboratories (Contract No. N62306-67-C-0044), NASA (Contract No. NAS 9-7175) and Project THEMIS. Parameter studies are being conducted for sea-ice measurements and include considerations of roughness, frequency, resolution area, polarization and antenna patterns.

A final memorandum[4] on the correlated split-gate altimeter has been completed under USNOO Contract NG2306-67C-0044. With the results of the range error statistics for square law[5] and linear[6] detection of independent pulses, the correlated or dependent pulse analysis provides a theoretical base for experimental studies on the split-gate altimeter. The split-gate tracking system was studied because it is frequently employed in the measurement and tracking of altitude with pulsed radar altimeters. The accuracy is affected by the deviation caused by random fluctuation of returns from surface scatterers. The resultant jitter creates range or altitude noise in altimeter response.

Analysis[7] of the backscattering cross section for sea states generated by fully developed winds has been completed in October, 1968.

The empirical sea wave spectra for different winds has been combined with rough surface scattering theory to provide angular dependence of cross section (σ_o versus theta) for these winds.

A series of scatterometer measurements made in the Arctic Ocean north of Point Barrow, Alaska, have demonstrated the capability of the 13.3 GHz system to differentiate different sea ice categories[8]. Differentiations have been achieved in winter and polar ice types.

TASK 4.3 DATA PROCESSING AND DISPLAY

The purpose of this task is to improve existing techniques for data display, such as those employed in the IDECS system, and to originate new techniques for processing and display of remote sensor data for improved interpretability. At this time, the working subtasks under 4.3 fall into two categories, 1) improvement of the IDECS system (Subtasks 4.3.1 and 4.3.3) and 2) implementation of adaptive and Bayes decision techniques (Subtasks 4.3.4 and 4.3.5). As work progresses in this categories, subtasks 4.3.2 (evaluation of color combinations of multiple images) and 4.3.6 (new display techniques) will be implemented. Ultimately, the adaptive and Bayes decision techniques will be instrumented and interfaced with the IDECS system in such a way that the IDECS operator will have maximum flexibility in enhancing data by direct combinations of images along with computer processed data.

Representative of the work accomplished to date under task 4.3 are three memoranda which are appended as Appendices E, F and G. The first of these (Appendix F) deals with the application of adaptive classification techniques to both spatial and measurement space clustering. The application of Bayes' statistical decision theory to data obtained from a remotely sensed environment is considered in Appendix F. The progress and mechanization of the IDECS system improvements are outlined in Appendix G.

TASK 4.4 DATA ANALYSIS AND APPLICATION

This task involves in part the analysis of the data obtained from the

broad-spectrum radar systems of task 4.1. Also included are studies relating to the increase of information content in multiple radar images over single image content.

Subtasks 4.4.2 (relation of image data to wavelength, polarization, depression angle, resolution, and bandwidth) and 4.4.3 (information increase with the use of multiple radar images) will not be implemented until broad-spectrum image data are available.

SUBTASK 4.4.1 EVALUATE GEOGRAPHIC AND GEOLOGIC INFORMATION AVAILABLE FROM SINGLE RADAR IMAGES

Since no data will be available from the broad-spectrum radar systems of task 4.1 before the second year, the efforts under this task are devoted to geographic and geologic evaluations of single image radar data. During the second and succeeding years this task will be changed to an evaluation of the IDECS and associated signature selection system as aids in image interpretation. A final report by Drs. Peterson and Simonett on the geomorphology of the Wasatch Range (Appended as a preliminary report, Appendix F, in the previous report) will be issued as a special interim report in the near future.

Work on single radar images has been done at CRES under Project SAND (Contract No. DAAK02-69-M-0255) to study the availability of construction materials in the Mekong Delta[9]. If more information on this work is desired, the reader can be supplied with a copy of CRES memorandum 156-1 which describes the investigations under Project SAND to date.

III. CONCLUSIONS AND RECOMMENDATIONS

Except for a few delays in delivery of components placed on order for subtasks 4.1.3 - 4.1.6 and task 4.3, the rate of progress of the overall program of Project THEMIS is as anticipated in the study plan. Due to these delays, subtasks 4.1.3 - 4.1.6 are about 90 days behind schedule; it

---

*DAAK02-1560-824

is anticipated that the broadband radar system will be in operation by early December 1968.

Appendices A through G of this report present the reader with a detailed picture of the efforts made under Project THEMIS since April 1968. Most of the work was concentrated under tasks 4.1 and 4.3. The output under task 4.2 was limited by shortage of funds, and major work on task 4.4 will be commenced after broad-spectrum image data are available and the IDECS system is fully operational.

BIBLIOGRAPHY

1. Interim Technical Progress Report, Project Themis: A Center for Remote Sensing, Contract No. DAAK02-68-C-0089, September 1967-April 1968.

2. Fung, A. K., and A. Leovaris, "Frequency Dependence of Ultrasonic Scatter from Statistically Known Rough Surfaces," 1968 WESCON Technical Papers, Session 22, August 20-23, 1968.

3. Rouse, J. W., Jr., "The Frequency Dependence of Backscatter from Rough Surfaces," Ph.D. Dissertation, The University of Kansas, Lawrence, Kansas.

4. Lee, H. L., "The Accuracy of the Correlated Split Gate Altimeter," Technical Memorandum 112-5, CRES Remote Sensing Laboratory, October 1968.

5. Lee, H. L., "Range Error Statistics for Split Gate Altimeter, Square Law Detection," Technical Memorandum 112-3, CRES Remote Sensing Laboratory, April 1968.

6. Lee, H. L., "Range Error Statistics for Split Gate Altimeter, Linear Detection," Technical Memorandum 112-4, CRES Remote Sensing Laboratory, April 1968.

7. Chia, R., "The Theory of Radar Scatter from the Ocean," Technical Report 112-1, CRES Remote Sensing Laboratory, October 1968.

8. Rouse, J. W., Jr., "Artic Ice Type Identification by Radar," Technical Report 121-1, CRES Remote Sensing Laboratory, August 1968.

9. Dellwig, L. F., E. Gillerman, and L. H. Jefferis, "Availability of Construction Materials in the Mekong Delta," Technical Memorandum 156-1, CRES Remote Sensing Laboratory, August 1968.

Appendix A

FREQUENCY DEPENDENCE OF ULTRASONIC SCATTER FROM STATISTICALLY KNOWN ROUGH SURFACES

A. K. Fung and A. Leovaris

FREQUENCY DEPENDENCE OF ULTRASONIC SCATTER FROM STATISTICALLY KNOWN ROUGH SURFACES

A. K. Fung and A. Leovaris
Center for Research in Engineering Science
University of Kansas
Lawrence, Kansas

SUMMARY

An acoustic simulator is used to model radar backscatter and the frequency dependence of the return signals from statistically known rough surfaces is studied. One of the model statistically rough surfaces is made of rubber polymer obtained with a clay mold and the other is made of steel. The profiles of the surfaces are measured with a depth gauge so that the correlation functions and the standard deviations of the surfaces could be calculated.

On each surface average backscattered power are measured at four different frequencies ranging from 0.5 MHz to 1.5 MHz. Comparison with the scattering law obtained under Kirchhoff's approximation shows real good agreement when the parameters in the scattering law are properly interpreted. It is believed that in the past the scattering law could not be verified due to an incorrect interpretation of one of its parameters. Certain precautions that must be taken in interpretating the scattering law are also pointed out.

INTRODUCTION

This study concerns the change in angular variation of the average backscattered power from statistically rough surfaces as a function of the incident frequency. It is clear that the angular variation of the return signal will depend on both the incident frequency and the nature of the surface under study. For a theoretical prediction assumptions must, therefore, be made about either the correlation function of the surface or its Bessel transform, the roughness spectrum. A case of great practical interest is when the correlation function is monotone decreasing but may have oscillating decaying tails. For simplicity, we assume that the tail is small and that the surface height distribution is Gaussian. We shall first establish some theoretical predictions for two different cases of surface roughness so as to obtain a qualitative picture of the backscattering behavior as a function of frequency. These predictions will then be compared with experimental results. Certain difficulties in interpretating experimental results are pointed out. It is found that previous interpretation of the parameters, that appear in the scattering law obtained under Kirchhoff's approximation, is incorrect and a new interpretation is presented.

FREQUENCY DEPENDENCE

For a plane wave incident upon a random surface with Gaussian height distribution, Kirchhoff's method predicts an average far zone backscattered power of the form[1]

$$P(\theta) = \frac{1}{(\lambda\cos\theta)^2} \int J_0(2k\sin\theta\xi) e^{-K(1-r(\xi))} \xi\, d\xi \quad (1)$$

where $K = 4k^2\sigma^2 \cos^2\theta$; θ is the incident angle; $k = 2\pi/\lambda$, the incident wave number; σ, the standard deviation of the surface, $r(\xi)$ the correlation function of the surface, and J_0 is the zero order Bessel function. In (1) we have left out a proportionality constant unimportant for our discussion. The integration in (1) is over the illuminated area.

If λ is large compared with σ, so that K is small compared with unity, (1) may be approximated as follows

$$P(\theta) = \frac{1}{(\lambda\cos\theta)^2} e^{-K} \int J_0(2k\sin\theta\xi)\xi d\xi + [1/(\lambda\cos\theta)^2] K e^{-K} \int r(\xi) J_0(2k\sin\theta\xi)\xi d\xi = P_1(\theta) + P_2(\theta) \quad (2)$$

For large enough illuminated area the first term in (2) contributes only at $\theta = 0$. The scattering component is the second term which may be rewritten in terms of the roughness spectrum of the surface, W,

$$P_2(\theta) = (1/\lambda)^4 \, 16\pi^2 \sigma^2 \, e^{-K} W(2k\sin\theta) \quad (3)$$

Eq. (3) is in agreement with the first order result obtained by small perturbation method.[2] The results, however, are not identical because (3) takes into account higher order surface slope terms. Looking at (3) we are tempted to say that it predicts an angular variation of the form exp (-K) W (2k sin θ). Actually, things are not as straight forward, since we always have finite beamwidth in performing our experiments. Thus, if our beamwidth is θ_0 and the incident angle is 10°, we cannot use W (2k sin 10°) but rather some average of W [2k sin (10° $\pm$ $\theta_0/2$)]. Hence, at a fixed incident angle, we are not concerned with just a single k' in W(k'), but a range of values of k'. Unless we maintain the same beamwidth as we change frequency, the problem will be further

complicated, since 2k increases with frequency and our beamwidth is likely to decrease with frequency. Similar kind of care must also be exercised when we consider frequency effect on return power at a fixed angle. Thus, it is clear that even if we know W(k'), a precise theoretical prediction is still difficult. One general conclusion for the case, $\lambda >> \sigma$, is that as the incident frequency increases the angular variation in $P_2(\theta)$ becomes smoother when the beamwidth is kept constant. For a monotone decreasing W(k') we expect, therefore, $P_2(\theta)$ to become flatter as frequency increases. The rate of flattening is smaller for a W(k') with more high frequency components.

Now let us turn to the more practical case when K is large compared with unity. Just how large K should be has never been established. Examining (1) shows that we can obtain a good approximation by applying a modified saddle point method. In the past[1,3], the practice is to expand $r(\xi)$ about $\xi = 0$, and take the first two terms. There are two objections to doing this. First of all, $\xi = 0$ is really not a saddle point, since the integrand vanishes at $\xi = 0$. Secondly, the derivative, $r'(0)$, if it exists, is nedessarily zero ($r'(\xi) = -\int W(k) J_1(k\xi) k^2 dk = 0$, at $\xi = 0$); Thus, we are forced to let $r(\xi) \approx 1 + r''(0)\xi^2/2$ which gives an incorrect prediction when compared with most of the experimental results. The maximum value of ξ $\exp[-K(1 - r(\xi))]$ really occurs at a point $\xi_o > 0$. It is easy to see, however, that ξ_o becomes smaller as K gets larger. Since we are now considering the case when K is large, ξ_o is necessarily a small number. Hence, the proper approximation to $r(\xi)$ is

$$r(\xi) = 1 + r'(\xi_o)\,\xi.$$

Note that $r'(\xi_o)$ is not zero since $r(\xi)$ is monotone decreasing at least for small values of ξ. If so, the integrated result of (1) is

$$P(\theta) = \frac{1}{16\pi^2} C(\cos^4\theta + C\sin^2\theta)^{-3/2} \qquad (4)$$

where $C = (\lambda/[4\pi\sigma^2 r'(\xi_o)])^2$. It is important to observe that C does not vary as λ^2. The reason is that ξ_o varies as K varies i.e., as λ, σ, or θ varies. Comparison with experimental results[4,5] indicates that C should decrease as λ decreases. There is, however, no definite pattern for C vs λ since for different surfaces $r'(\xi)$ may be different. When we express $r(\xi)$ in terms of W(k), we see that the magnitude of $r'(\xi)$ is larger if the surface has more high frequency components. If a rougher surface is defined to have more high frequency components, then a rougher surface calls for a smaller C. We may also want to say that the surface is rougher if its σ is larger. If so, smaller C indicates a rougher surface in both cases. From the dependence of C upon σ and $r'(\xi_o)$, it is clear that this theory is difficult to pin down by experiments unless we know the surface in great details. A general conclusion for the case when K is large is that $P(\theta)$ tends to be independent of λ and gets flatter with angular change as frequency increases.

Comparison between the two cases shows that it is easier to check the surface roughness spectrum for the case $\lambda >> \sigma$ since the effect of σ is independent of the variations of W(k'). When K is large, σ^2 acts together with $r'(\xi_o)$ to determine C. This may lead to unexpected results. For example, we may have $\sigma_1 > \sigma_2$ and $r_1'(\xi_{o1}) < r_2'(\xi_{o2})$ resulting in $\sigma_1^2 r_1'(\xi_{o1}) < \sigma_2^2 r_2'(\xi_{o2})$. Thus we get $C_1 > C_2$ although $\sigma_1 > \sigma_2$. Consequently, $P(\theta)$ curves for surface no. 1, which has larger standard deviation than surface no. 2, drop off faster with incident angle.

The above discussion for both cases shows that a precise theoretical prediction on frequency behavior using Kirchhoff's theory is difficult. However, meaningful qualitative picture may be obtained. When the properties of the surface under study is known, verification of the theory is possible. No verification was possible in the past[1,3] since $r'(0)$ was used in place of $r'(\xi_o)$ and $r'(0)$ was interpreted as one over the correlation distance.

COMPARISON WITH EXPERIMENTAL RESULTS

Two model surfaces with different statistical properties are considered. Surface no. 1 is made of rubber polymer with a clay mold and surface no. 2 is made of steel. Both surfaces have gentle slopes so that Kirchhoff's theory is applicable. Profiles of these surfaces are measured with a depth gauge at intervals 0.25 mm and 0.5 mm apart for surfaces no. 2 and 1, respectively. The standard deviations, the correlation functions (see Fig. 1 and 2) and the slopes of the correlation functions (see Fig. 5) are then computed from the profiles obtained.

The acoustic simulator facilities of the Center for Research at the University of Kansas are employed for measuring the average backscattered power. This is done at frequencies ranging from 0.5 to 1.5 MHz (see Fig. 3 and 4). Only incident angles in the range 0° to 30° measured from the vertical are considered, since there is no general agreement as to the validity of the theory for large angles of incidence. (It is not clear how large the incident angle can be before the theory breaks down). Also, for this range of incident angles we are sure that the scattering behavior of the acoustic waves is the same as that of the electromagnetic waves. Hence, the conclusions arrived at in this paper applies equally well to electromagnetic scattering.

To check the theory given by (4), we proceed as follows. First of all, for each frequency we can fit (4) to the corresponding experimental curve to determine the parameter C. Secondly, we calculate $r'(\xi_o) = \lambda/(4\pi\sigma^2 C^{1/2})$. Thirdly, we determine ξ_o as the point where the factor, $\xi \exp [-K(1-r(\xi))]$, is maximum. The $\cos^2\theta$ factor that appears in K is evaluated at $\theta = 15°$ assuming C gives the closest fit at $\theta = 15°$. Actually, the effect due to cos θ is not significant as compared with $r(\xi)$ at least for θ between 0° and 20°. The $r'(\xi_o)$ thus obtained is our predicted slope for $r'(\xi)$ at ξ_o. Now on the $r'(\xi)$ curve calculated from the profile of the surface, we can also find a value for $r'(\xi)$ at ξ_o. Let us call this $r'(\xi_o)$ our measured slope as opposed to the predicted slope for $r(\xi)$. Comparison of the predicted with measured values of $r'(\xi_o)$ at different frequencies is shown in Fig. 5. Very good agreement is obtained. The result for surface no. 2 is more satisfactory, however, since the slopes are larger. As for surface no. 1, its slopes are of the size, 10^{-2} - 10^{-3}. Hence, a small error in the third place after the decimal in evaluating the slopes from the profile-data will produce large percentage error. However, we can still see that the order of magnitude is correct and the agreement is within experimental error.

CONCLUSION

Measurements for the backscattered power from statistically known rough surfaces are made at various frequencies. Results are used to verify the scattering law obtained under Kirchhoff's approximation. When the parameters in the scattering law are properly interpreted good agreement is obtained.

ACKNOWLEDGEMENT

This work is supported by the National Science Foundation under grants GK 875 and GK 1153.

REFERENCES

1. Hagfors, T., "Relationship of Geometric Optics and Autocorrelation Approaches to the Analysis of Lunar and Planetary Radar," J. Geophys. Res., vol. 71, p. 379-383, January 1966.
2. Rice, S. O., "Reflection of Electromagnetic Waves from Slightly Rough Surfaces," Comm. Pure Appl. Math 4, pp. 351-378, 1951.
3. Beckmann, P., "Scattering by Composite Rough Surfaces," IEEE, vol. 53, pp. 1012-15, August 1965.
4. Chapman, R. P. and H. D. Scott, "Surface Backscattering Strengths Measured Over an Extended Range of Frequencies and Grazing Angles," J. Acous. Soc. Am., vol. 36, pp. 1735-1737, September 1964.
5. Beckmann, P. and W. K. Klemperer, "Interpretation of the Angular Dependence of Backscattering from the Moon and Venus," N.B.S., Radio Science, vol. 69D, pp. 1669-76, December 1965.

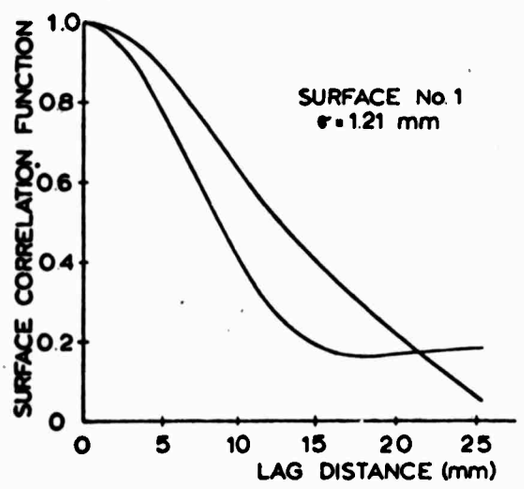

Figure 1. Statistical Properties of Surface No. 1

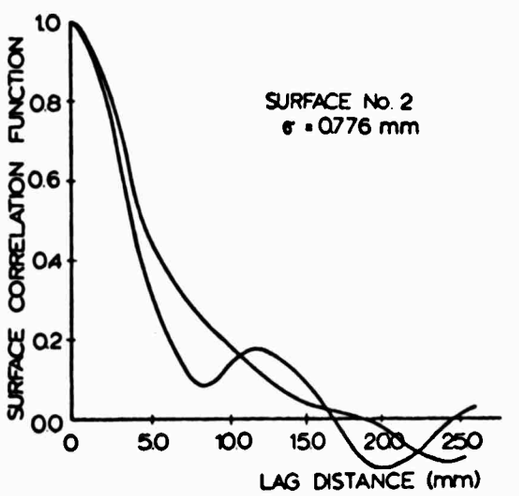

Figure 2. Statistical Properties of Surface No. 2

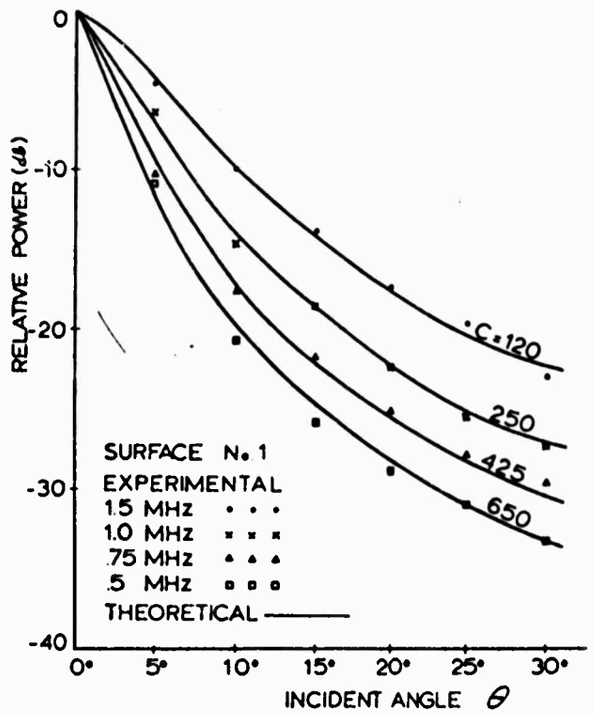

Figure 3. Average Relative Backscattered Power vs Angle of Incidence from Surface No. 1

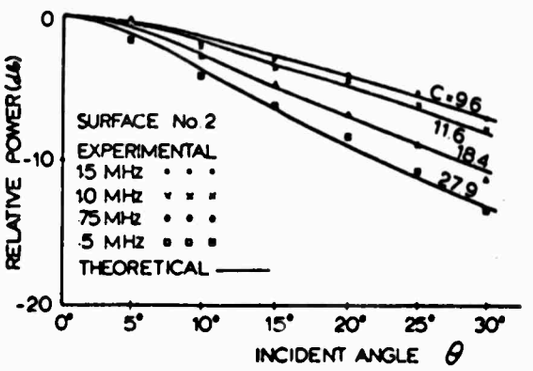

Figure 4. Average Relative Backscattered Power vs Angle of Incidence from Surface No. 2

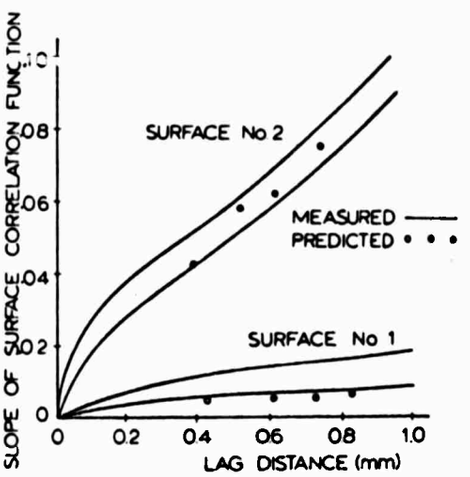

Figure 5. Comparison Between Predicted and Measured Slopes of the Correlation Functions for Surfaces No. 1 and No. 2

Acknowledgement: This work was supported by National Science Foundation Grants GK 875 and GK 1153.

BLANK PAGE

Appendix B

RESULTS OF SCATTERING AND IMAGING EXPERIMENTS

J. W. Rouse

Condensed Version of Chapters 5 and 6 of Dr. J. W. Rouse's Ph. D. Dissertation

RESULTS OF SCATTERING AND IMAGING EXPERIMENTS

Condensed Version of Chapters 5 and 6
of Dr. J. W. Rouse's Ph. D. Dissertation [1]

The University of Kansas
Lawrence, Kansas 66044

I. RESULTS OF SCATTERING EXPERIMENT

The scattering experiment consisted of the measurement of backscatter from two statistically rough surfaces. The fundamental surface was gently undulating surface having slopes large relative to the incident wavelength. The other surface was produced by adding sand particles to the fundamental surface. As shown by the results, the effect of superimposing small scatterers onto the fundamental surface was to convert the frequency dependent scattering coefficient curve from a negative slope to a positive slope. An attempt was made to explain this and other behavioral characteristics and to relate the results to theoretical predictions of frequency dependence.

The experiment results presented in this chapter were recorded as described in Chapter 4 of Reference [1] and, to the degree possible by repetitive measurements, are considered to be accurate to within equipment tolerances. Data that could not be repeated were not included in the results. These include a sharply rising behavior of the scattering coefficient curve in the region 2.5 MHz to 3.0 MHz discovered in the measurement of the fundamental surface, which could not be checked due to subsequent malfunction of the transducer pair used in this frequency region. This malfunction, and the unreliable behavior of the 0.3 MHz to 0.1 MHz region of the low-frequency transducer pair, restricted the range of the available data.

A. Measurement Results of Fundamental Surface

The behavior of the scattering coefficient as a function of frequency for the fundamental, gently undulating rough surface is shown in figures 1 through 5 at incidence angles of 0°, 15°, 30°, 45°, 60°. Figure 6 shows all the curves plotted together.

The curves show two behavioral regions; one below and one above about 1.25 MHz (λ = 1.2mm). In the region below 1.25 MHz the 0° and 15° data have a negative slope which increases above 1.25 MHz. For 30°, 45°, and 60° the lower frequency region, at least down to 0.5 MHz (λ = 3.0mm), the slope is approximately zero. Below 0.5 MHz a positive slope is suggested, especially at 45° and 60°, however the confidence level of these data is not as high as that above 0.5 MHz.

The region above 1.25 MHz has a pronounced negative slope for all angles. This slope is confirmed to 2.5 MHz (λ = 0.6mm) and is believed tc continue to higher frequencies, however some measurements indicated a rapid change to a large positive slope in the region above 2.5 MHz. These measurements could not be confirmed and no physical explanation was found for such behavior, therefore the data were discarded.

The data were also plotted as a function of angle for several discrete frequencies in figure 7. The plots indicate a greater negative slope near vertical for the low frequencies with a gradual flattening out to about 1.2 MHz (λ = 1.2mm). Thereafter the plots hold approximately the same shape but gradually drop in overall amplitude.

B. Measurement Results of Sanded Surface

The frequency dependence of the scattering coefficient measured for the fundamental surface densely coated with 0.595-0.825mm sand particles are shown in figures 8 through 12 at incidence angles of 0°, 15°, 30°, 45°, and 60°. Figure 13 shows all curves plotted on the same graph.

As in the case of the fundamental surface, these data exhibit different behavior in two frequency regions. In the region below 1.25 MHz the curves have a positive slope of approximately the same magnitude for all angles. Above 1.25 MHz the data tend to become frequency independent. There was some support for defining a third region above about 2.0 MHz (λ = 0.75mm) where the data exhibit a positive slope such as was found for the fundamental surface. Unfortunately this could not be confirmed due to the malfunction of the transducer pair used in this region.

These data were also plotted as a function of angle for several discrete frequencies in figure 14. The plots indicate a greater negative slope near vertical for the low frequencies with a gradual flattening as the frequency increases out to about 1.25 MHz (λ = 1.2mm) just as in the case of the fundamental surface. The measurements at 45° incidence confuse the interpretation of the data and an immediate explanation is not available for this phenomenon. The readings tend to conform to expectations as the frequency increases. Above 1.25 MHz the curves remain almost unchanged within the equipment accuracy tolerances.

C. Comparison of Results with Experiments

Following the analysis procedure used extensively by Katz[2] the scattering coefficient frequency dependence curves were fit to a function: $\sigma^\circ = a\lambda^\alpha$. The fit was done by frequency regions and a determination of the best α was made for all data. In figures 15 and 16 the variation of the coefficient α is plotted as a function of incidence angle for the fundamental surface. In figures 17 and 18 the coefficients are plotted for the sanded surfaces.

In the next section an attempt will be made to explain the behavior of the curves using the guidelines offered by the Kirchhoff theoretical method of expressing the scattering processes, however as reference to other experimental results, the values of the coefficient α for angular backscatter measurements of sea clutter, cities, snow covered terrain, grass surfaces, the moon, and asphalt and concrete roads are shown in figure 19. These data were compiled by Katz[2] using data from the Ohio State University and Naval Research Laboratory measurements programs. These data were obtained by polychromatic systems, hence the slope factors were obtained using widely spaced points. Such subtleties as were found in the measurements of the surfaces used in this program could not have been detected.

D. Comparison with Theory

Although some degree of matching of the measured and theoretical results was obtained, considerable doubt exists as to the ability of the

Kirchhoff method to predict the frequency dependence of backscatter, at least in cases where the actual surface autocorrelation is approximated by an autocorrelation function. A point of major concern is that the best fit occurs using the expressions derived for an exponential autocorrelation function, which clearly cannot fit the measured surface autocorrelation. This contradiction is somewhat overcome by the approach used by Fung and Leovaris[3], which allows incorporation of autocorrelation functions other than the exponential. Even with this approach the maximum wavelength variation is λ^{+2} (at $\Theta = 0°$), and the coefficient must decrease as Θ increases. This characteristic is contradicted by the measurements of the fundamental surface (see figure 6) and the results of Wiltse, et al.[4]. Likewise the theory cannot predict results such as those compiled by Katz.

The effective parameter approach is supported by the physical reasoning that different subranges of structure sizes dominate the return at different incidence angles and/or wavelengths. These subranges have autocorrelations and variances which are not the same as the autocorrelation and variance of all subranges combined, i.e. the entire surface. Several attempts have been made to incorporate this character into the scattering expressions to describe the angle dependence[5, 6, 7, 8]. These attempts have been only moderately successful.

In summary, the measurements obtained in this program, as well as those of other programs, suggest, in agreement with Davies[8], that use of the autocorrelation function approximation of the surface autocorrelation does not give sufficient statistical information to describe the scattering from the surface.

II. IMAGE EXPERIMENT

In recent years the use of imaging radar systems for both military reconnaissance and geoscience investigations has expanded rapidly. Associated with this expanding demand has been the growing realization that the monochromatic nature of such systems handicaps their utility, especially in military reconnaissance applications. This chapter presents an experiment with a panchromatic imaging system. In this experiment

monochromatic images of complex targets are compared with panchromatic images to show the effect of frequency averaging. The substantial improvement in target definition obtained is impressive, especially in view of the fact that less than a ± 10% bandwidth is employed, and that little increase in system power or complexity is required to gain this improvement.

The theme of the chapter is illustrated in Figure 20 which shows an acoustic image of two spheres. The images actually show an expanded view of a small area of the sphere's surface near the apex. The return signal strength from regions away from the apex is below the noise level. In 20 (a) the spheres are imaged monochromatically and lobing is evident. In 20 (b) the frequency is swept ± 10% from the center frequency. The frequency averaging of the lobes is obvious. The monochromatic lobes are investigated in detail in section II-C and the effect of frequency averaging is illustrated.

A. Measurement Technique

Acoustic images were obtained in a manner completely analogous to an airborne imaging radar system. The antennas (transmitting and receiving transducers) were moved past the targets at a fixed distance and uniform velocity. The transducers were mounted on a linear motion carriage that was capable of a wide range of movement velocities and transducer position settings. The position geometry is shown in Figure 21 and a photograph of the arrangement is also shown.

The system operation associated with obtaining acoustic images was as follows: The signal return is envelope detected and applied to the grid of an imaging CRT. Each return, i.e. the return associated with each transmitted pulse, intensity modulates one horizontal line trace on the CRT. Sequential returns form sequential intensity-modulated line traces each vertically displaced from each other. The end result is an intensity modulated raster display. A photographic image is obtained by exposing the film during the entire vertical traverse time interval. The producure is illustrated in figure 22.

The imaging experiment was designed around the limitation presented by the transducers. That is, the available piston transducers provide only

conical beams and have relatively high sidelobes. The use of spherical targets insured that the sidelobes of the antenna did not influence the return over the area of investigation of the reradiation pattern. Ideally the experiment would concentrate on imaging area-extensive targets such as those of concern to imaging radar systems, however the lack of a fan-beam antenna discouraged this approach. Fortunately, as will be shown in section II-B, the spherical targets provided the information needed to relate to the area extensive imaging problem, hence the limitation to a conical beam did not restrict the value of the experiment.

The parameters of the experiment were set with the following consideration. The objective of the experiment was to determine the effect of introducing a broad-spectrum signal in place of a monochromatic signal. The targets examined were complex and consequently provide a reradiation pattern consisting of a multiple of fine lobes. To determine the effect of frequency averaging required that the effect of sample averaging be excluded. That is, the image would be altered if the number of "looks" were changed by the fact that more or less lobes would be seen. To eliminate this variable, the sampling rate (PRF) was set sufficiently high that all lobes would be recorded and the rate was not altered when the swept frequency was introduced. The darriage velocity was set at 6.5 mm/sec and the PRF was set at approximately 130 Hz. This provided one sample for each .05mm of carriage travel.

The system employs the "slow-sweep" mode. This mode of operation consists of sampling the swept frequency at the pulse-rate frequency. Ideally broad-spectrum imaging would be done using a "fast-sweep" mode, that is the entire spectrum would be transmitted during each pulse. This could conceivably be simulated by increasing the PRF proportional to the sweep time. That is, if the PRF for monochromatic imaging os 100 Hz, set the sweep time at (1/100) sec and increase the PRF to 400 Hz to provide 4 samples per sweep. Unfortunately this reintroduces the effect of increasing the sampling rate and hence for this experiment the PRF for both monochromatic and swept frequency signals was the same, 130 Hz. The sweep time was adjusted to give 4 samples per sweep (about 23.5 m sec). The samples

were not synchronized with the sweep, and hence the frequency sampling varies sweep-to-sweep. In this manner the full sweep is effective even though the sampling rate is very low.

The width of the pulse was set at .6 - .8 m sec to provide a return segment which did not include the effect of the high frequency components in the leading and trailing edge of the transmitted pulse. It was determined that the spherical targets caused the return signal to be restricted to an area near the apex, hence the leading edge effect decayed rapidly. Therefore by extending the pulse width beyond this decay interval, the leading edge effect was excluded. This effect is evident in the images shown in figure 20.

The useful bandwidth of the swept signal was restricted by the frequency response of the transducers. The response curves fall so rapidly that variations greater than about $\pm$ 10% from resonance were impractical.

B. Targets

Three primary targets were used in this experiment: (1) a 4.5 cm diameter rubber sphere; (2) a 7.8 cm diameter styrofoam sphere; and (3) an 8-element planar array consisting of 2.5 cm diameter wooden spheres located on 3.2 cm centers in two rows of 4-elements each. The targets are shown in the photograph as they were positioned in the tank. The rubber sphere is on the left.

1. Rubber Sphere. This target is a relatively smooth, soft rubber sphere selected to provide a broad, hopefully frequency-insensitive, lobe in the direction of backscatter. Although the exact composition of the sphere is unknown, it is reasonable to assume negligible shear waves and a reasonably high reflection coefficient. The diameter of the sphere is very large relative to the incident wavelength, but is smaller than the illuminated area of the beam. Under these conditions the scattering cross section should be almost independent of wavelength[9] and the sphere would provide the necessary calibration reference for other measurements.

The measurements presented in section II-C verify the presence of a strong, almost frequency insensitive, reflection in the backscatter direc-

tion, however the fact that the sphere is not perfectly smooth to the incident wavelength is evident.

2. Styrofoam Sphere. This target was selected to illustrate an effect very common to imaging systems but one that is difficult to simulate acoustically in a controlled manner; that is, an area extensive surface consisting of various size randomly oriented scatterers. The surface of the sphere is rough in the somewhat facet-like manner typical of styrofoam. Consequently some scatterers are sufficiently close together to form highly directional reradiation patterns similar to closely spaced arrays. In addition the multilobe pattern of widely spaced elements exists, and scatterer sizes both large and small relative to the incident wavelength are present. The spherical configuration reduces the illumination area edge effects and helps accent the behavior of the surface reradiation lobes by restricting the contributing area to a much smaller size than is otherwise possible using the available acoustic transducers.

3. Array. The array target consists of eight spheres arranged as shown in figure 23. The purpose of this target is to provide a large number of narrow lobes of different amplitudes. The array is an extension of a 4-element array (one row of spheres) which provided the desired fine lobe structure, but the lobes were of almost equal amplitude. The effect of variations in incident wavelength is better illustrated by use of the more directional pattern of the 8-element array.

The reradiation pattern of an array of point scatterers spaced several wavelengths apart can be calculated, and the results show a number of lobes proportional to the number of elements. The width of each lobe is also proportional to the number of elements[10]. The spherical elements of the target array cannot be interpreted as point scatterers; however the area on the sphere contributing to the reradiation is sufficiently small that a very similar pattern to that calculated is created.

C. Results

The results clearly indicate that the addition of frequency averaging of the reradiation pattern of complex targets substantially improves the de-

finition of the target. The reader should bear in mind that the results presented represent only the addition of a swept frequency during transmission, done in such a manner that each pulse modulated a different carrier frequency on a repetitive sweep basis. Several other techniques are possible, some perhaps more optimum than the method used here[11, 12, 13]. However, the point is well made that the addition of frequency averaging warrants consideration in the design of imaging radar systems.

1. Rubber Sphere. Figure 24 shows the acoustic image of the rubber sphere for four separate frequencies and a swept frequency. The images were recorded from a distance of 51 cm., and consequently the illumination region of the transmitted beam was 6 cm in diameter. The target diameter was 4.5 cm.

The images of the styrofoam sphere and the array show the existence of, what may properly be termed, multiple lobes. The return from the rubber sphere consists of multiple "specular points." That is, the sphere is obviously not perfectly smooth to the incident wavelength, but the roughness does not produce an array effect such as the styrofoam sphere. The significance of this distinction is that for an array the lobes "move" with frequency and hence an averaging is obtained. This effect does not occur with the rubber sphere. The distinction evident between images at different single frequencies is that each "specular point" has a different amplitude from frequency-to-frequency. The swept frequency image clearly shows the target to have two major "specular points", where one is 6 db greater than the other. Other such points are indicated to exist at lower levels. No single frequency image clearly defines both points, and limited to any one single frequency image the definition of the target is misleading. In comparing figure 24 to figure 20, both of which show the rubber sphere, the reader should note that figure 20 was obtained by imaging a region of the sphere slightly off-center and hence the dynamic range of the "specular point" return was less than the returns shown in figure 24, which are from the apex.

2. Styrofoam Sphere. Figure 25 shows the acoustic image of the styrofoam sphere for several single frequencies. In figure 26 one of the mono-

chromatic images is compared to swept frequency images of ± 3% and ± 6% from center frequency. The images were recorded at a distance of approximately 1 m and a beam illumination region of 11.6 cm diameter. The reradiation lobe pattern is more complex than the simple rubber sphere and the effect of varying frequency is marked. Of special interest is the phase cancellation of the center main lobe (well defined at 1520 KHz and 1626 KHz) at 1427 KHz, 1744 KHz, and 1816 KHz. The effect occurred at numerous intermediate frequencies as well.

The application of swept frequency illumination (figure 26) smoothed the monochromatic lobes and formed a uniform, broad backscatter lobe. The effect of increasing the bandwidth was to strengthen the off-center lobes found at the higher and lower frequencies and hence "fill" the sphere return. Unfortunately at sweeps above about ± 10% the frequency response curve of the transducers has decreased such that only a small contribution is obtained from the extreme frequencies of the sweep, hence the full effect of frequency averaging could not be investigated. This is especially evident in the array target data.

3. Array. Figure 27 shows the acoustic images of the 8-element array at three monochromatic frequencies. The images were recorded for several gain settings to show the various amplitude levels of the multiple lobes. As the gain is increased the lower level lobes become evident. Because of the gain level sensitivity and the large number of lobes it is difficult to determine the difference in the lobe structure at different frequencies. Figure 28 compares three monochromatic images at approximately the same loop-gain levels, i.e. the receiver gain is set to compensate for the decrease in transducer gain.

Figure 29 shows the effect of adding a swept frequency signal of two different sweep widths: ± 100 KHz and ± 50 KHz. As in figure 27, the lobe levels were interrogated by varying the receiver gain. The ± 50 KHz swept signal was inadequate to completely smooth the reradiation pattern, however the ± 100 KHz swept signal provided good smoothing at nearly all intensity levels. It is evident that a greater sweep width is required to completely "fill" the image.

Acknowledgement: This work was supported by Project Themis (USAETL Contract DAAK02-68-C-0089, ARPA order No. 1079) and NASA Contract NAS 9-7175.

BIBLIOGRAPHY

1. Rouse, J. W., Jr., 1968, "The Frequency Dependence of Backscatter from Rough Surfaces," An Experiment with Broad-spectrum Acoustic Waves, Ph. D. dissertation, University of Kansas, Lawrence, (in press).

2. Katz, I., 1966, "Wavelength Dependence of the Radar Reflectivity of the Earth and the Moon," J. Geo. Res., vol. 71, no. 2.

3. Fung, A. K. and Leovaris A., 1968, "Frequency Dependence of Ultrasonic Scatter from Statistically Known Rough Surfaces," WESCON.

4. Wiltse, J. C., Schlesinger, S. P., and Johnson, C. M., 1957, "Backscattering Characteristics of the Sea in the Region from 10 to 50 K mc/s," Proc. IRE, vol. 45, pp. 220-228, February.

5. Beckmann, P., 1965, "Scattering by Composite Rough Surfaces," Proc. IEEE, vol. 53, no. 8, pp. 1012-1015.

6. Fung, A. K. and Moore, R. K., 1964, "Effects of Structure Size on Moon and Earth Radar Returns at Various Angles," J. Geophys. Res., vol. 69 (6), pp. 1075-1081,

7. Fung, A. K. and Moore, R. K., 1966, "The Correlation Function in Kirchhoff's Method of Solution of Scattering of Waves from Statistically Rough Surfaces," Journal of Geophys. Res., vol. 71, no. 12,

8. Davies, H., 1954, "The Reflection of Electromagnetic Waves from a Rough Surface," Proc. IEEE, Part IV, vol. 101, pp. 209-214.

9. Stratton, J. A., 1941, Electromagnetic Theory, McGraw-Hill, New York.

10. Silver, S., 1964, Microwave Antenna Theory and Design, Boston Technical Publisher,

11. Gustafson, B. G. and Ås, B-O, 1964, "System Properties of Jumping Frequency Radar," Phillips Telecommun. Rev., vol. 25, no. 1, pp. 70-76.

12. Kosowsky, L. H., Brody, S. S., Chanzit, L., and Saslovsky, S., 1963, "The Reduction of Angle-of-Arrival Scintillation by a Frequency Shifting Technique," Presented at the 1963 Natl. Electronics Conf., New York.

13. Ray, M., 1966, "Improving Radar Range and Angle Detection with Frequency Agility," Microwave J., pp. 63-68, May 1966.

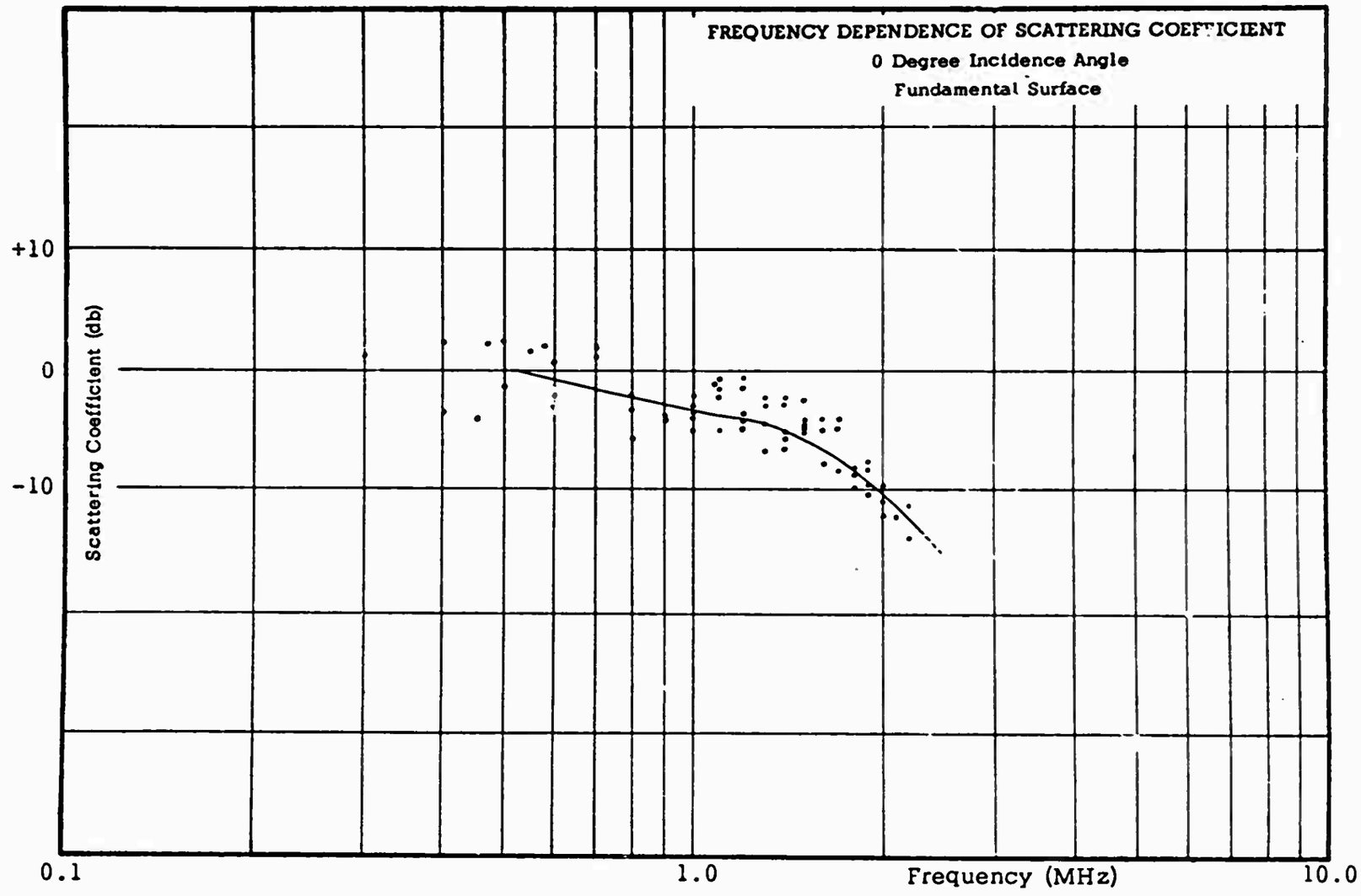
FREQUENCY DEPENDENCE OF SCATTERING COEFFICIENT
0 Degree Incidence Angle
Fundamental Surface
+10
0
-10
Scattering Coefficient (db)
0.1
1.0
Frequency (MHz)
10.0

Figure 1

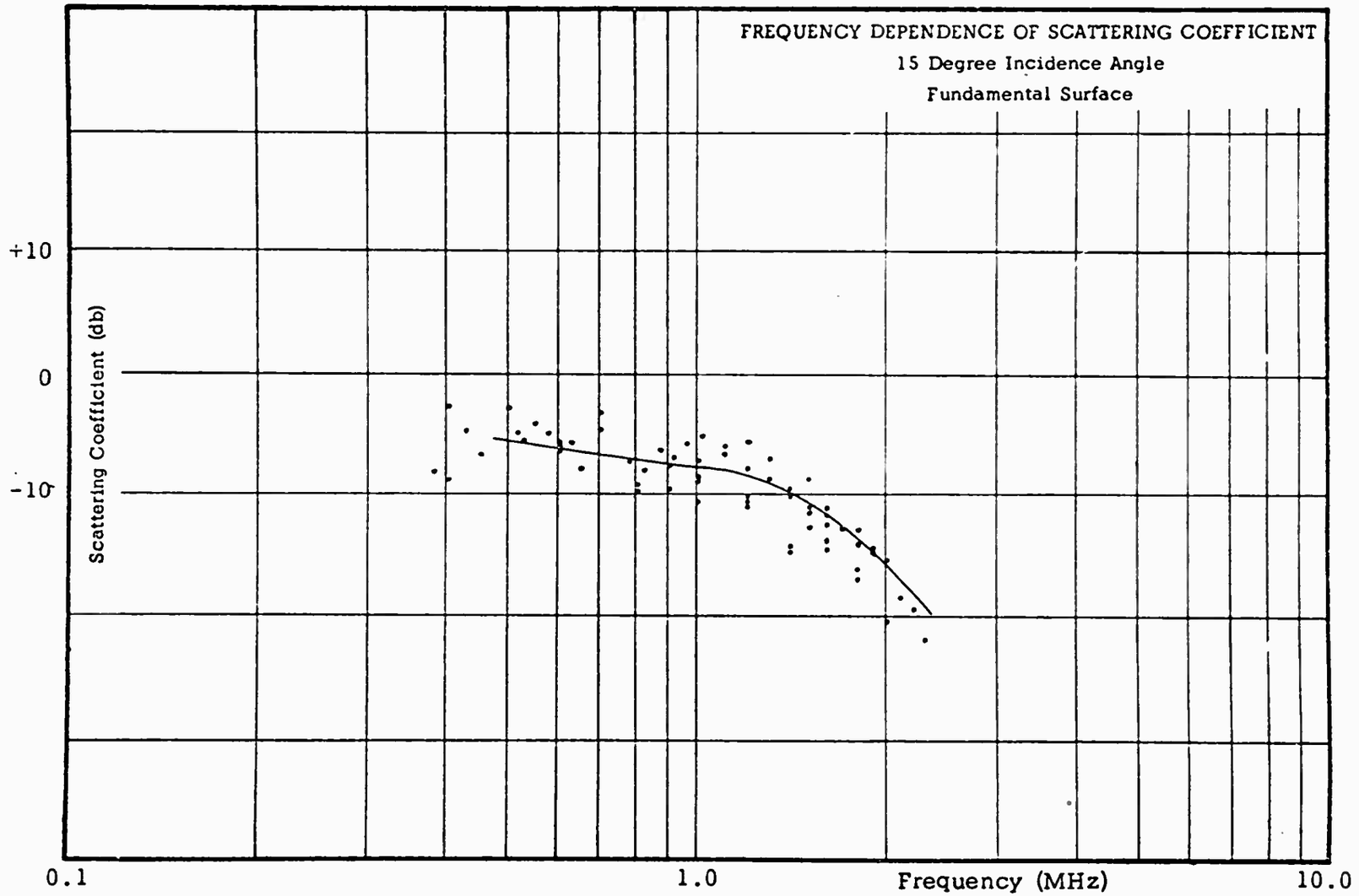
FREQUENCY DEPENDENCE OF SCATTERING COEFFICIENT
15 Degree Incidence Angle
Fundamental Surface
+10
0
-10
Scattering Coefficient (db)
0.1
1.0
10.0
Frequency (MHz)

Figure 2

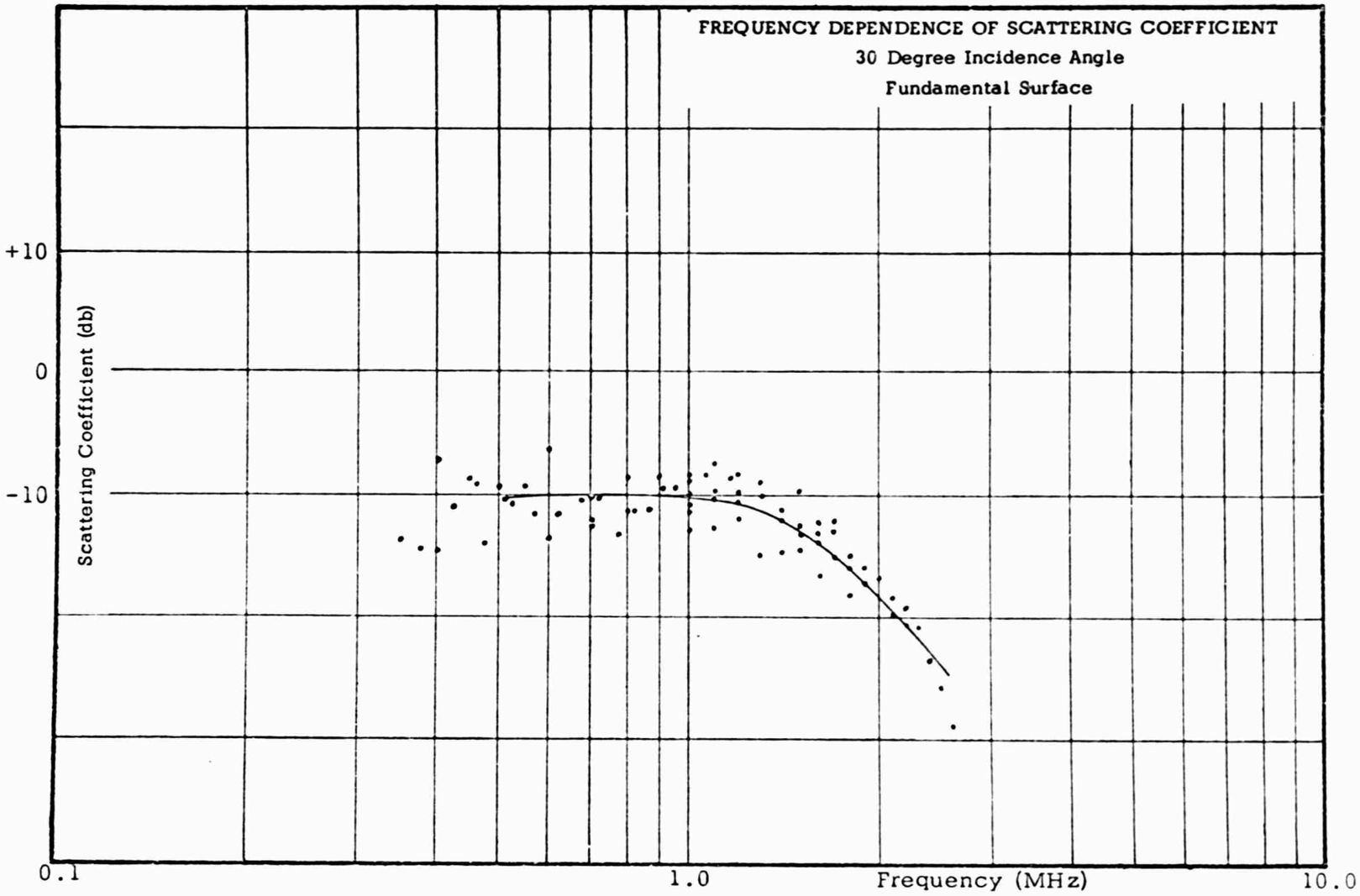
FREQUENCY DEPENDENCE OF SCATTERING COEFFICIENT
30 Degree Incidence Angle
Fundamental Surface
+10
0
-10
Scattering Coefficient (db)
0.1
1.0
Frequency (MHz)
10.0

Figure 3

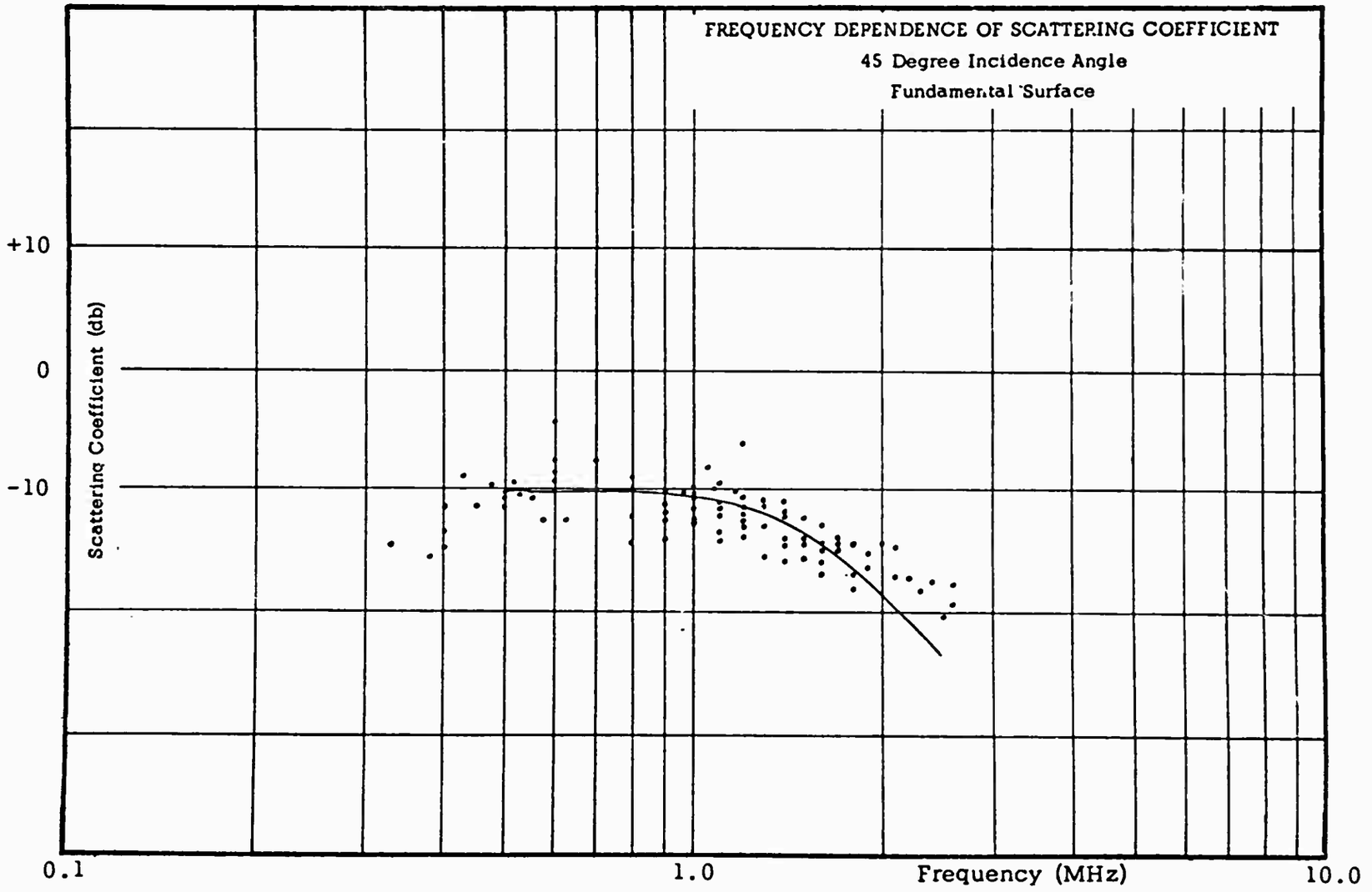
FREQUENCY DEPENDENCE OF SCATTERING COEFFICIENT
45 Degree Incidence Angle
Fundamental Surface
+10
0
-10
Scattering Coefficient (db)
0.1
1.0
Frequency (MHz)
10.0

Figure 4

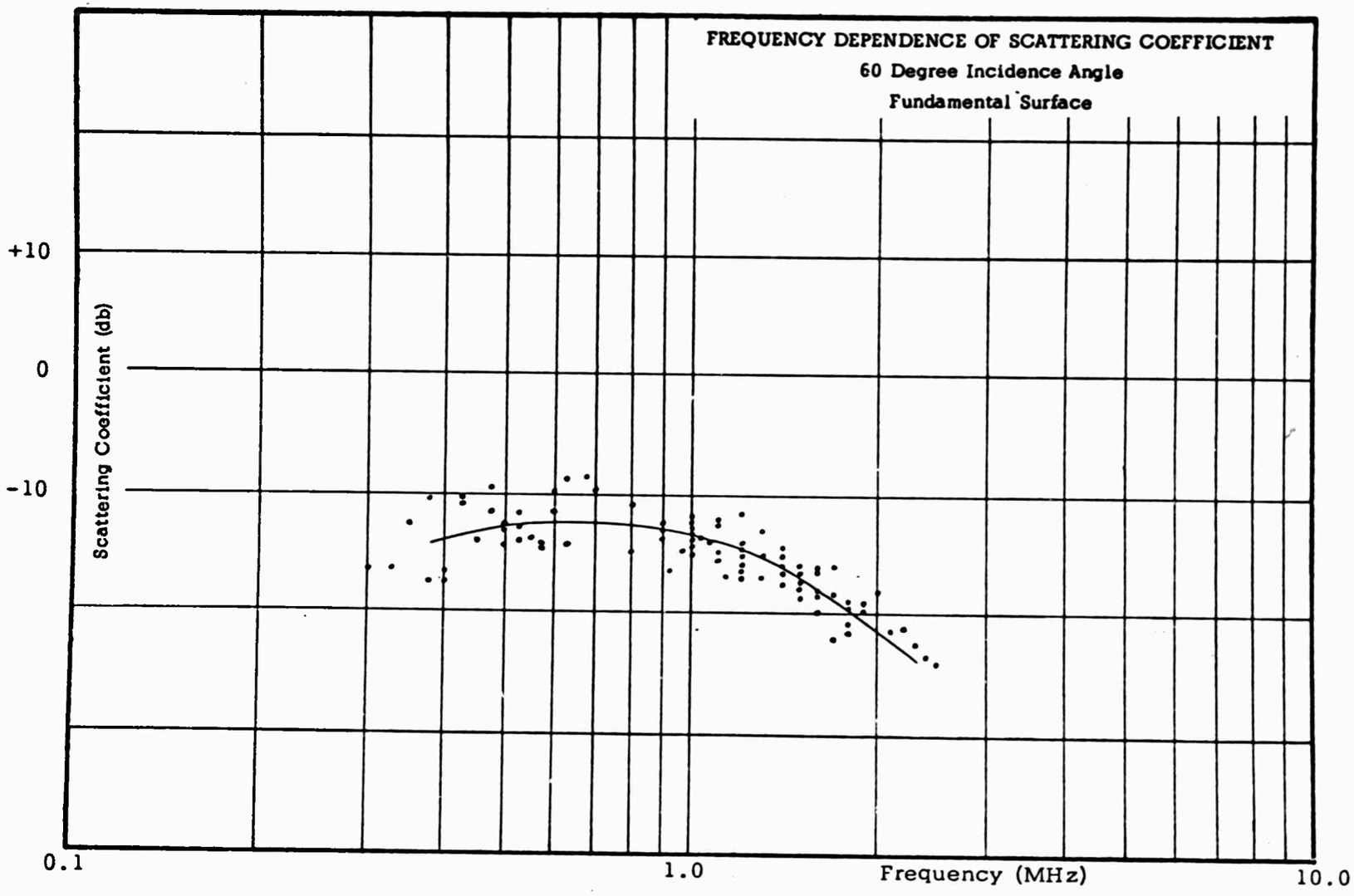
FREQUENCY DEPENDENCE OF SCATTERING COEFFICIENT
60 Degree Incidence Angle
Fundamental Surface
+10
0
-10
Scattering Coefficient (db)
0.1
1.0
Frequency (MHz)
10.0

Figure 5

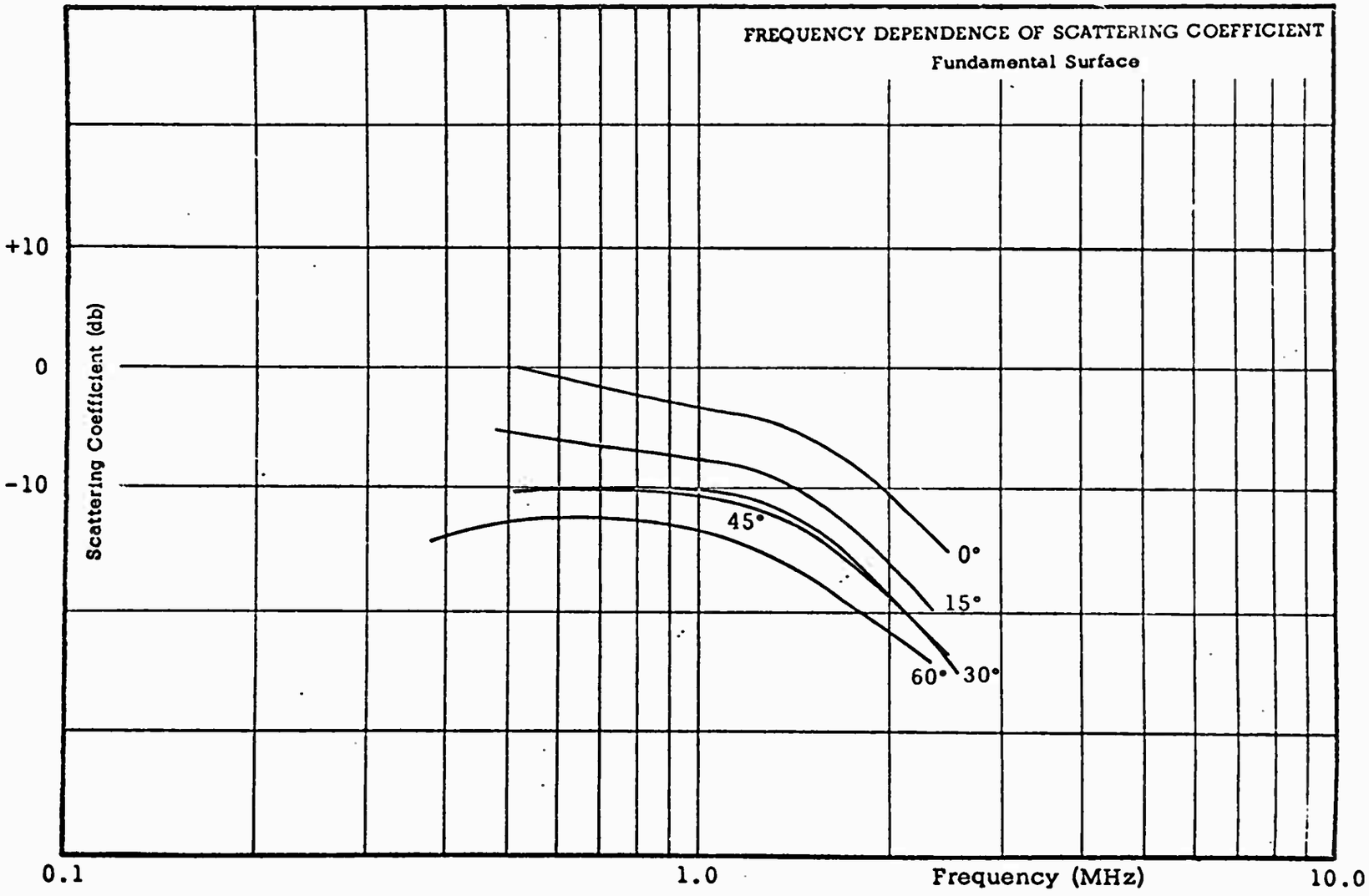
FREQUENCY DEPENDENCE OF SCATTERING COEFFICIENT
Fundamental Surface
+10
0
-10
Scattering Coefficient (db)
45°
0°
15°
60°
30°
0.1
1.0
Frequency (MHz)
10.0

Figure 6

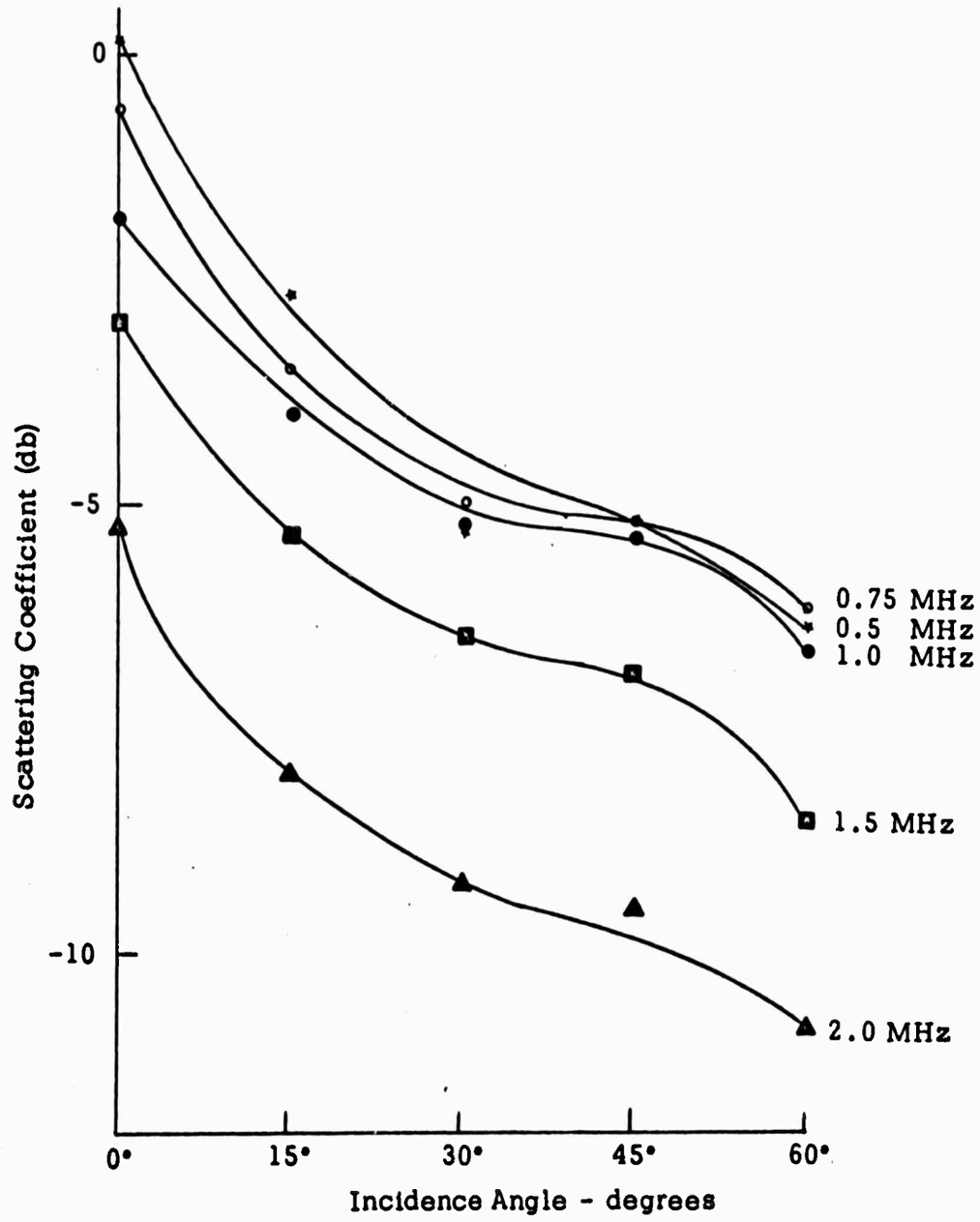

Figure 7 Variation of scattering coefficient with angle and frequency - fundamental surface.

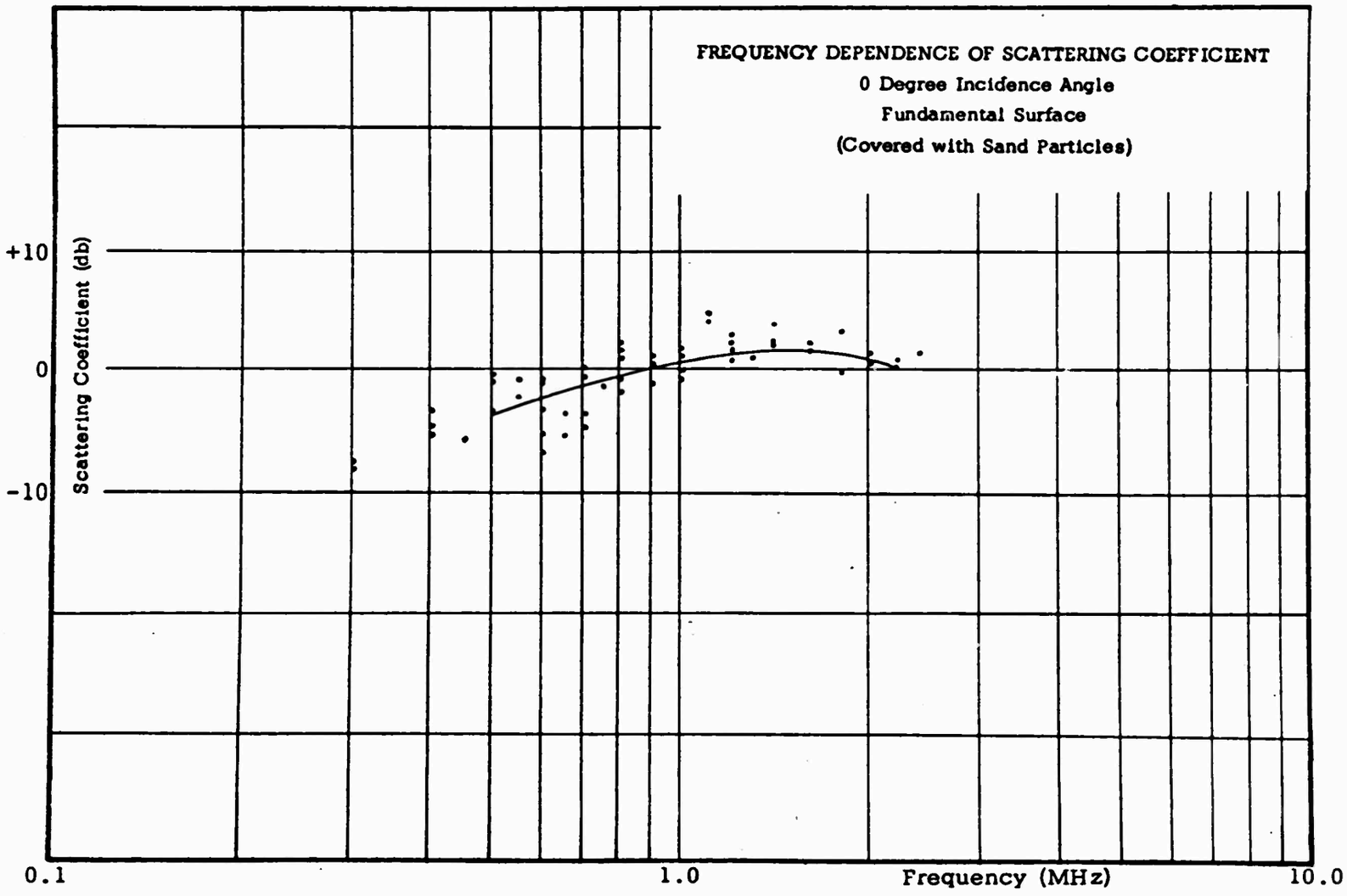
FREQUENCY DEPENDENCE OF SCATTERING COEFFICIENT
0 Degree Incidence Angle
Fundamental Surface
(Covered with Sand Particles)
+10
0
-10
Scattering Coefficient (db)
0.1
1.0
Frequency (MHz)
10.0

Figure 8

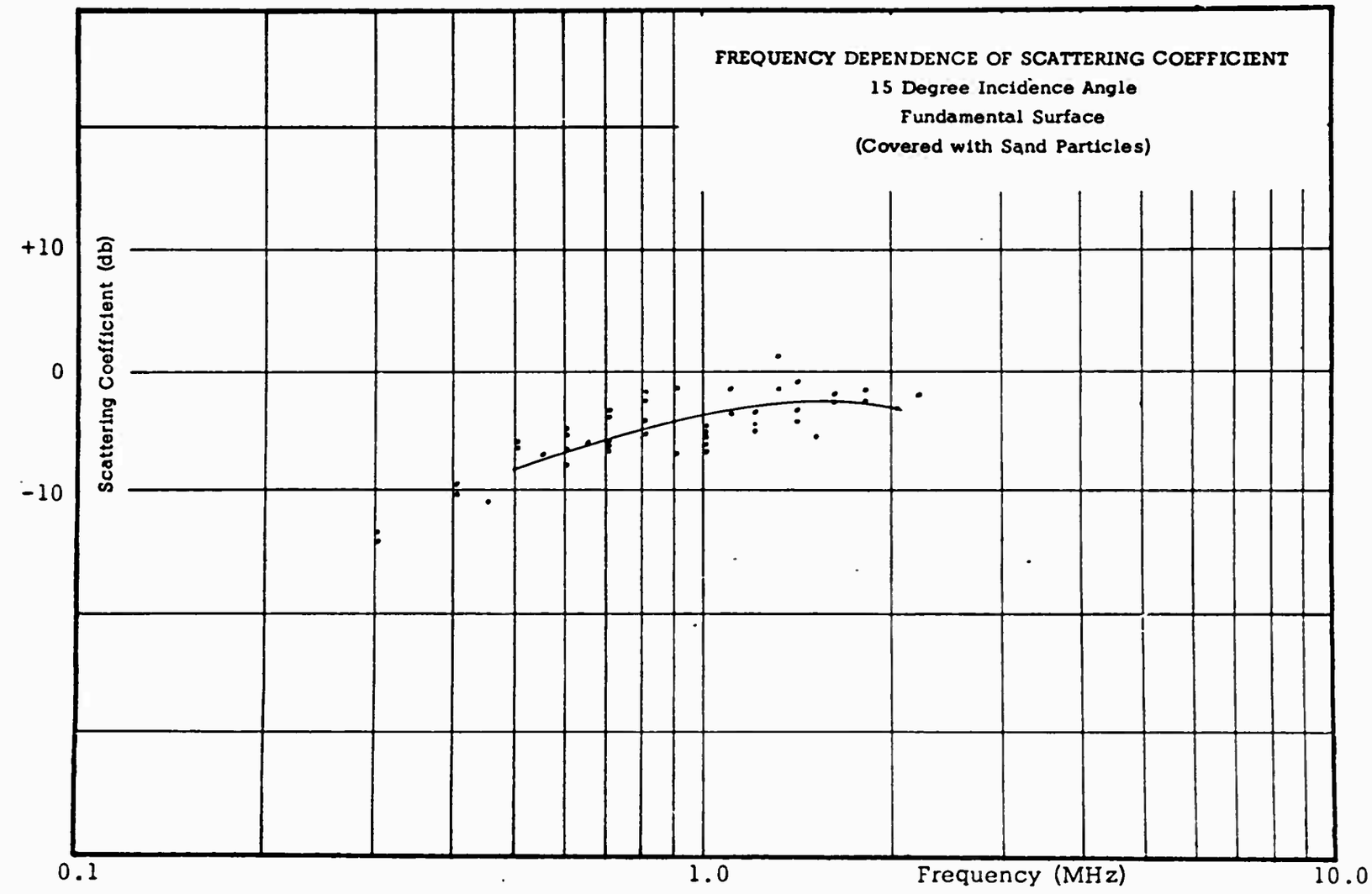
FREQUENCY DEPENDENCE OF SCATTERING COEFFICIENT
15 Degree Incidence Angle
Fundamental Surface
(Covered with Sand Particles)
Scattering Coefficient (db)
+10
0
-10
0.1
1.0
10.0
Frequency (MHz)

Figure 9

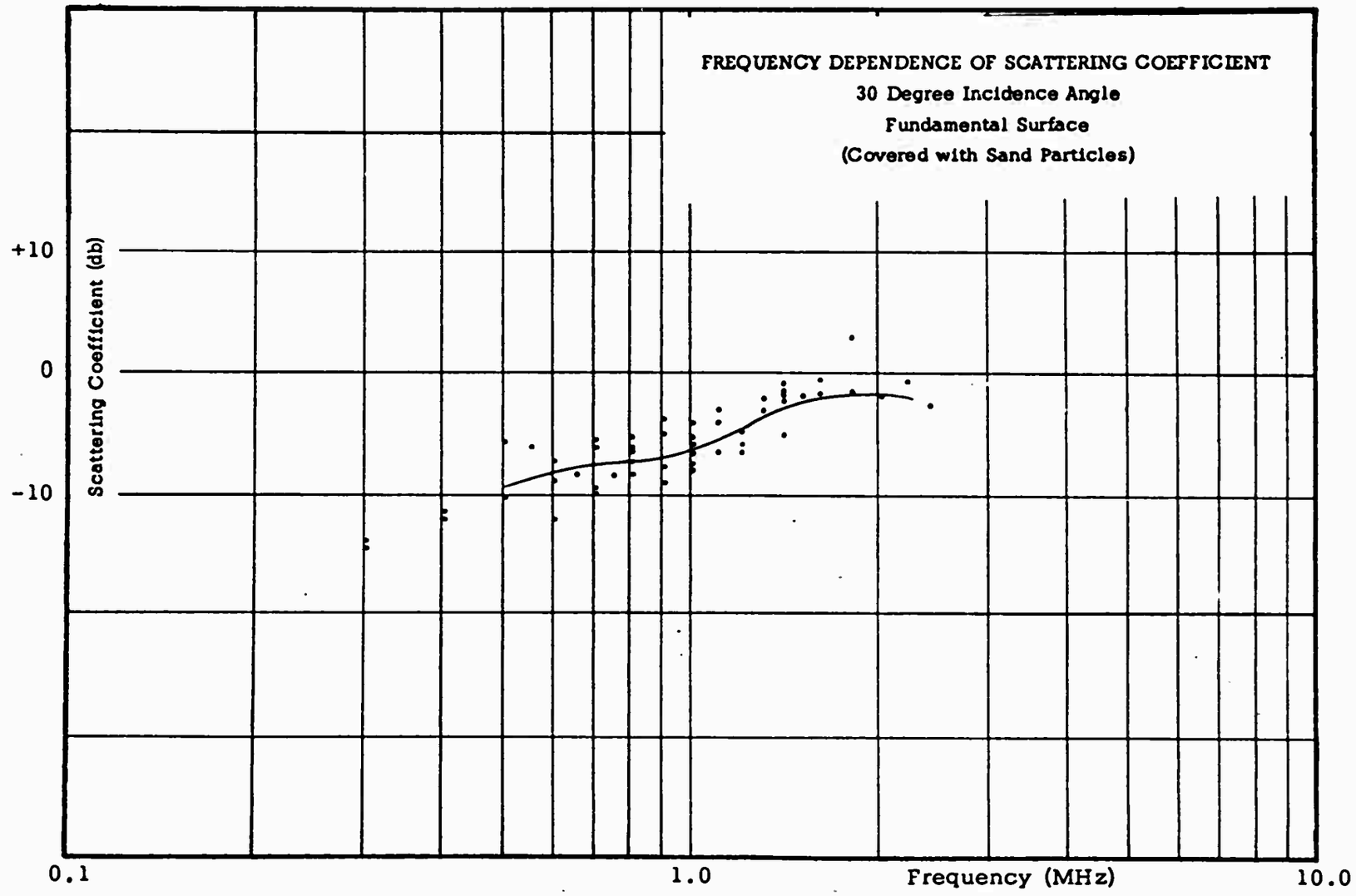
FREQUENCY DEPENDENCE OF SCATTERING COEFFICIENT
30 Degree Incidence Angle
Fundamental Surface
(Covered with Sand Particles)
+10
0
-10
Scattering Coefficient (db)
0.1
1.0
10.0
Frequency (MHz)

Figure 10

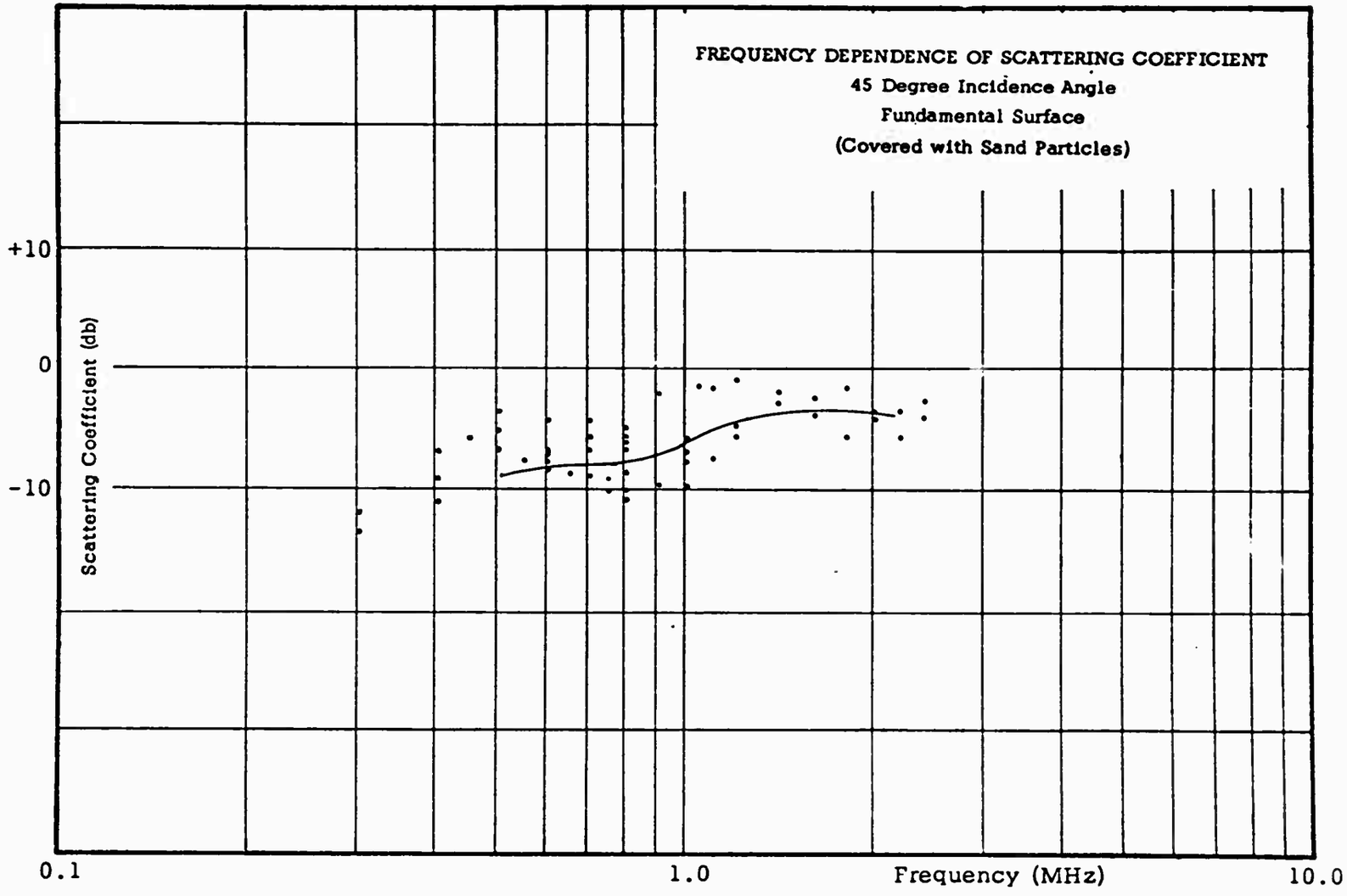
FREQUENCY DEPENDENCE OF SCATTERING COEFFICIENT
45 Degree Incidence Angle
Fundamental Surface
(Covered with Sand Particles)
+10
0
-10
Scattering Coefficient (db)
0.1
1.0
Frequency (MHz)
10.0

Figure 11

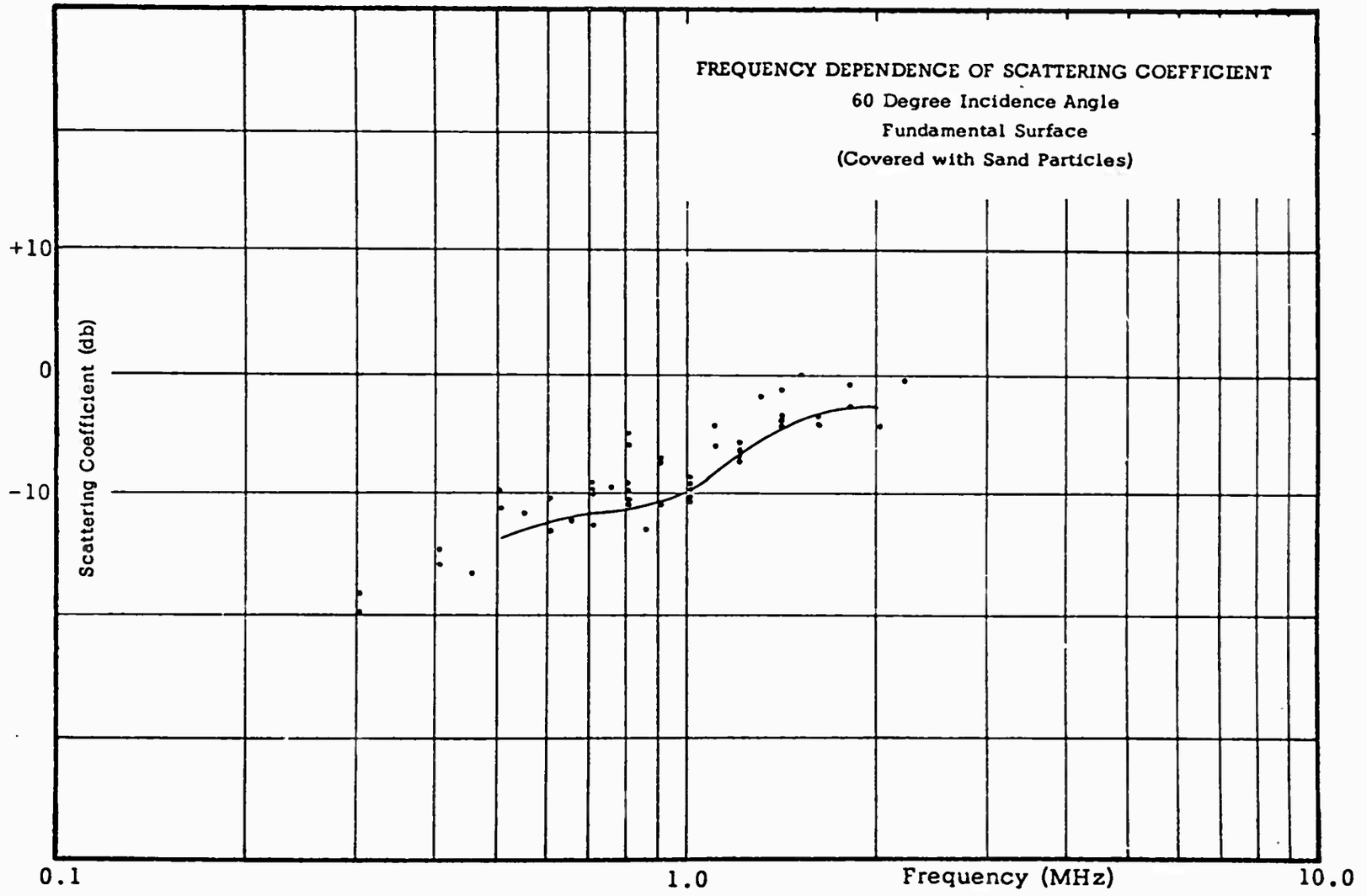
FREQUENCY DEPENDENCE OF SCATTERING COEFFICIENT
60 Degree Incidence Angle
Fundamental Surface
(Covered with Sand Particles)
+10
0
-10
Scattering Coefficient (db)
0.1
1.0
10.0
Frequency (MHz)

Figure 12

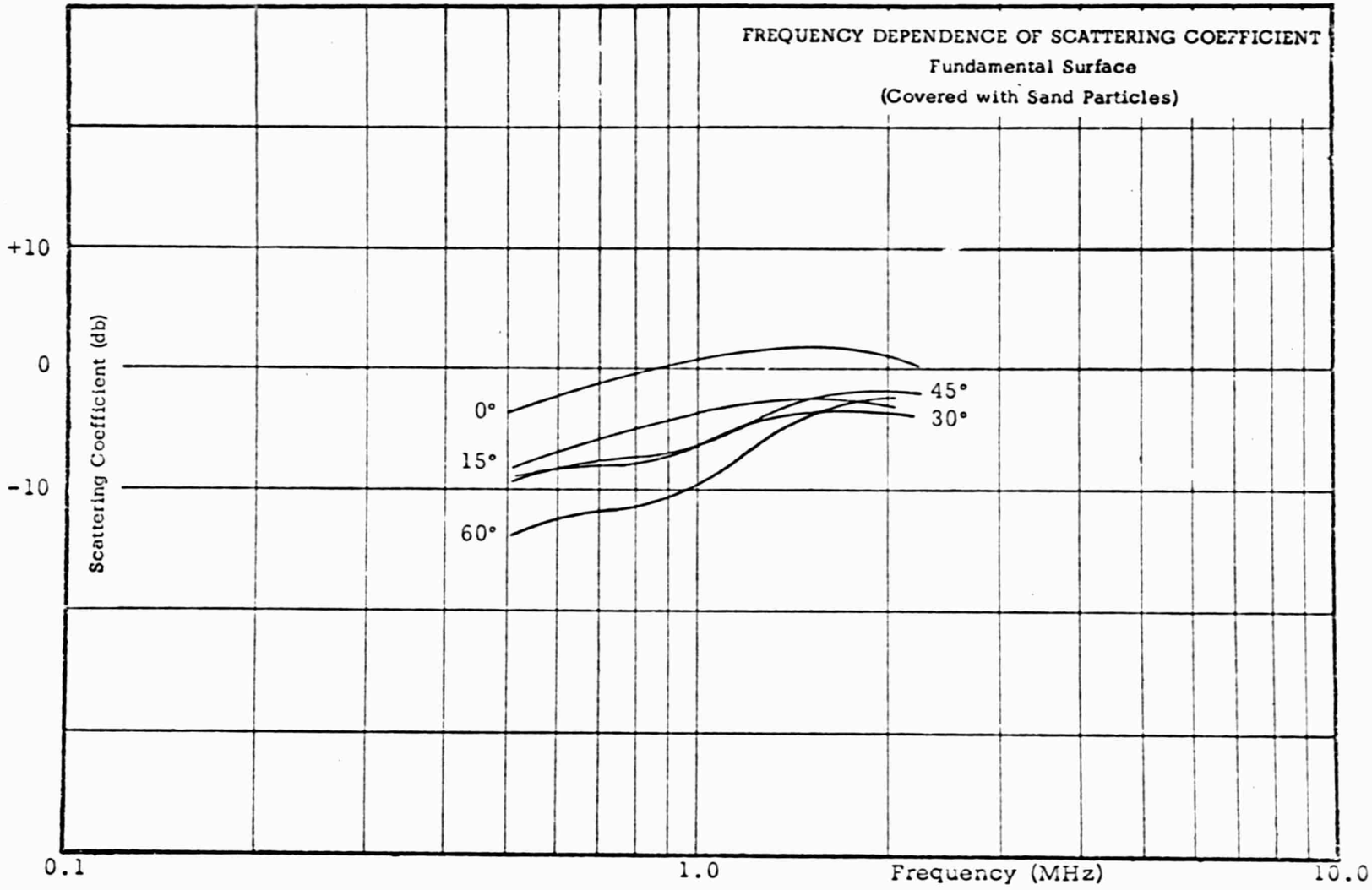
FREQUENCY DEPENDENCE OF SCATTERING COEFFICIENT
Fundamental Surface
(Covered with Sand Particles)
+10
0
-10
Scattering Coefficient (db)
0°
15°
60°
45°
30°
0.1
1.0
Frequency (MHz)
10.0

Figure 13

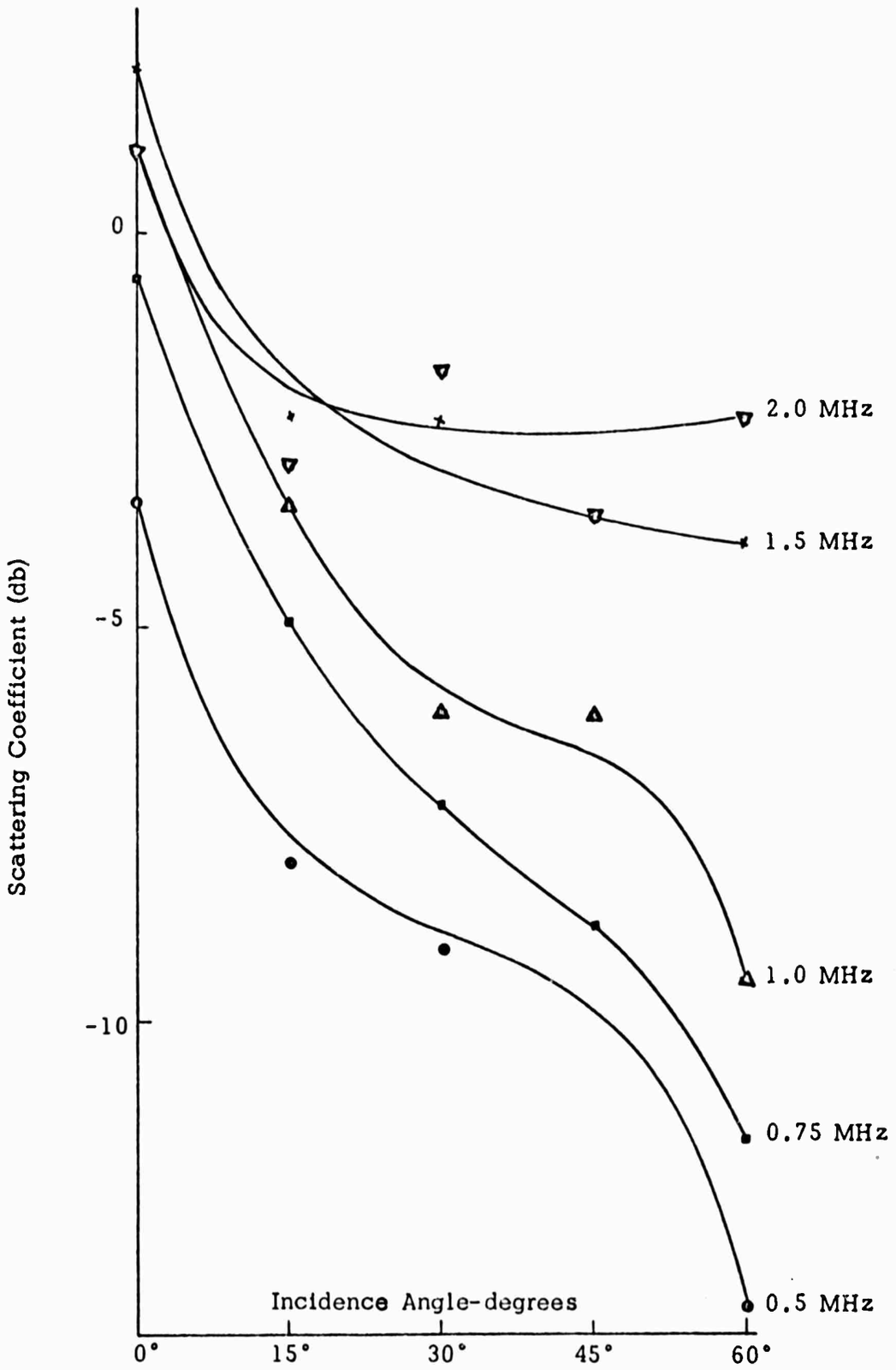

Figure 14 Variation of scattering coefficient with angle and frequency - sanded surface.

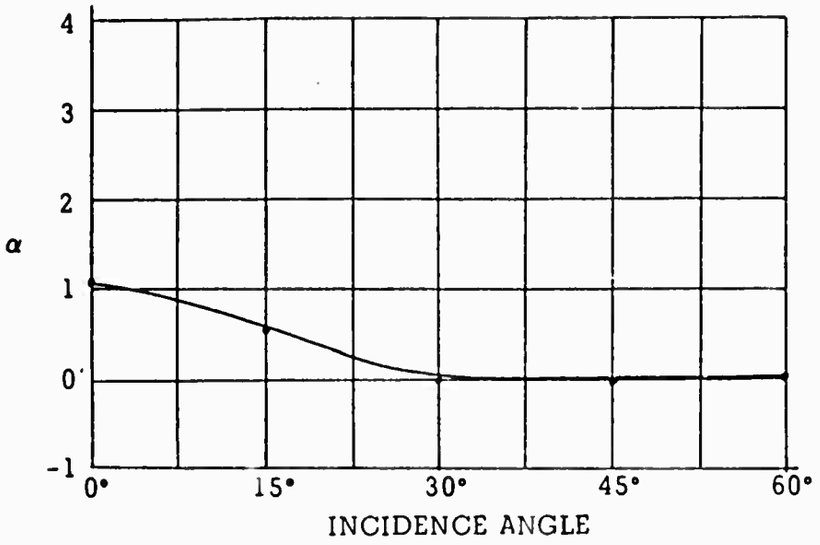

Figure 15 Variation of slope for fundamental surface data below 1.25 MHz

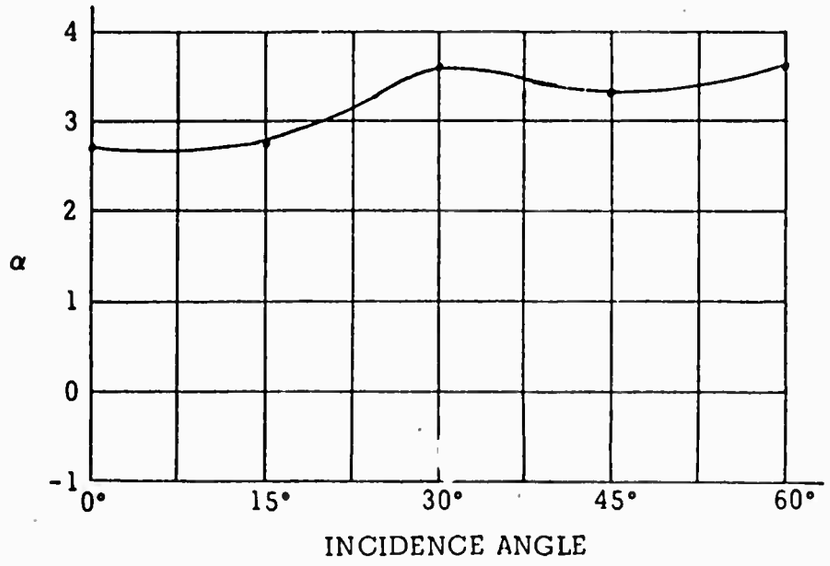

Figure 16 Variation of slope for fundamental surface data above 1.25 MHz

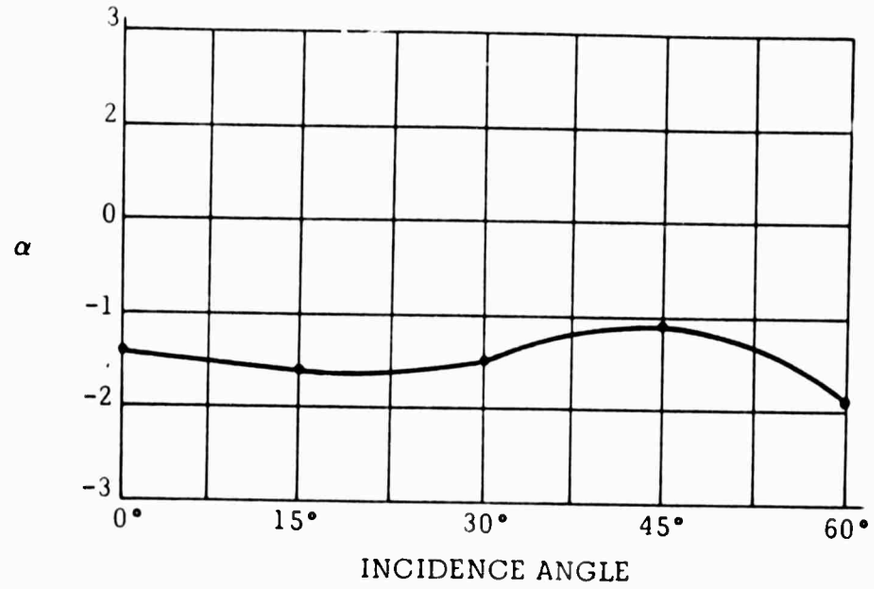

Figure 17. Variation of slope for sanded surface data below 1.25 MHz

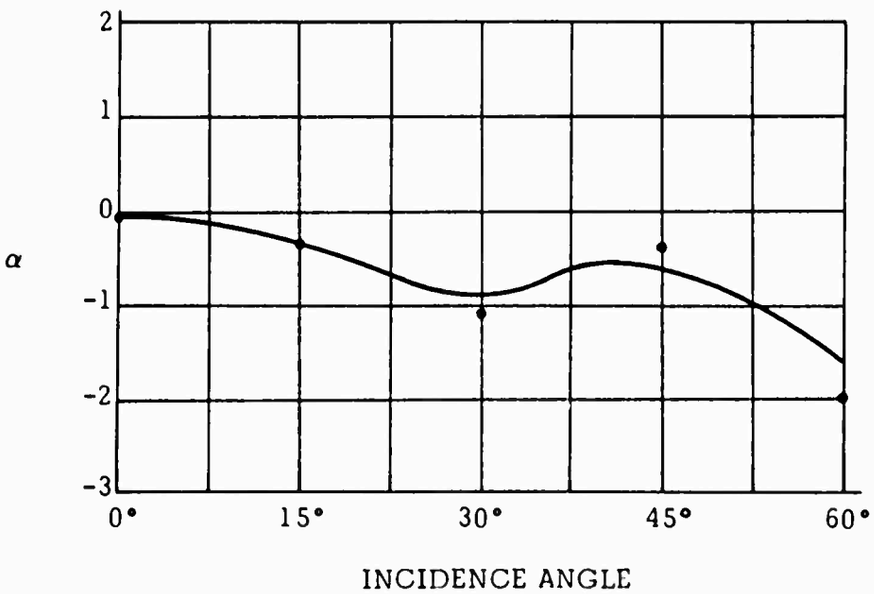

Figure 18. Variation of slope for sanded surface data above 1.25 MHz

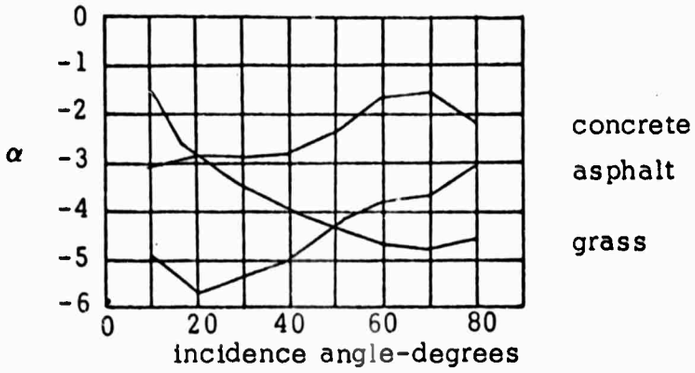

(a) Wavelength dependence of grass, concrete, and asphalt surfaces.

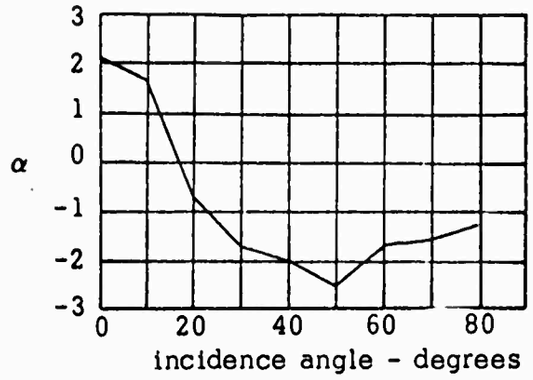

(b) Wavelength dependence of sea clutter. This figure covers the microwave region from 0.86 to 71 cm and applies to rough sea conditions.

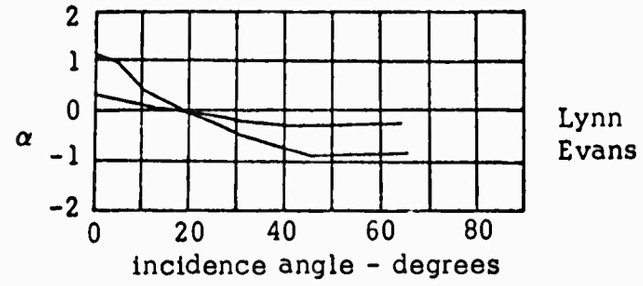

(c) Wavelength dependence of the moon's surface.

Figure 19 Variation of slopes for natural surfaces (after Katz 1966)

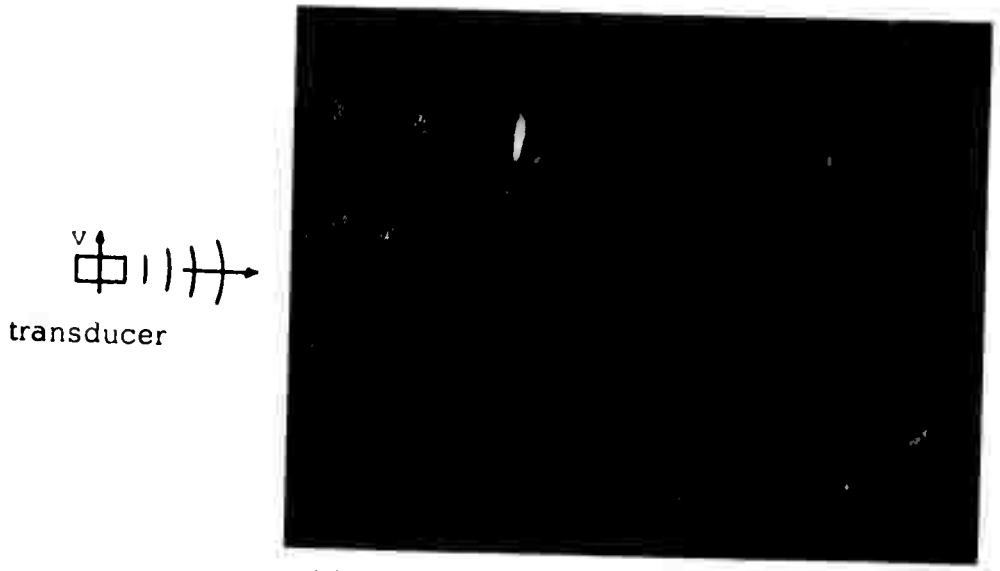

(a) Monochromatic image of two spheres
(f = 1.5 MHz)

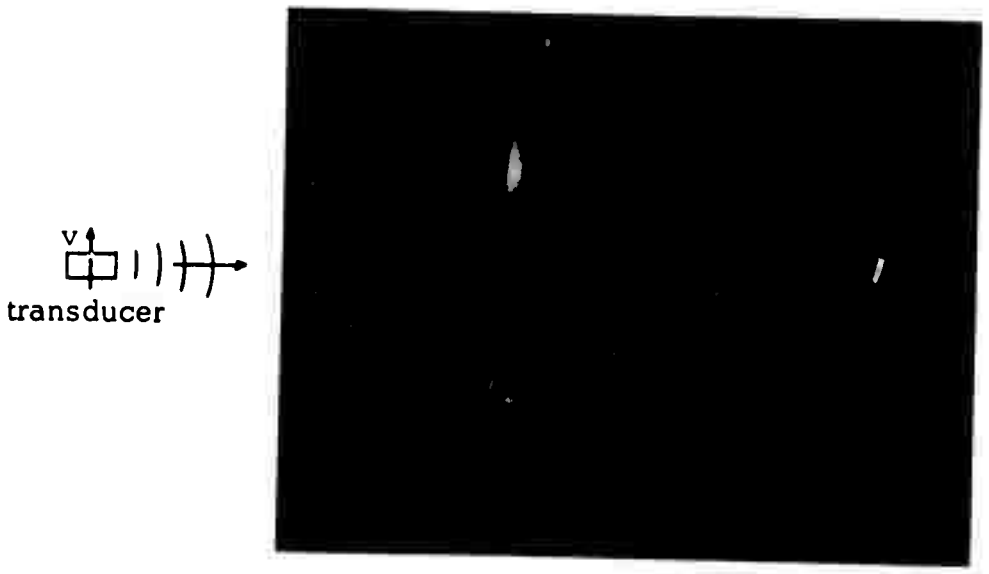

(b) Swept frequency image of two spheres
(f = 1.5 MHz ± 10%)

Figure 20 Effect of frequency average on image of sphere targets

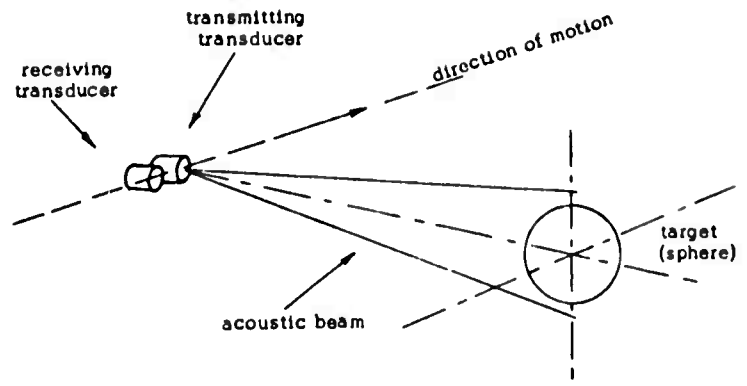

Figure 21 Positioning for acoustic imaging.

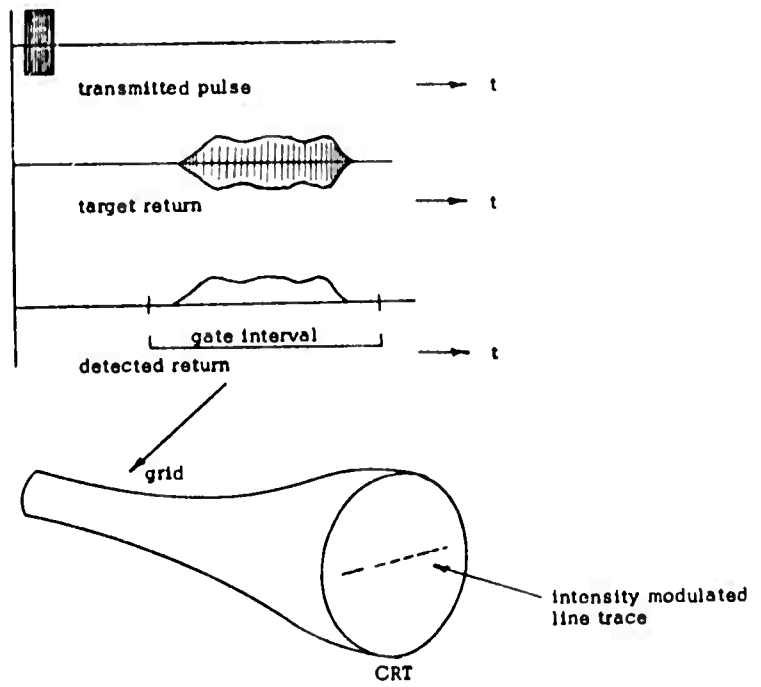

Figure 22 Image recording of target return.

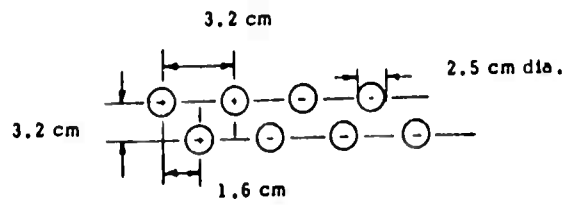

Figure 23 8-element array.

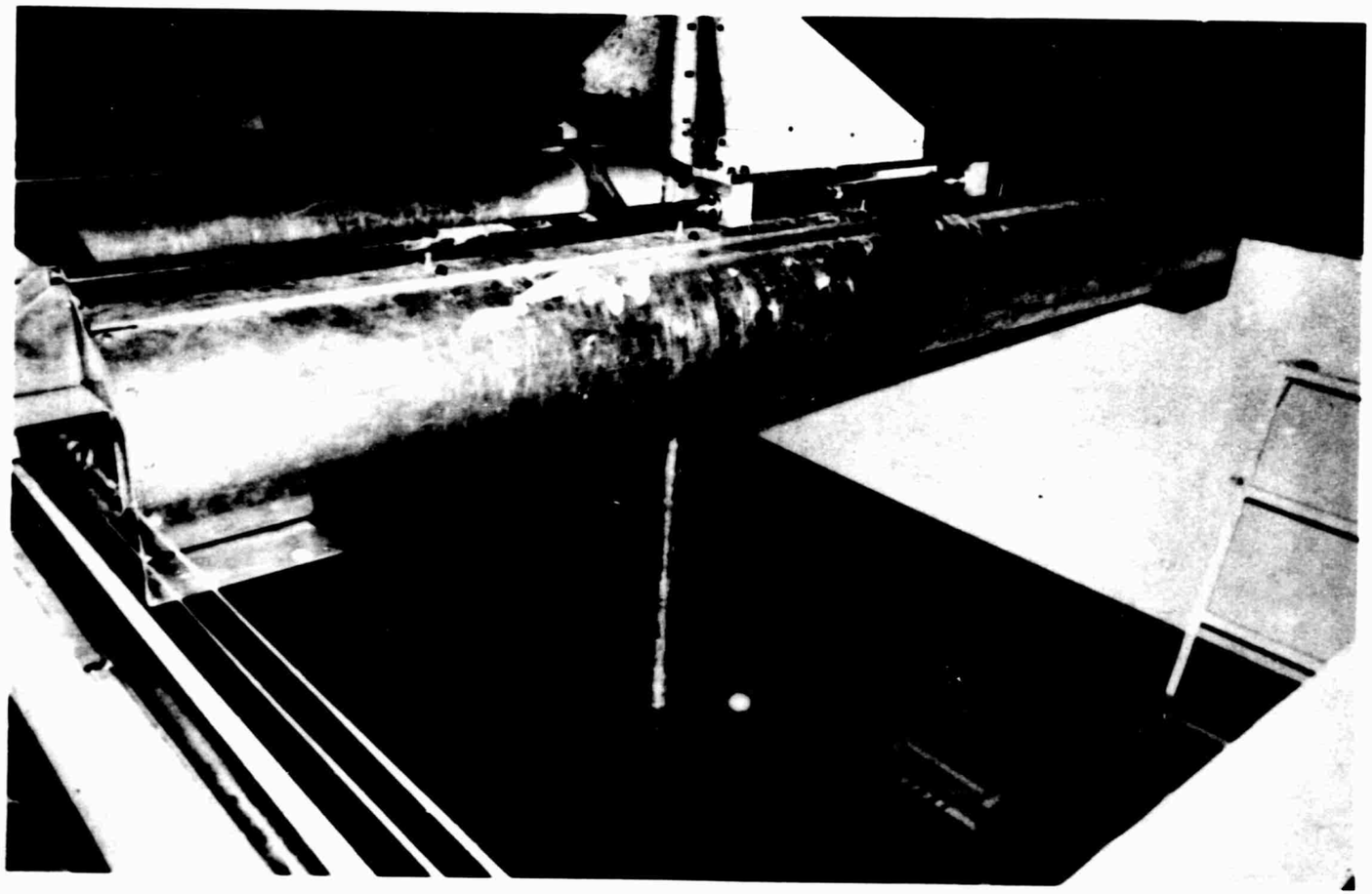

LINEAR MOTION CARRIAGE

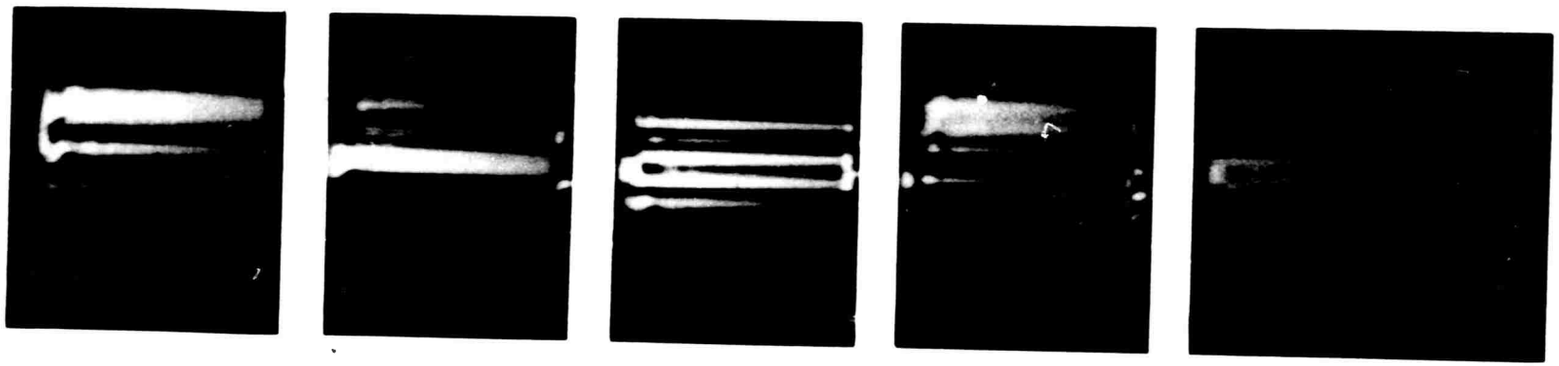

f = 1523 KHz	f = 1637 KHz	f = 1750 KHz	f = 1819 KHz	f = 1640 ± 100 KHz
G = 15 db	G = 16 db	G = 17 db	G = 21 db	G = 21 db

Figure 24 Acoustic images of rubber sphere target

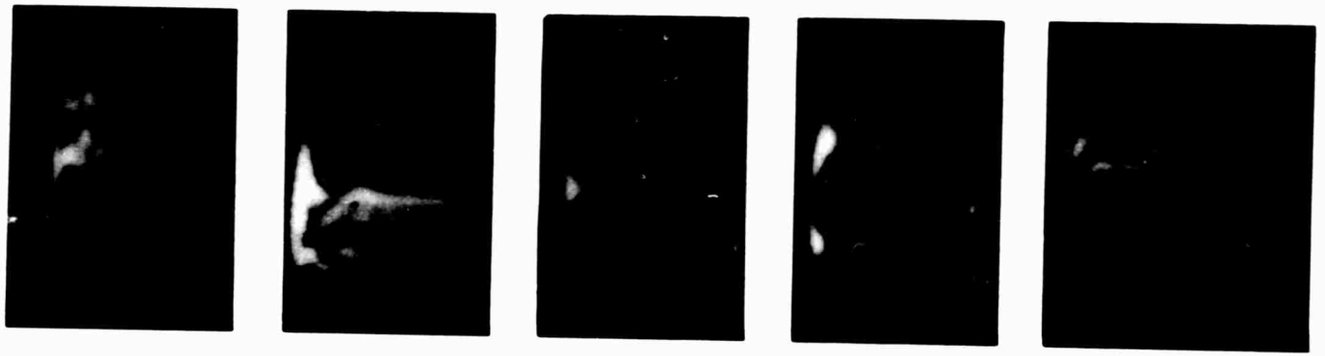

f = 1.43 MHz f = 1.52 MHz f = 1.64 MHz f = 1.74 MHz f = 1.82 MHz

Figure 25 Comparison of different frequency images of styrofoam sphere target

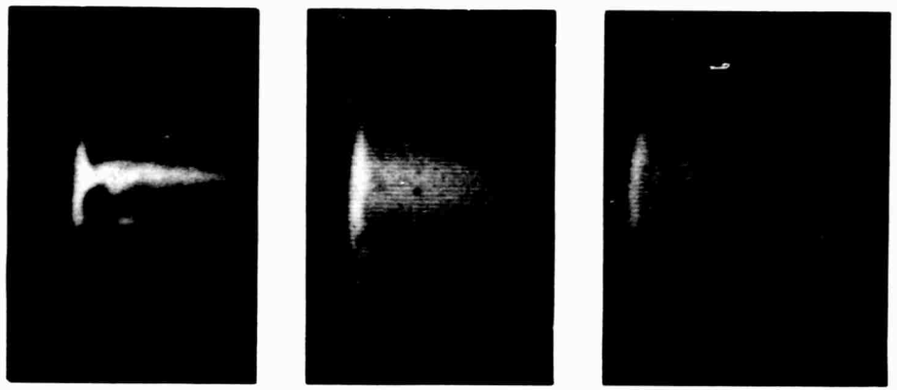

F = 1.64 MHz f = 1.64 ± 0.05 MHz f = 1.64 ± 0.1 MHz

Figure 26 Comparison of monochromatic and swept frequency images of styrofoam sphere target

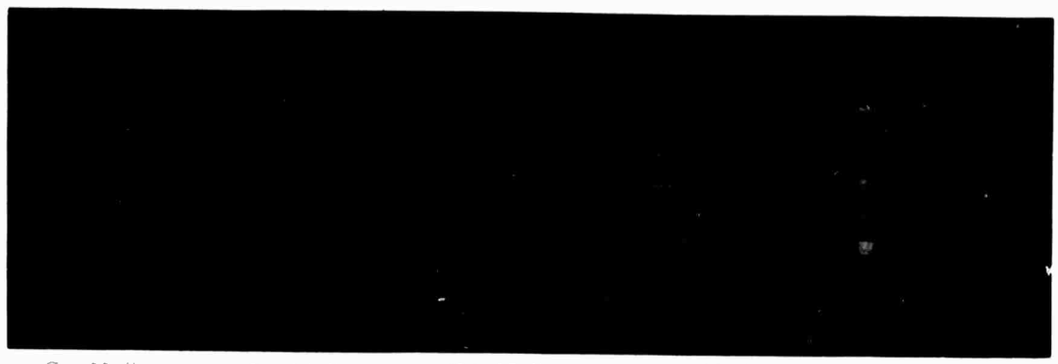

G = 22 db G = 24 db G = 27 db G = 30 db G = 32 db

(a) f = 1745 MHz

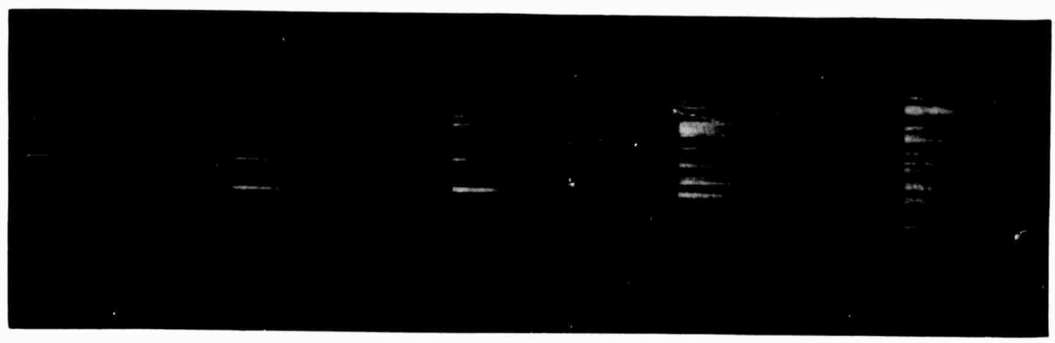

G = 20 db G = 23 db G = 25 db G = 27 db G = 30 db

(b) f = 1640 MHz

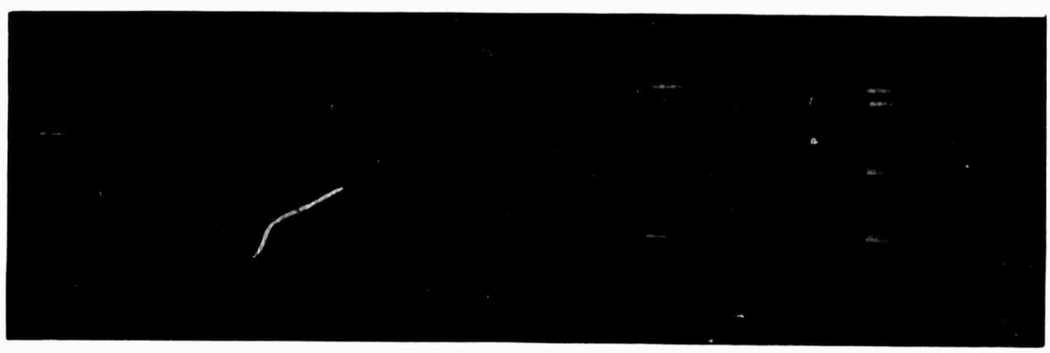

G = 30 db G = 32 db G = 34 db G = 35 db G = 37 db

(c) f = [illegible]

Figure 27 Effect of receiver gain variations on images of 8-element array at three monochromatic frequencies

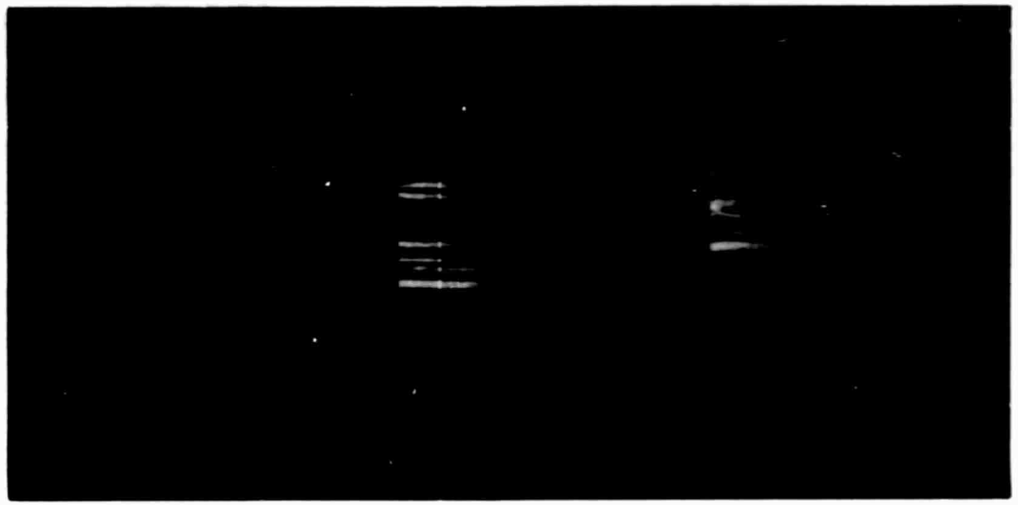

f = 1500 KHz
G = 36 db

f = 1640 KHz
G = 26 db

f = 1750 KHz
G = 30 db

Figure 28 Image of major lobes of 8-element array for three monochromatic frequencies.

G = 11 db G = 14 db G = 17 db G = 20 db G = 23 db

(a) Frequency = 1640 ± 100 KHz

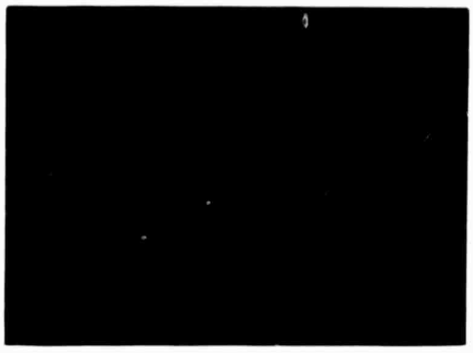

G = 11 db G = 14 db

(b) Frequency = 1640 ± 50 KHz

Figure 29 Effect of swept frequency on image of 8-element array

BLANK PAGE

Appendix C

SYSTEM AND COMPONENT CONSIDERATIONS FOR THE POLYPANCHROMATIC RADAR

P. D. Shaw

Technical Memorandum 133-1-2

SYSTEM AND COMPONENT CONSIDERATIONS FOR THE POLYPANCHROMATIC RADAR

by

P. D. Shaw

1.0 INTRODUCTION

The polypanchromatic radar is a device for performing broad spectrum electromagnetic scattering and imaging measurements. The calculations necessary to define the transmitter power and antenna were previously performed (Reference 1). Since publication of this memorandum the system functional arrangement has been changed. Consideration will be given to the revised system and the components necessary to implement it. The post detection processing (Reference 3) and the digital control system (Reference 4) are described separately.

2.0 SYSTEM REVIEW

The basic design goals have been described (Reference 1). These are:

1. Operation over a bandwidth of one octave (4-8 GHz)
2. Measurement of backscattering cross section as a function of
   a. Frequency
   b. Bandwidth
   c. Incidence angle
3. Production of panchromatic imagery as a function of
   a. Frequency
   b. Bandwidth

These objectives are most economically achieved with a slow sweep, pulse modulated system in which the frequency does not change appreciably within the pulse period. The frequency range is divided into separated narrow bands. Full spectrum coverage is achieved by the overlapping spectra of the transmitted pulses (Figure 12).

Figure 1 shows the functional units in the radar while Figure 2 shows the component arrangement. It will be noted that the components have been divided into two sections. Two methods of construction are possible.

1. All components mounted on the ground with the signal transmitted to the antenna, at the end of the boom, by coaxial cable (Reference 1). This has the advantage of component accessibility and simplified duplex switching, but gives a high signal loss due to the cable.
2. The signal loss may be reduced by mounting the transmitter and receiver T.W.T.'s and associated components next to the antenna.

The first method of mounting will be used initially to simplify adjustment. The second method can be used later to increase the range of the radar.

3.0 THE TRANSMITTER

3.1 The T.W.T. Amplifier

As described (Reference 1) a transmitted power of 20 watts is required. The frequency of the transmitted signal must vary in frequency from 4 GHz to 8 GHz. The only suitable amplifier is a traveling wave tube. A T.W.T. manufactured by Alto Scientific was purchased. Its relevant characteristics are shown (Spec. 1).

When using this amplifier it is necessary to consider the harmonic power generated by the tube. The most important component will be the second harmonic generated when the fundamental is a low frequency. At this point both fundamental and second harmonic are within the pass band of the tube and the second harmonic may be only 3 to 6 db less than the fundamental. It is most important that these higher harmonics not be reflected back into the tube output. We must, therefore, use an isolator at the tube output. If these higher harmonics are to be isolated from the load it will be necessary to use a switched filter (Figure 3).

We can calculate the signal power required from the source as follows:

TWT Gain	= 58 db (min.)
TWT output	= 44 dbm (max.)
Isolator insertion loss	= 0.4 db (max.)
2x Diode Switch insertion loss	= 3 db (max.)
Signal Power	= -10.6 dbm

This amount of power is obtained from the source output through a directional coupler.

3.2 The Sweep Frequency Source

A source is required which is able to rapidly sweep the 4-8 GHz frequency range. The source chosen was a sweep frequency oscillator manufactured by Hewlett Packard. The relevant characteristics are shown (Spec. 2). This oscillator has an internal P.I.N. leveling system (Section 6.0). The relevant components were removed and used externally to facilitate power division.

4.0 THE RECEIVER

4.1 The Preamplifier

The requirements for the amplifier are

a. Low noise figure (< 10 db)
b. Frequency range 4-8 GHz
c. High gain
d. Reasonable cost

A T.W.T. Amplifier is necessary. The specifications of the model chosen are given in (Spec. 3).

4.2 Intermediate Frequency Amplifier

An amplifier manufactured by R.H.G. Labs was chosen (Spec. 4). The factors influencing this choice and the associated components are described.

4.2.1 Choice of Bandwidth

The maximum spectral width of transmitted signal is obtained when the pulse has the minimum width of 20nS. This would have a bandwidth.

$$B = \frac{1.2}{\tau} = 60 \text{ MHz}$$

This gives a sufficient spectral overlap between the frequency shifted pulses to approximate continuous frequency coverage.

The maximum range we will assume to be 915 m which gives a signal delay of 6.1 μS. We will allow 100 ns for delay through the system giving a total delay of 6.2μs. If the frequency source is sweeping at its maximum rate of 4 GHz in 10 ms, the frequency will change by 2.4 MHz. We will assume that the doppler effect is negligible in our static system. The bandwidth of the receiver must be great enough to accommodate both the bandwidth of the individual pulse and the frequency change within the delay time. A receiver bandwdith of 100 MHz was chosen, which will accomplish this and still leave room for possible future reduction of the individual pulse width.

4.2.2 I.F. Amplifier Gain

We will estimate the maximum gain required in the IF stage. Dynamic range will be considered later.

The minimum received signal

$$P_r = KTBFS$$

B = 100 MHz = receiver bandwidth
F = 10 db = receiver noise figure
S = 3 db = signal to noise ratio

If the required IF power out is 1 mw

Receiver Gain = 90.1 db

Actual Receiver gain = 32.2 + 23 + 55 = 110.2 db.

∴ We must attenuate the received signal by 20 db.

4.3 Receiver Dynamic Range

4.3.1 R.F. Section

We must first estimate the maximum signal power that appears at the receiver TWT input. This occurs when we look at a target at minimum range and vertical incidence.

We have

$$P_r = \frac{P_t \epsilon^2 \pi^2 d^2 \sigma_o}{R^2 256} \qquad \text{(Ref. 1)}$$

Where P_r = return signal power (max.)

P_t = 20 watts = transmitted power (max.)

ϵ = 0.5 = antenna efficiency

d = 0.61 m = diameter of antenna

σ_o = 20 db = radar scattering cross section/unit area (max.)

R = 11.1 m = range (min.)

P_r = 58 mw = 17.6 dbm

The maximum power out of the I.F. preamp is -10 dbm, to avoid saturating the preamp output. The corresponding gains are preamp 23 db, and TWT 32.2 db.

Max signal into receiver TWT = -23 -10 -32.2 = -65.2 dbm,

We must attenuate the received signal by 17.6 + 65.2 = 81.8 db.
The minimum received signal is -93.2 dbm

Dynamic power range of the receiver = 93.2 - 65.2 = 28 db

The dynamic range sets the limits of received signal variation at a constant attenuator setting. The effective dynamic range will be reduced since we will wish to use finite steps of attenuation. These received signal variations are due to Rayleigh signal fading (Ref. 1) and system parameter variations. We will consider the effect of these parameters.

At angles of incidence away from the vertical we have

$$P_r = \frac{P_t \epsilon^2 \pi^2 d^2}{64 R^2 \sin \Theta} \sigma_o \quad \text{[Beam width limited mode]}$$

$$P_r = \frac{P_t \pi \epsilon^2 d^3 f \tau \sigma_o}{128 R^3 \sin \Theta} \quad \text{[Pulse length limited mode]}$$

Where P_r = return signal power
P_t = transmitted power
ϵ = antenna efficiency
d = diameter of antenna
τ = pulse length
σ_o = radar scattering cross section/unit area
f = signal frequency
Θ = angle of incidence

To obtain the scatterometry data we will operate in the beamwidth limited mode with approximately a constant range. The only frequency dependent term in the expression for the return power is the radar scattering cross-section. Since the variation of this scattering cross-section with frequency is expected to be small we can obtain a set of measurements, at a constant angle of incidence, whilst frequency is varied, without changing the R.F. attenuator setting.

For the imaging measurements we will operate in a pulse length limited mode to improve the range resolution at far range. For targets where the fading effect is great, the dynamic range may be insufficient.

It will then be necessary to make measurements over restricted frequency and range bands and to superimpose the results.

An R.F. attenuator which has steps of 5 db and a maximum of 90 db will probably be sufficient. This can be achieved using attenuators of 5, 10, 20, 40, 80 db in series combinations.

A linear IF amplifier does not allow great dynamic range. The dynamic range can be increased, by using a logarithmic IF amplifier. We would then be limited by the noise power of the receiver TWT and the maximum power that can be applied to its mixer load. It would increase the dynamic range in this case by 23 db.

4.3.2 IF Section

The maximum output of the preamp is -10 dbm while that of the post amp is 0 dbm and the post amp gain is 55 db. Under the condition of maximum signal return we must insert 45 db attenuation between the IF preamp and IF postamp. A switched IF attenuator has been purchased for this purpose.

4.3.3 Automatic Gain Control

The automatic gain control input of the amplifier can be used to change the amplifier gain with signal frequency to match the change in antenna gain with frequency. This reduces the dynamic range requirements of the post detection components.

5.0 DUPLEXING

5.1 Isolation Requirements

The arrangement of the required switches and circulator are shown in Figure 4. The specifications of the required components are given (spec. 5), (Figures 10, 11).

A_1 A_2 A_4 is the isolation of each switch in db when the switch is OFF (power reflected). A_3 is the isolation between reverse ports of the circulator.

B_1 B_2 B_4 is the insertion loss when the switch is ON (power transmitted).
B_3 is the insertion loss between forward ports of the circulator.

There are two system states:

Transmit	S_1 S_2 ON S_4 OFF
Receive	S_1 S_2 OFF S_4 ON

On transmit it is necessary to prevent the receiver from saturating.

On receive it is necessary that the power at the receiver input due to transmitter TWT noise and signal leakage be much less than the received radar return power.

We will now define the system parameters:

Transmitter TWT maximum pwer out	P_T max = 139db*
Transmitter TWT gain	G_T = 43.5 db
Transmitter TWT noise figure	N_{FT} = 35 db
Receiver TWT gain	G_R = 32.2 db
Receiver TWT noise figure	N_{FR} = 7.3 db
IF Preamplifier gain	G_{IF} = 23 db
IF Preamplifier power out	$P_{IF\ max}$ = 94 db
IF Post amplifier gain	G'_{IF} = 55 db
IF Post amplifier power out	$P'_{IF\ max}$ = 94 db

On transmit:

$$P_{IF\ max} = P_{T\ max} + G_R + G_{IF} - A_3 - A_4$$

$A_3 + A_4 = 100.2$ db

But $A_3 = 18$ db

$\therefore A_4 = 82.2$ db

But P.I.N. diode switch isolation = 2 x 38 db = 76 db

$\therefore$ We will use 10 db of fixed attenuation between the receiver TWT amplifier and the IF preamplifier.

---

* All power is referenced to the Thermal noise, KTB, where B is the receiver bandwidth = 100 MHz.

To prevent the post amplifier from saturating we must put a diode switch between the pre amplifier and post amplifier with an isolation of greater than 55 db and a switching speed of less than 20 nS.

On receive:

We will make the TWT noise and signal leakage power at the receiver TWT input 3 db above the thermal noise level.

Power due to transmitter TWT noise = $N_{TF} + G_T - A_2 - A_3$

$A_2 + A_3 = 35 + 43.5 - 3 = 75.5$ db

Power due to signal leakage = $P_{T\ max} - A_1 - A_2 - A_3$

$A_1 + A_2 + A_3 = 139 - 3 = 136$ db

5.2 Switch Power Rating

The pulse to be transmitted has a peak power to 20 w and is applied to the switch S_2 only when the switch is in the open condition. The switch S_2 must be able to pass this signal safely and without signal degradation. The limiting factor will be diode voltage breakdown, while the switch is in the open position, and average power dissipation. From the specifications of the switch we see that the maximum insertion loss with zero bias is 1.5 db. For this value the average power must not exceed 10 watts and a peak power of 80 watts.

Due to the high cost of the P.I.N. diode switches and the many possible failure modes we must find some method of protecting switch S_2 since the continuous rating is exceeded. This cannot be achieved electro-mechanically since the diode switch can fail in less than 2 μS at the applied power levels. Probably the only method available is to have separate drive circuitry for each of the switches in S_1.

5.3 Switching Time

The "cherry picker" boom system (Ref. 1) will position the antenna at a maximum height of 40 feet above the ground for a vertical incidence measurement. The signals are carried from the equipment truck to the antenna by coaxial cable. The minimum signal return time is thus 150 ns referred to the duplexing circulator.

The timing sequence is shown (Figure 5) with the delay times indicated for the chosen switches. If the switch S_2 were mounted on the boom together with the transmitter and receiver TWT's, the signal delay between switches would become important.

5.4 The Circulator

The circulator must be able to pass the maximum peak power of 20 watts and have sufficient isolation between reverse ports.

6.0 FREQUENCY CONVERSION

In order to reduce the bandwidth of the receiver it is necessary to mix the received signal with a local oscillator signal ($f_s + f_\ell$) displaced in frequency from the transmitted signal (f_s) by the chosen IF frequency (f_ℓ) this can be accomplished in three ways.

1. A double frequency conversion. (Fig. 6)
2. Using a voltage tuned filter. (Fig. 7)
3. Using quadrature hybrid phase shifters (Fig. 8)

The second method was chosen since we were unable to obtain suitable components for the other two methods. Mixers were not available with the required bandwidth on the IF port for method 1 and Quadrature hybrid phase shifters with the required isolation and defined phase shift were not available for method 3.

The specifications of the required components are given (Spec. 6). The specifications of the mixer are not at the required power levels. We must therefore estimate the conversion loss and isolation.

We will examine the signal levels in the frequency conversion system:

Leveled signal from PIN modulator	= 15 mW
LO power required	= 100 mW (estimate)
Conversion loss	= -10 db (estimate)
Power in each side band	= 1.5 mW
YIG insertion loss	= 5 db
Isolator insertion loss	= 0.4 db
Effective directional coupler insertion loss	= 1.2 db
Sideband power output	= 0.33 mW

The IF amplifier mixer combination requires a local oscillator power of greater than 0.25 mW.

7.0 LEVELING

Two closed leveling loops are included in the system, the first to level the transmitted power and the second to level the frequency converter output. The method of leveling is shown (Figure 9, Ref. 4). One of the required amplifiers is included in the sweep frequency oscillator; the other was purchased separately (Reference 5).

System Power Requirements

Motor Generator Output	15,000 watts
Sweep Oscillator	350 watts
TWT Receiver	8.5 watts
TWT Transmitter	644 watts
D.C. Power Supplies	300 watts
Oscilloscope (585)	550 watts
Sampling Oscilloscope	500 watts
Leveler Amplifier	2 watts
Signal Generator	9 watts
Tape Punch	138 watts
Digital Volt Meter	30 watts
Antenna Positioner	1,300 watts
Total Load	4,031 watts

BIBLIOGRAPHY

1. Antenna and Output power considerations for the polypanchromatic radar system - W. F. Waite, CRES Technical Memorandum 133-1-1.

2. A digital system to control sampling measurements - for a polypanchromatic radar - 1 Dinstein, CRES Technical Memorandum 133-1-3.

3. Method of signal sampling for the polypanchromatic radar system - to be published, CRES Technical Memorandum 133-1-4.

Index to Figures

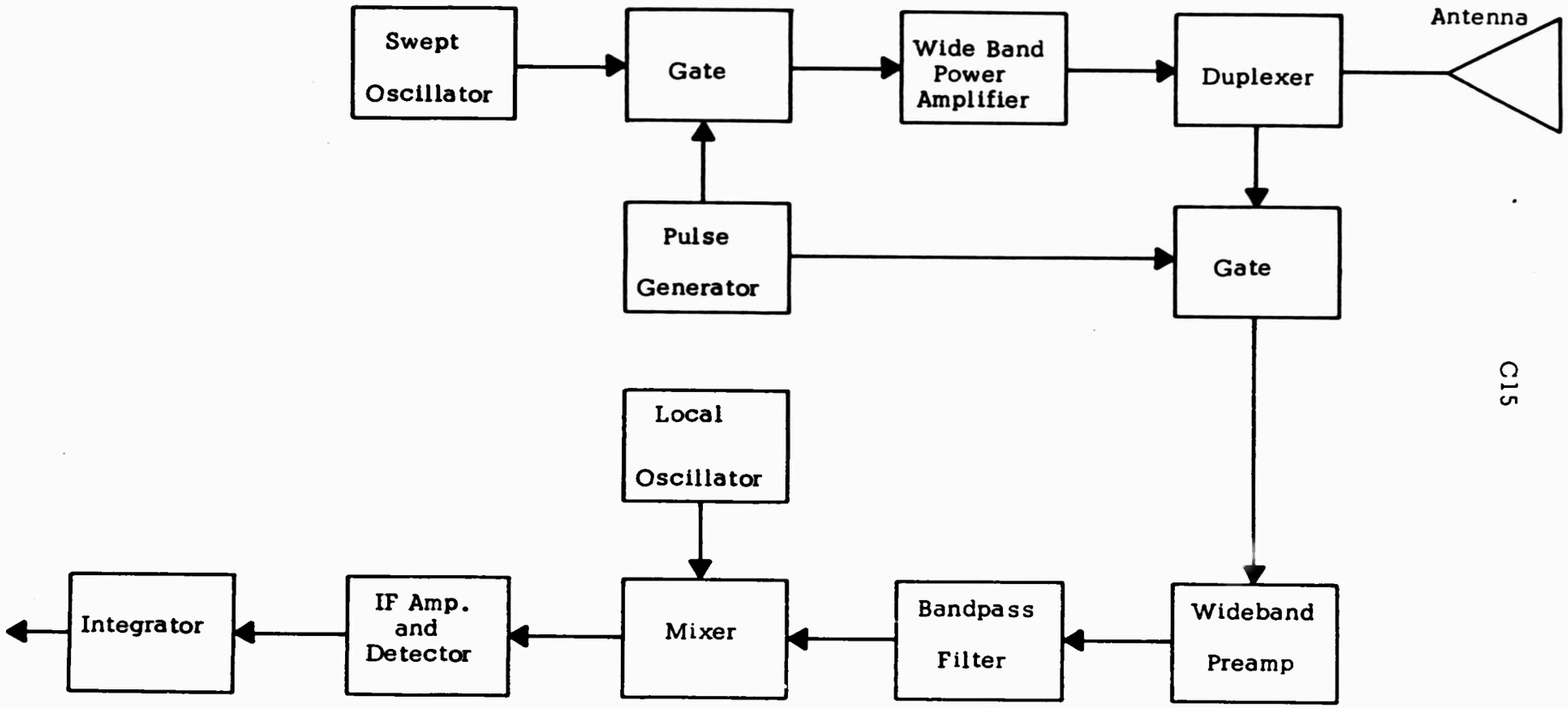

C15

Figure 1. Slow-Sweep System Block Diagram

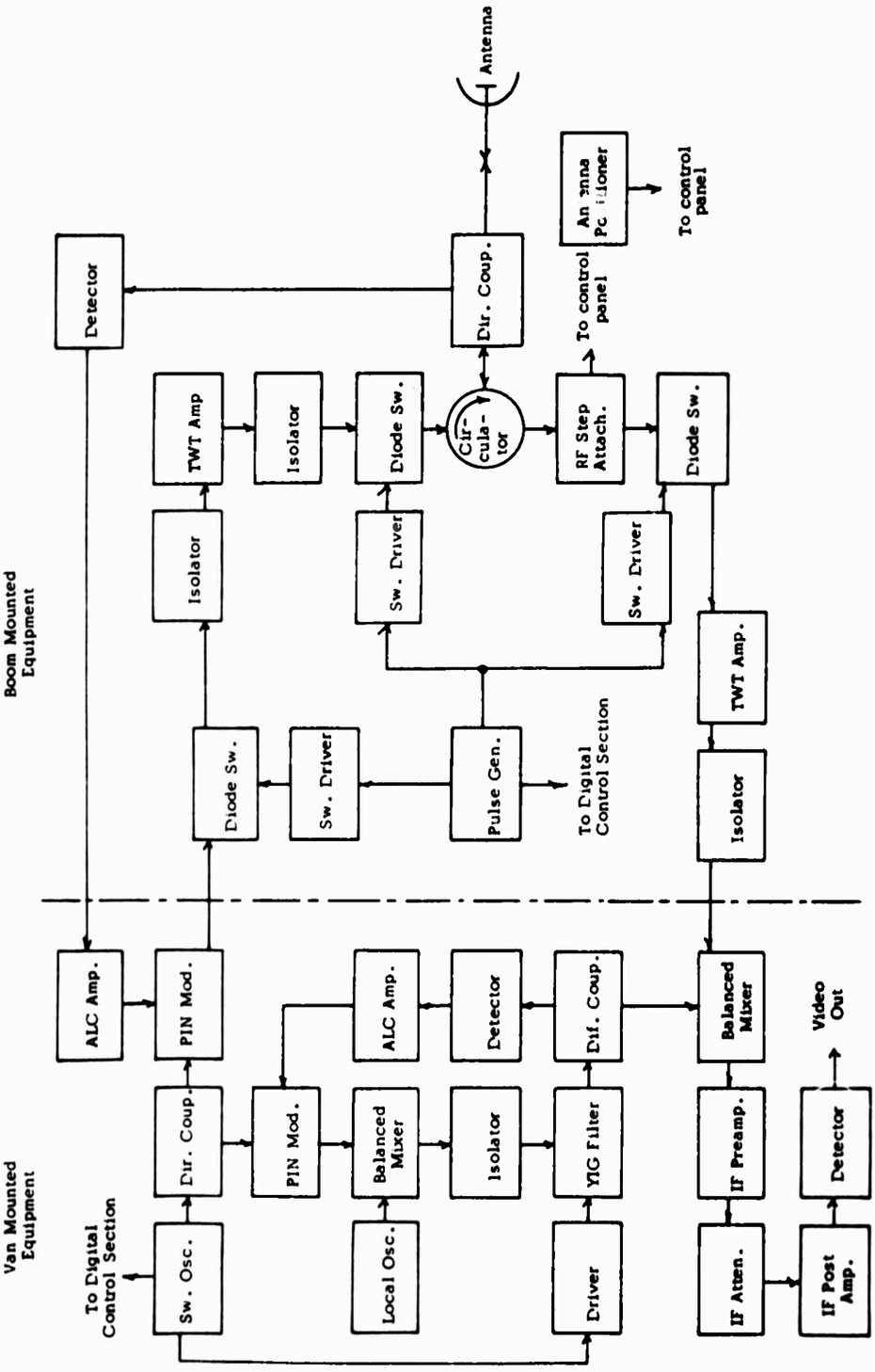

FIGURE 2

POLYPANCHROMATIC RADAR - RF SECTION BLOCK DIAGRAM

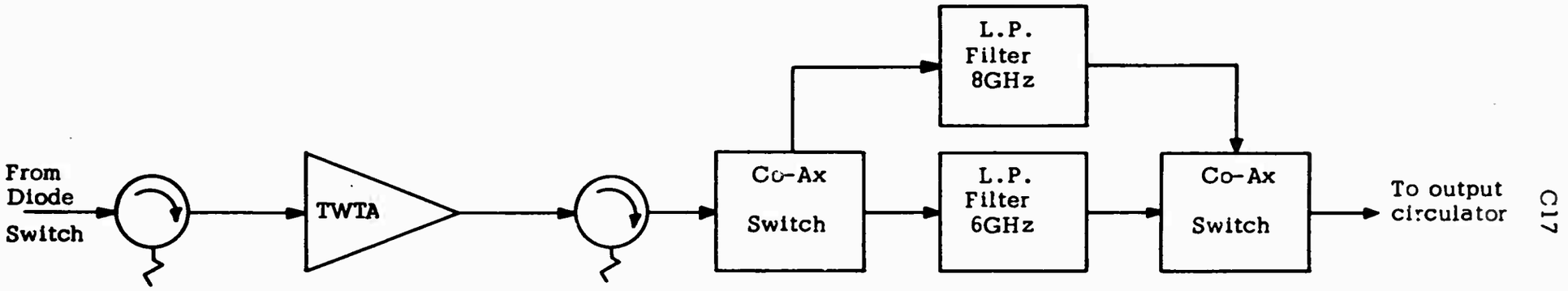
From
Diode
Switch
TWTA
Co-Ax
Switch
L.P.
Filter
8GHz
L.P.
Filter
6GHz
Co-Ax
Switch
To output
circulator

Figure 3.

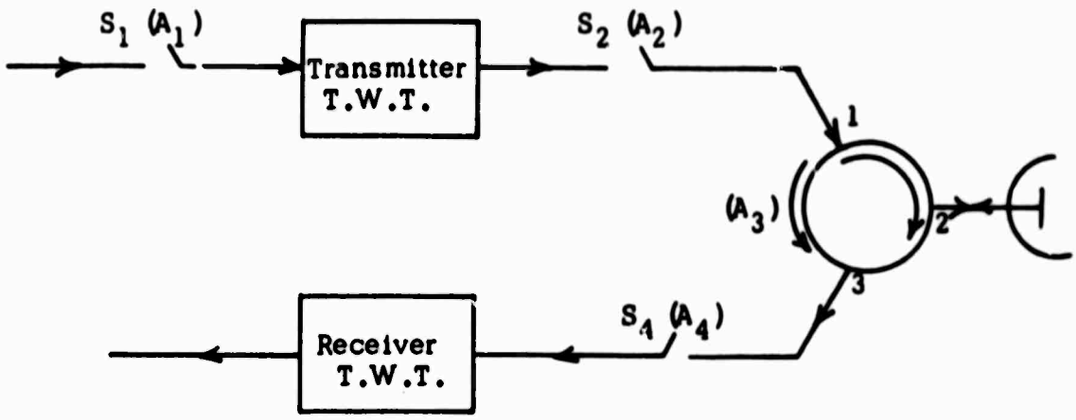

Figure 4. R.F. Switch Arrangement

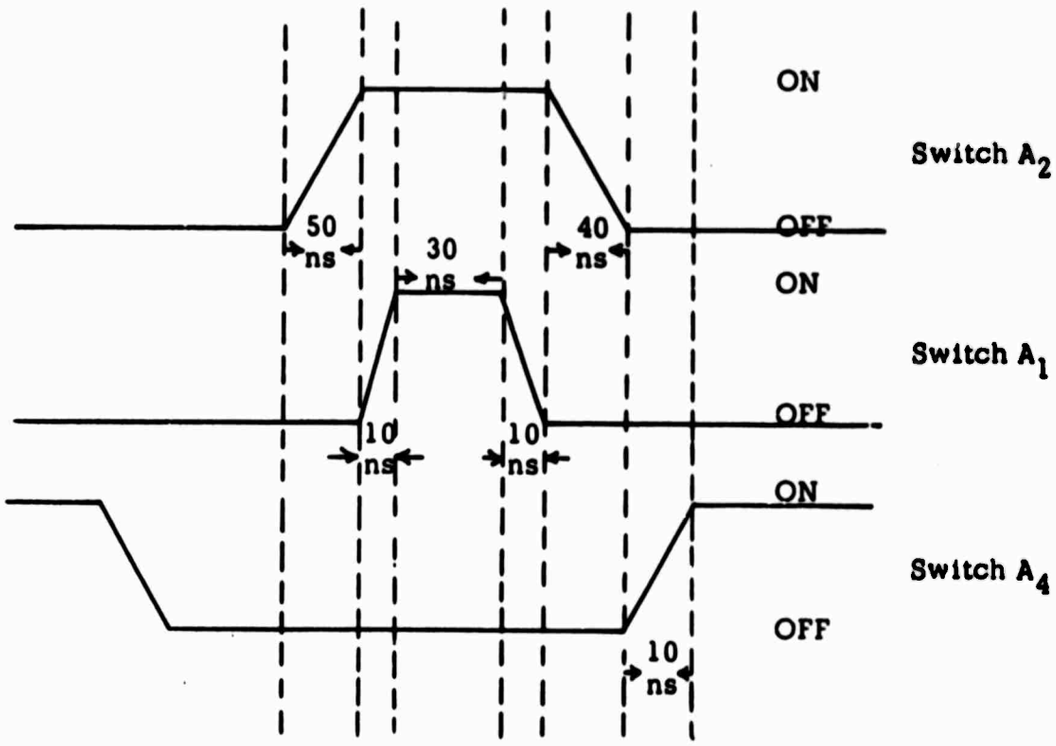

Figure 5. R.F. Switching Sequence

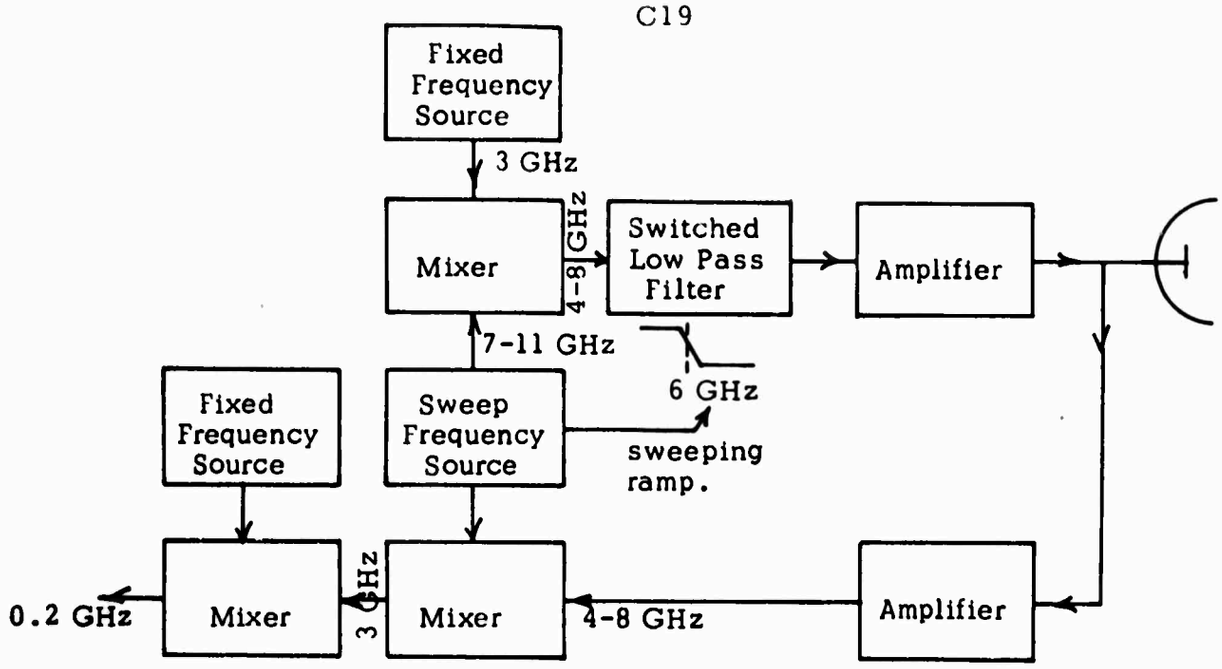

a. 1st IF Below Band

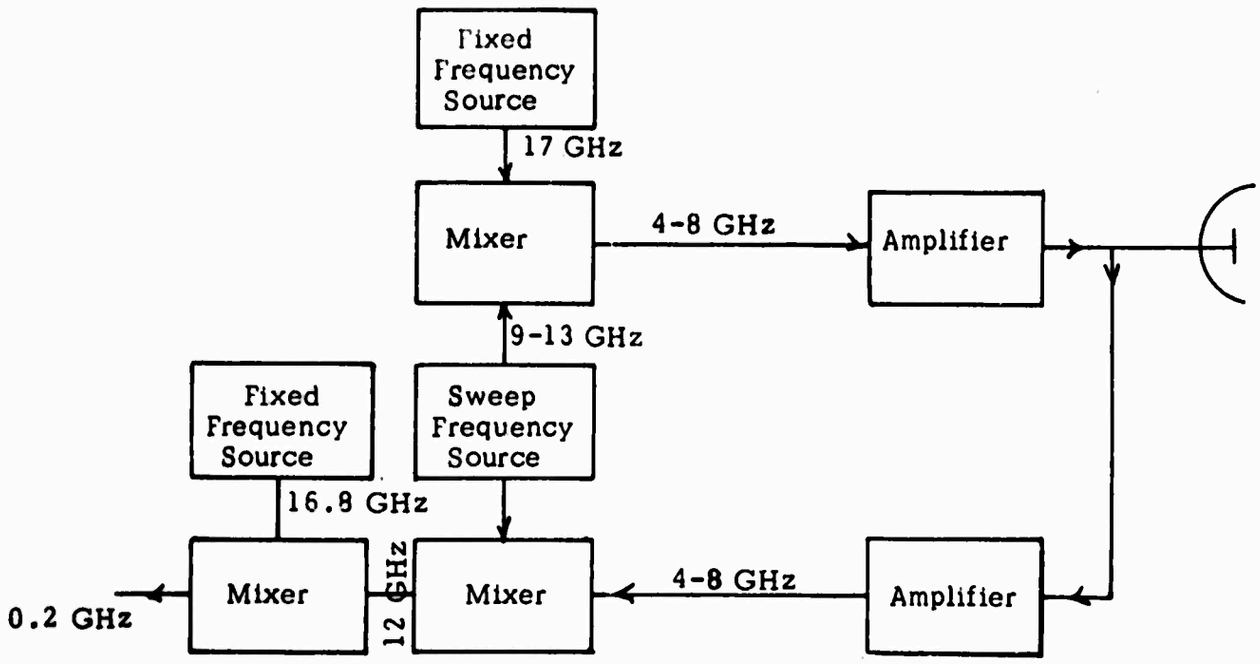

b. 1st IF Above Band

Figure 6. Frequency Conversion by 2-Stage Mixing

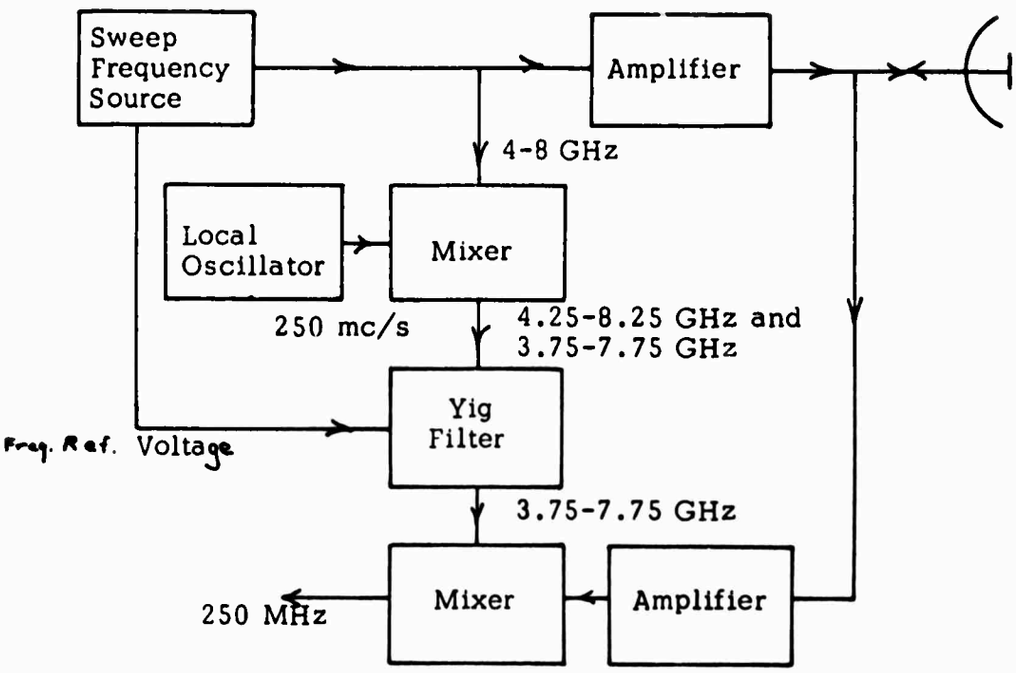

Figure 7. Frequency Conversion Using Voltage Tuned Filter

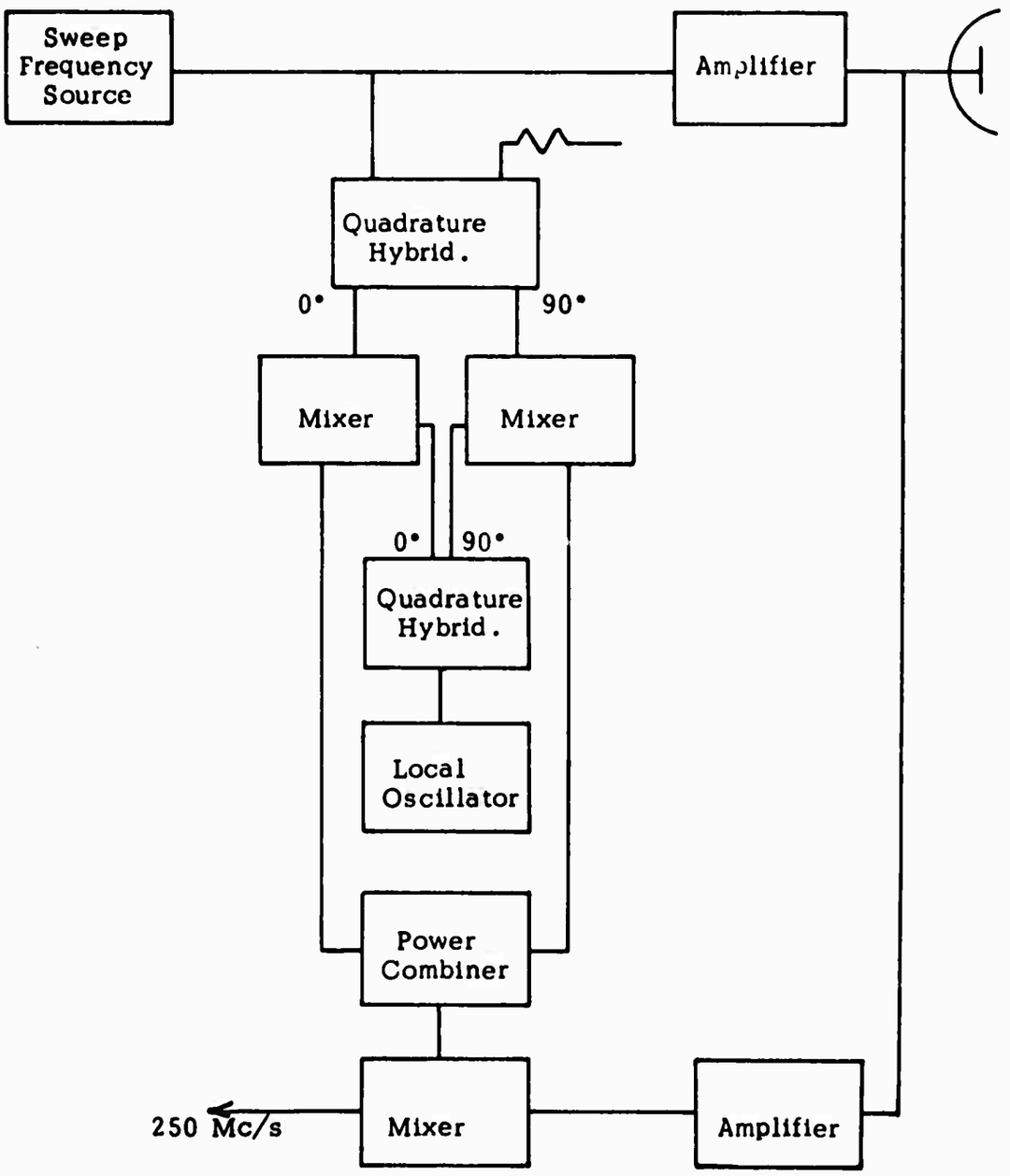

Figure 8. Frequency Conversion Using Quadrature Hybrid Phase Shifter

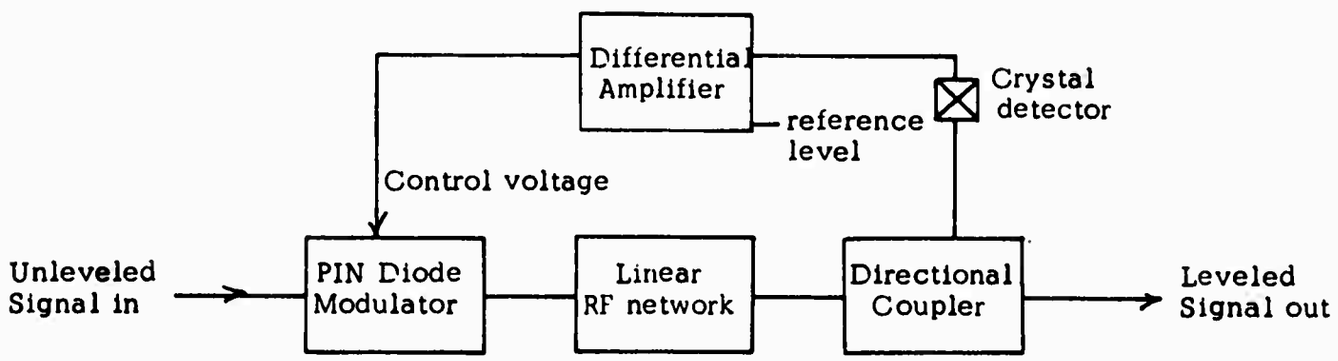
Differential Amplifier
Crystal detector
reference level
Control voltage
Unleveled Signal in
PIN Diode Modulator
Linear RF network
Directional Coupler
Leveled Signal out

Figure 9

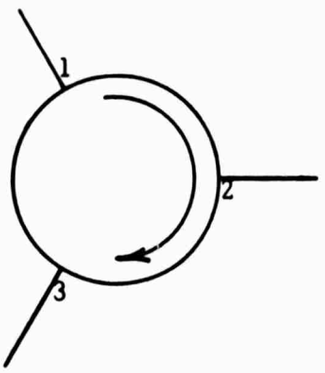

Circulator Schematic

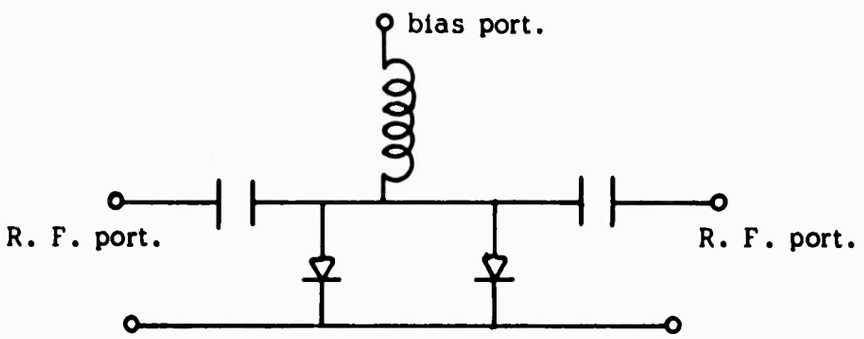

Diode Switch 3570 Schematic

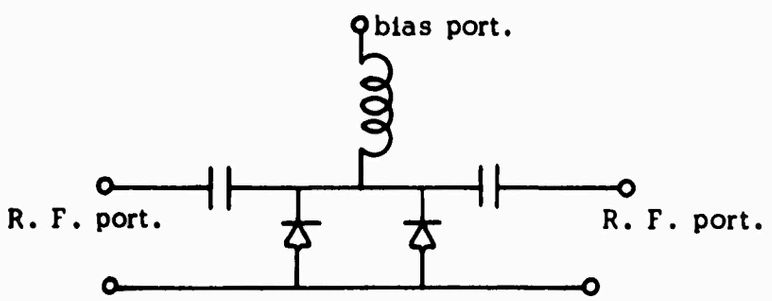

Diode Switch 3603 Schematic

Figure 10

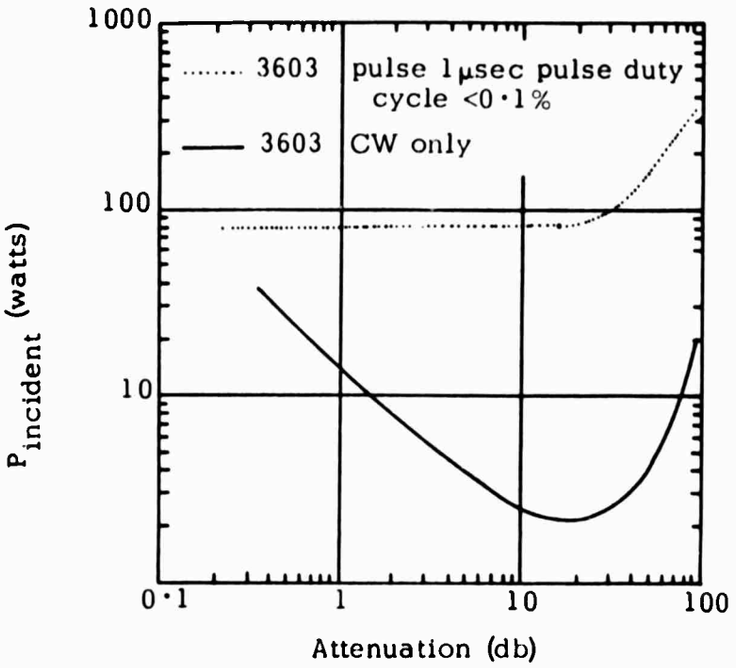

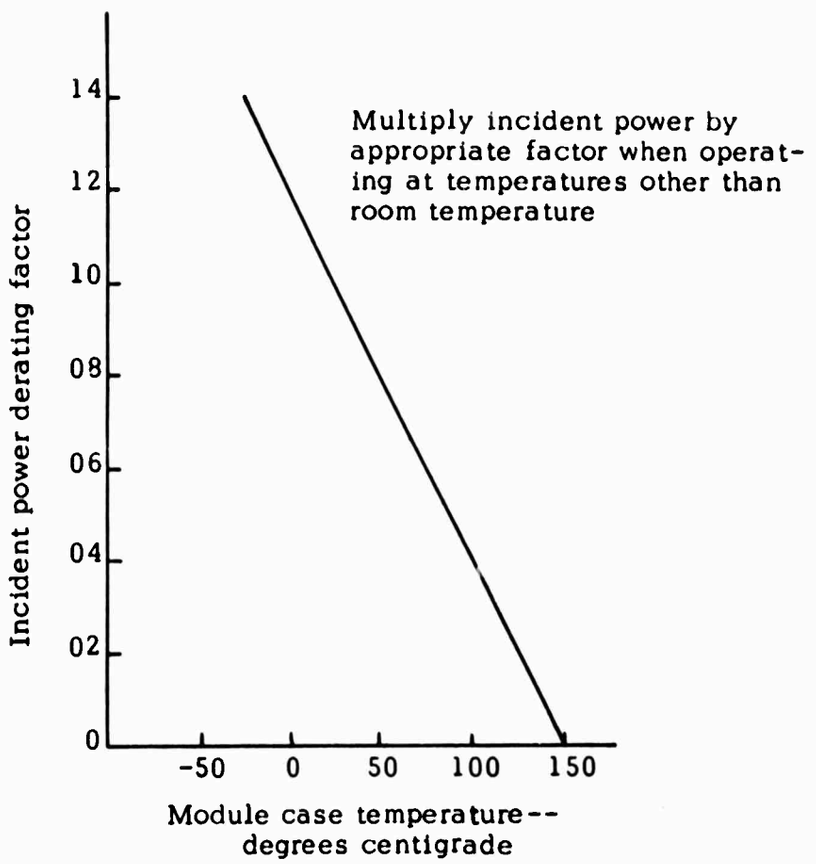

Figure 11. Incident Power Rating at 25°C for 3603 at 4-8 GHz

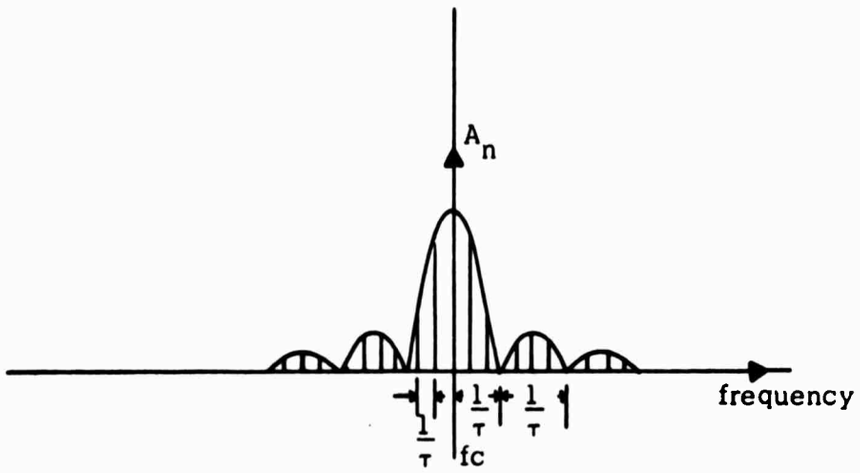

Frequency domain amplitude spectrum of a pulse-modulated carrier

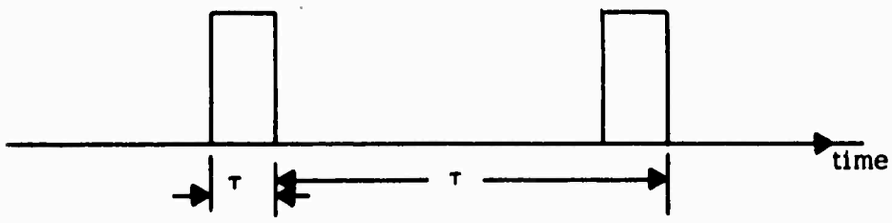

Time domain. Envelope of pulse-modulated carrier

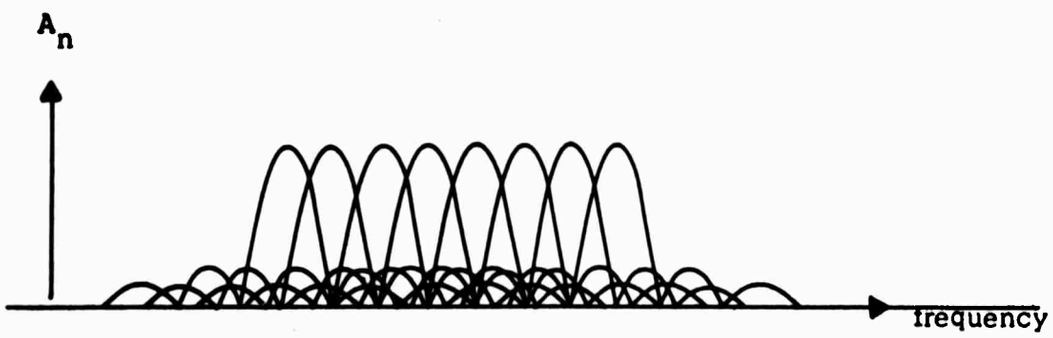

Overlapping spectrum due to slow change of carrier frequency

Figure 12

Index to Specifications of Components

SPECIFICATION 1

Transmitter T.W.T. Amplifier
Manufacturer -- Alto Scientific Co., Inc.
Type -- 20C 4.0 - 8.0 Q 60
Frequency -- 4.0-8.0 GHz
Small Signal Gain -- 60 db
Noise Figure -- 30 db nom. 35 db max.
Max. R.F. input -- 1 watt

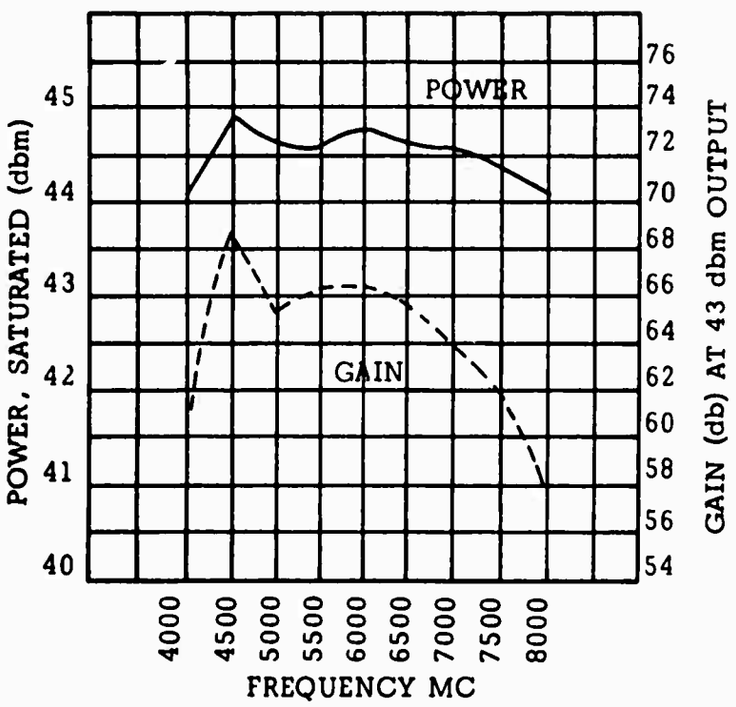

Reference. Alto Scientific Instruction Manual -- Alto Scientific Engineering Note 5-66.

SPECIFICATION 2

Sweep Frequency Oscillator

Manufacturer -- Hewlett Packard

Model -- 8690A sweep oscillator

8693B RF unit

Frequency Range -- Adjustable from 4-8 GHz (manual or internal sweep)

Frequency Accuracy -- $\pm$ 20 MHz

Leveled Power Output -- 15 mW

Sweeptime Adjustable in 4 decades 0.01 to 100 secs.

Associated Outputs -- Sweep Output

Sweep reference output

Blanking

Market

Leveling Amp. Input -- -20 to -350 mV

Reference. Hewlett Packard Manual 8690A, 8693B.

C29

WATKINS JOHNSON COMPANY

SPECIFICATION 3

FINAL DATA SHEET

LOW-NOISE TWT AMPLIFIER

The data as recorded below is the result of tests performed by our test department just prior to shipment of this tube, and is provided as a special service to our customers.

Tube Type WJ- 423 Serial No. 5

SUPERSEDES ALL PREVIOUS DATA

Frequency (GHz)	VSWR Maximum		Small Signal Gain (dB)	Noise Figure (dB) *	Saturation Power Output (dBm)
	Input	Output			
4.0			31.8	7.3	+15.0
4.4			34.3	6.8	+15.7
4.8			34.8	6.7	+15.8
5.2			34.8	6.5	+15.8
5.6	1	1	34.6	6.3	+15.7
6.0	..	..	34.2	6.0	+15.1
6.4	0	0	33.5	6.1	+14.7
6.8	.	.	33.4	6.2	+14.4
7.2	2	2	32.4	6.6	+13.4
7.6	^	^	32.3	6.9	+13.4
8.0			32.2	7.3	+12.9

*N.F. measured with H.P. noise sources G347A and J347A and H.P. noise figure meter model 340B.

Tube Requirements

Input Voltage: 105-125 V ac

Input Current: 165 mA

Input Power: 8.5 Watts

Tested by: M. Slaughter Date: 21 March 1968

3333 Hillview Avenue Stanford Industrial Park Palo Alto, California

SPECIFICATION 4

IF Amplifier

Manufacturer -- R.H.G. Labs
Model No. Preamp. MP 4-8m37, Post Amp. EBT106MGC
RF Frequency -- 4-8 GHz
IF Frequency -- 250 MHz
IF Bandwidth -- 100 MHz
Power Gain Preamp. (RF to IF) 23 db, Postamp. 55 db
Noise Power -- 4 db (at 0.25 mW LO)
Maximum Output Preamp. 10 dbm, Postamp. 0 dbm

Reference. RHG Electrical Test Data Form MP1 and Form EVT1

SPECIFICATIONS 5

Duplexing Components (Figure 10)

Circulator (Test Data Supplied)

Manufacturer -- Melabs. Model 6317-264
Frequency -- 4-8 GHz
Insertion loss port 1-2 -- 0.36 db max.
1-3 -- 19.0 db max.

Switch S_1 S_4 (Two each in series)

Manufacturer -- Hewlett Packard
Model PIN Diode Switch 3570
Frequency -- 4-8 GHz
Insertion loss -- 1.5 db max. at -20v bias
Isolation -- 38 db min. at 100 mA bias
VSWR -- 2.5:1 max. at -20v bias
Max. RF power -- 1 watt at 25° C.
Maximum bias current -- 100 mA
Maximum bias voltage -- -36v
Switching speed -- RF ON 15 nS max. 9 nS typ.
RF OFF 10 nS max. 6 nS typ.
Switching speeds are measured over a range of 10 db detected power (OFF) to 0.45 db detected RF power (ON)

Switch S_2

Manufacturer -- Hewlett Packard
Model PIN diode switch C00433603A
Frequency -- 4-8 GHz
Insertion loss -- 1.5 db max. 0v bias
Isolation -- 60 db min. -150 mA bias
VSWR -- 2.0:1 max. at 0v bias

SPECIFICATION 5 CONT'D.

Max. RF power -- see Figure 11
Max. forward bias -- -675 mA
Max. reverse bias -- -100 v
Switching speed -- RF ON 50 nS max.
RF OFF 40 nS max.

SPECIFICATION 6

Frequency Conversion Component

Mixer

Manufacturer -- Sage
Model 2543 NOCM
Frequency -- 4-8 GHz
IF -- 200 MHz
Isolation -- 8 db min.
Conversion loss - 7.5 db min. (Sig. -20 dbm L.O. 3 dbm)

Local Oscillator

Manufacturer -- Frequency Sources
Frequency -- 250 MHz (Mechanical adj.)
Power -- 200 mW (Min.)

Yig Filter

Manufacturer -- Watkins Johnson
Model -- 617-8 Four Stage Yig Filter
922-4 Voltage to Current Driver, 250 MHz
Frequency -- 4.25-8.25 GHz
Bandwidth -- 45-80 GHz
Tuning Voltage -- 0-10 v.
Insertion Loss -- 5 db max.
Off resonance isolation -- 70 db min.
Off resonance spurious -- 50 db min.
Passband ripple -- 1.0 db
Passband ripple spurious -- 1.5 db (max.)
Passband VSWR -- 2:0 (max.)
Limiting level -- 10 dbm min.
Hysteresis -- 2- MHz
Deviation from linear -- $\pm$ 8 MHz max.

SPECIFICATION 6 CONT'D.

Frequency Deviation -- 10 GHz (0° C to 60° C)
Frequency Selectivity -- 24 MHz/octave (of bandwidth)

BLANK PAGE

Appendix D

A DIGITAL SYSTEM TO CONTROL SAMPLING MEASUREMENTS FOR A POLYPANCHROMATIC RADAR

Its'hak Dinstein

Technical Memorandum 133-1-3

A DIGITAL SYSTEM TO CONTROL SAMPLING MEASUREMENTS FOR A POLYPANCHROMATIC RADAR

by

Its'hak Dinstein

The digital control system is designed to control the time sampling in the frequency domain of reflected pulses in a wide bandwidth radar system. The memorandum is written in a general way and is almost independent of the radar system. The block diagram of the whole system is given here briefly.

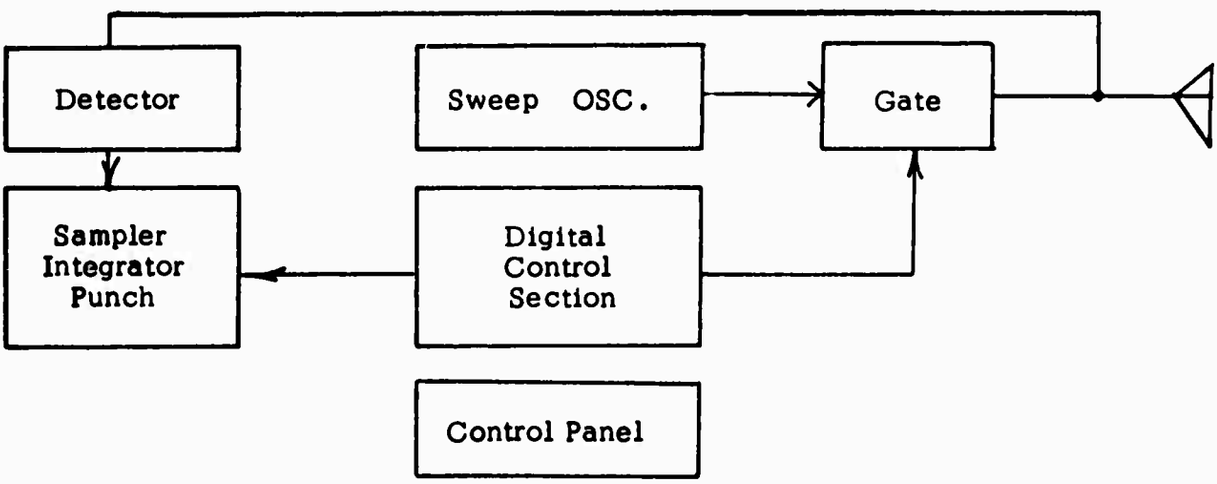

The Digital Control Unit will be operated with -5 Volts, (V_{cc} of the TTL's connected to ground and ground of the TTL's connected to -5 Volts) in order to be compatible to signals to and from the sweep OSC.

The format of this memorandum is that of a step-by-step procedure. This seems to describe the logical and switching nature of this system better than the more usual narrative description.

THE PROBLEM

1.1 Given a periodic function of time f(t) (See Figure 1)

1.2 Divide the period τ_0 into 1000 increments.

1.3 To be able to choose any time interval t_1 to t_2 so that $t_2 - t_1 = \tau_1$, and to produce an output signal during this time.

1.4 To repeat this output signal during the time $t_1 + \tau$ to $t_2 + \tau$ (see Figure 1) and again during the time $t_1 + 2\tau$ to $t_2 + 2\tau$, and so on n times till the time $t_2 + (n - 1)\tau$.

1.5 Then starting again from t_0, to choose another interval t_3 to t_4 so that $t_4 - t_3 = \tau_1$ and $t_3 - t_1 = \tau_2$ (see Figure 1) , and to produce an output signal during this time interval.

1.6 To repeat this output signal during the time $t_3 +$ - to $t_4 + \tau$ and so on n times till the time $t_4 + (n - 1)\tau$

1.7 To repeat this procedure till m intervals are covered.

THEORY OF OPERATION

2.1 An internal clock produces a time base. The frequency of the clock is adjusted to be $\frac{1000}{\tau_0}$ (Figure 1)

2.2 The unit of time is equal to $\frac{\tau_0}{1000}$.

2.3 The timing is controlled by 5 counters:

1) Start Counter (STR. CNT)
2) Bandwidth Counter (BND. CNT)
3) Repetitions Counter (REP. CNT)
4) Spacing counter (SPC. CNT)
5) Number of Bands Counter (NMB. CNT)

Each counter consists of 3 decimal digits. The counters can be preset to any number defined by the DIGISWITCHES (Figure 2)

2.4 The beginning of the first interval of time is defined by the START COUNTER. The STR. CNT is preset to the complement number of t_1 (Figure 1). Therefore, the counter will be full after counting t_1 pulses. When the STR. CNT starts to count at t_0, it reaches t_1 when it is full.

2.5 The length of the time interval is defined by the BANDWIDTH COUNTER. The BND. CNT is preset to the complement number of τ_1. (Figure 1) . The counter will be full after counting τ_1 pulses. The BND. CNT starts its counting when the STR. CNT starts its counting when the STR. CNT is full, therefore it will be full at t_2.

2.6 The number n (see sec. 1.4) is defined by the REPETITION COUNTER. The REP. CNT is preset to the complement of n, and is advanced by one after every interval of time. When the REP CNT is full, the system begins to cover the next interval.

2.7 The beginning of the next interval is defined by the SPACING COUNTER and by the START COUNTER. When moving to the K^{th} interval, the SPC. CNT will count $(K - 1) \times \tau_2$ pulses, and when it will be full, the STR. CNT will count t_1 pulses. The beginning of the K^{th} interval is at $t = t_1 + (K - 1) \times \tau_2$.

2.8 The sequency is finished when the NUMBER OF BANDS COUNTER is full. The NMB. CNT is preset to the complement number of m (see Sec. 1.7). The counter is advanced by one when the system is moving from one interval to the next.

OPERATION

3.1 Calibration

3.1.1 The CALIBRATION COUNTER (CLB. CNT) starts counting at t_0, triggered by an external start marker.

3.1.2 When the CLB. CNT counts 999 pulses this state is decoded and then the D input of FF 10 (see the overall scheme) is going high. If the external end marker of τ_0 (Figure 1) comes between the 999^{th} pulse and the 1000 pulse, the clock is calibrated and the calibration lamp will be on.

3.1.3 If the CLB. CNT is full before τ_0, FF 11 will be triggered and the overflow lamp will be on. It indicates that the frequency of the clock should be decreased.

3.1.4 When the clock is calibrated, the CAL lamp is on and the overflow lamp is off.

3.2 The RUN MODE (see overall scheme)

3.2.1 All the Digiswitches have to be adjusted to the proper numbers. The system has to be reset and then preset.

3.2.2 The given function (Figure 1 is produced by the sweep OSC. The sweep OSC has to be triggered manually, to start the sequence.

3.2.3 When the sweep begins, FF 1 is triggered to on and then:
a) The STR. CNT begins to count α-pulses (through gate 6)
b) FF 3 is reset.

3.2.4 When the STR. CNT is full, it triggers FF 7 and gate 19 is opened. then:
a) The SAMPLER and the RF UNIT DRIVERS are triggered by α pulses (this is the output signal).
b) The BND. CNT is not counting α pulses (through gate 19)

3.2.5 When the BND. CNT is full, it triggers FF 8, and gate 19 is closed.

3.2.6 When the sweep comes to its end:
a) FF 7 and FF 8 are reset by β pulses (through gate 3 and gate 8).
b) The STR. CNT and BND. CNT are preset by the β-pulses.
c) The REP. CNT is triggered (through gate 3) and it is advanced by one.

3.2.7 If the REP. CNT is not full, the sweep OSC is triggering itself (by the blanking pulse through gate 1) and the procedure repeats again.

3.2.8 When the REP. CNT is full, then:
a) It triggers the monostable, and gate 1 is closed and the sweep OSC is not triggered by itself.
b) An output signal from the monostable indicates that the system is moving to the next interval.
c) FF 2 is triggered by the REP. CNT, gate 7 is opened, the number of SPACES CNT preset by β-pulses and the NMB. CNT is advanced by one by β pulse (through gate 7).

3.2.9 When the monostable returns to its stable state it triggers the sweep OSC.

3.2.10 The comparator is now not equal, because the number of SPACES CNT was preset and the NMB. CNT was advanced by one. Therefore, gate 5 is now open and the SPC. CNT is counting α pulses.

3.2.11 When the SPC. CNT is full:

a) It advances the number of SPACES CNT by one

b) It triggers FF 4, then the β pulses preset the SPC. CNT and the next α pulses reset FF 4.

3.2.12 The comparator is now equal and therefore gate 5 is closed and gate 6 is opened.

3.2.13 The STR. CNT counts α-pulses and the procedure continues as before.

3.2.14 When the NMB. CNT is full, the sequence is completed, FF 9 is on, gate 19 is closed and there is no more output signal.

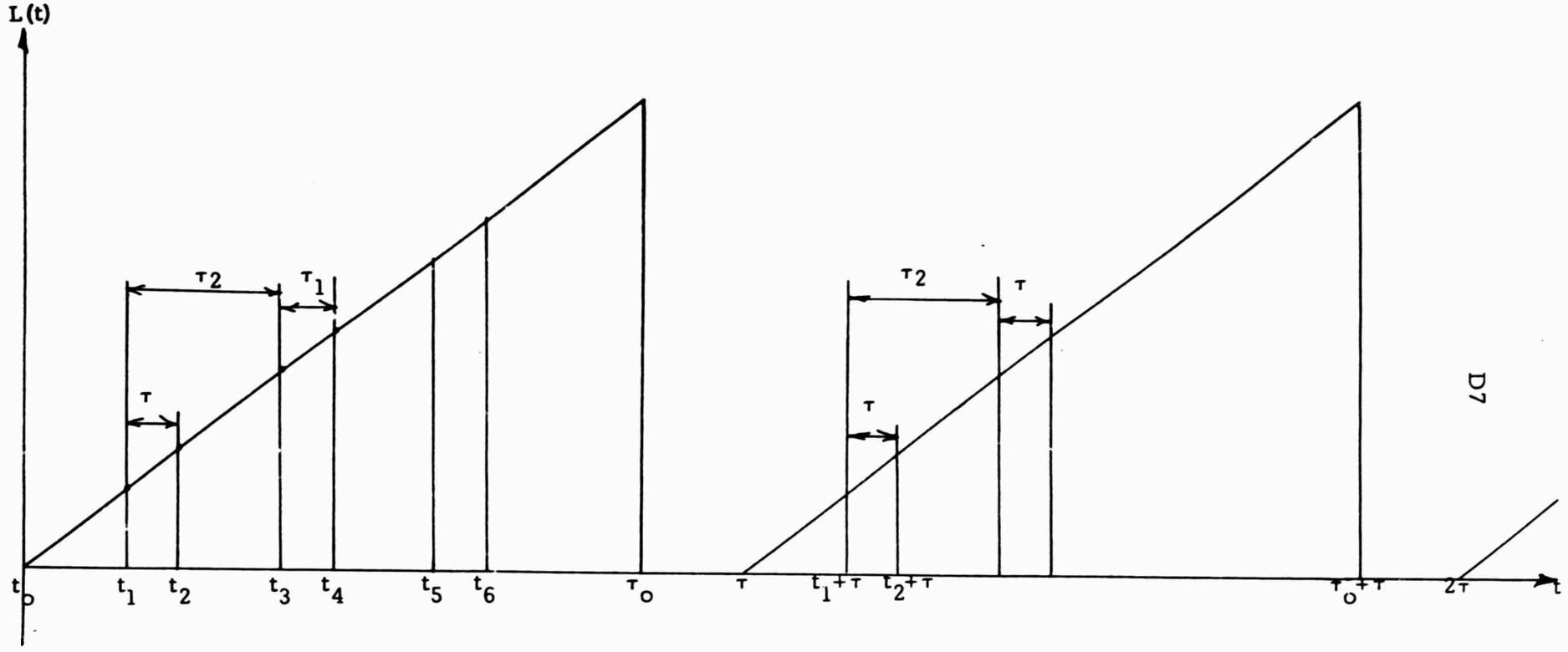

Figure 1

DECADE COUNTER

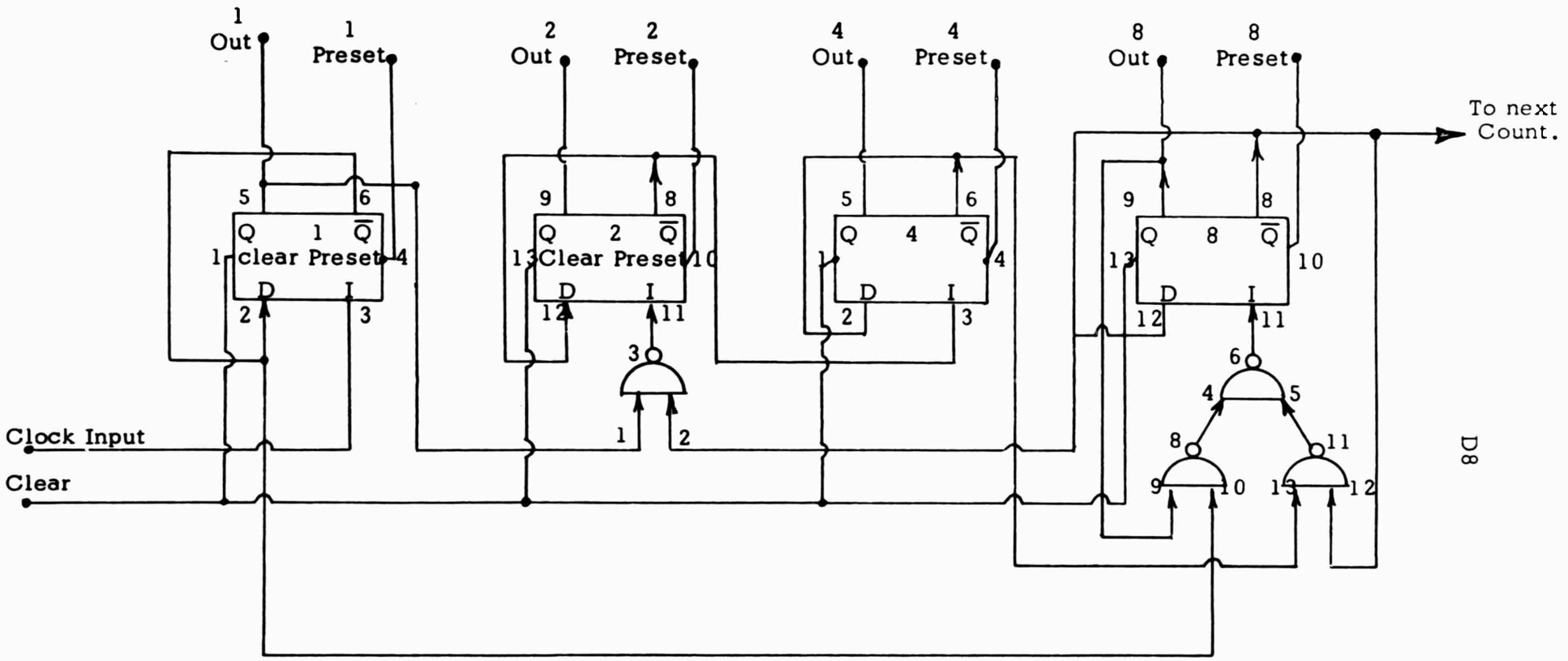

The Flip Flops SN 7474N Dual D Type

The gates SN 7400 Quadruple 2 Inputs Positive Gate

Figure 2

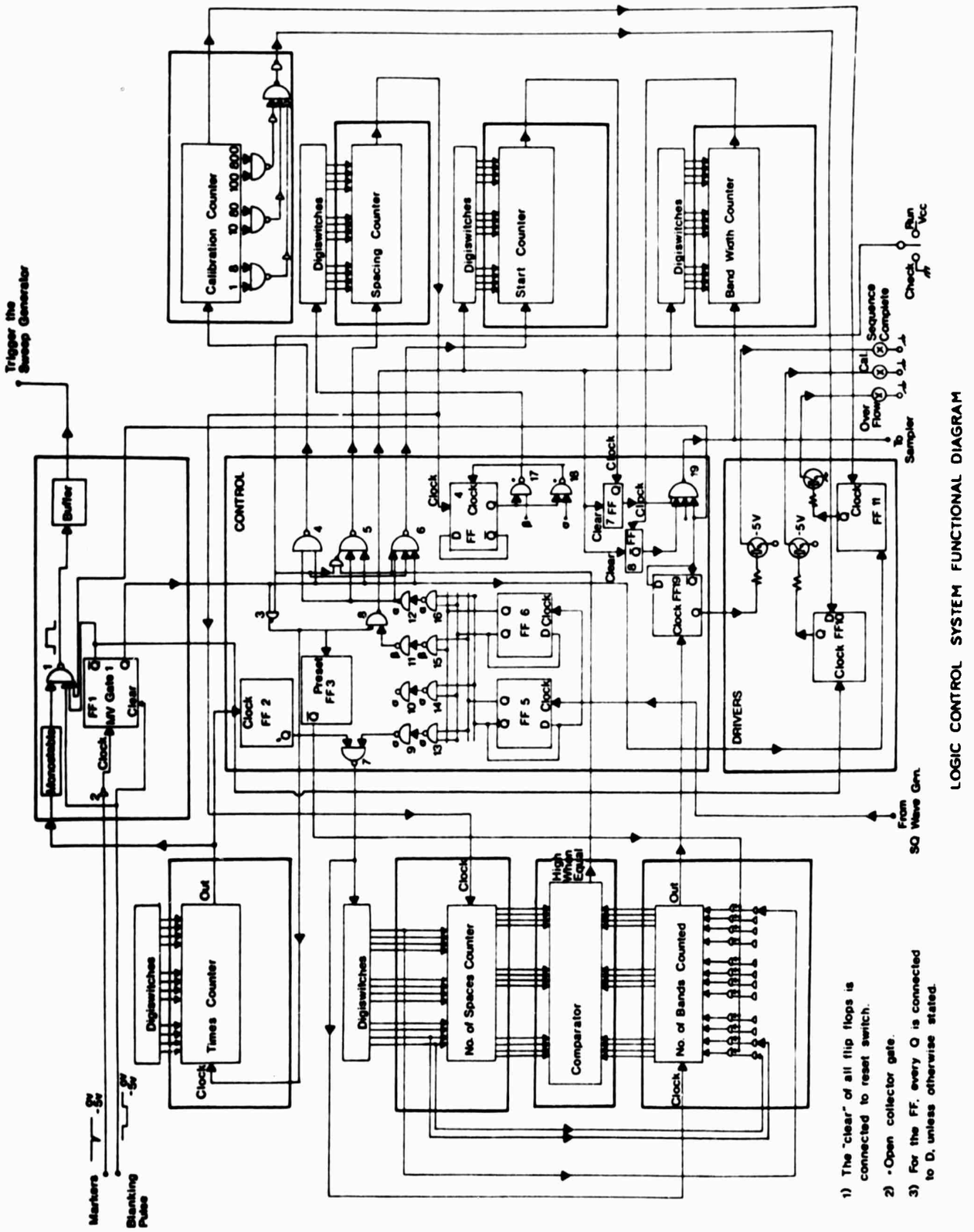

LOGIC CONTROL SYSTEM FUNCTIONAL DIAGRAM

Figure 3

Appendix E

MULTIPLE IMAGE CLASSIFICATION WITH SPATIAL AND MEASUREMENT SPACE CLUSTERING

R. M. Haralick

Technical Memorandum 133-6

MULTIPLE IMAGE CLASSIFICATION WITH SPATIAL AND MEASUREMENT SPACE CLUSTERING

R. M. Haralick
Remote Sensing Laboratory
Center for Research in Engineering Science
University of Kansas
Lawrence, Kansas 66044

We have done work in texture analysis, adaptive clustering, and spatial clustering. We have also implemented various optimizing, statistical and Bayes decision theory techniques for the computer. Included in this report is a preliminary description of this research. Detailed technical reports will be forthcoming for each area. The spatial clustering report will be out shortly and it is not discussed here.

Basic research in texture analysis (as part of the color combination and texture study of multiple images) was undertaken because we feel that the local spatial structure of the image densities has much information about its classification. This has been further illustrated with our spatial clustering results. On a test set of three images, the classification obtained using spatial clustering had about half the errors which the classification using measurement space clustering had.

The adaptive clustering technique which was briefly described in the study plan was programmed. Difficulty was found in getting the procedure to converge for arbitrary starting points. If the starting point was sufficiently close to a solution then the procedure worked fine. Attempts are now being made to simplify the algorithm by breaking it up into parts which work independently. In this manner each part can converge without upsetting the other parts. We are testing various measures of similarity to find the one which works best.

We are also investigating the possibility of combining the adaptive techniques with standard optimizing procedures. In this vein we

have written gradient search, dynamic allocation, generalized matrix inverse, matrix inverse accuracy increaser, and eignvector-eigenvalue routines. We have continued our work with Bayes theory, updating our Bayes program to include many general options. A brief description of both Bayes theory and the programs which can be used in optimizing procedures are included.

COLOR COMBINATION AND TEXTURE STUDY OF MULTIPLE IMAGES

The intent of this task was to examine color and texture combinations of imagery during the summer of 1968. However, it became apparent, in our discussions with the visual perception psychologist Dr. Epstein, that if we wanted to study both color and texture together, we would first have to study texture in black and white. Much more is known about color than about texture, and since we eventually want to perform a factorial experiment involving both color and texture we must be equally knowledgeable about both. Our first goal was to create a set of abstract textures with different texture gradients in order to determine where subjects would perceive the most convincing edge or boundary. With this information we hoped to be able to create, by superposition, multiple texture images which were simple textural-map representations of actual radar imagery.

Our first problem was to decide whether dots, lines, or other various geometric figures should be the basic pattern in the texture. We decided upon short lines because groups of scattered short lines had least similarity to common textured objects: other texture patterns such as various types of checkerboard patterns could easily be perceived as a wall, floor or receeding surface; it was this kind of identification which we wished to avoid. In addition, textured patterns of lines are easy to generate on the plotter available at the KU Computation Center.

The principal goal was to produce a continuum of computer generated textures which, as a function of known parameters, range from those suggesting a uniform flat surface to those strongly suggesting two

surfaces meeting at a boundary, thus forming an edge. Two different approaches have been tried: one using a simple geometric projection model to determine the distribution gradients, and the other using a set of gradients, resulting from no single model, but empirically showing the desired visual effect.

Boundaries are caused by an abrupt change of texture gradients. An edge is produced by introducing a discontinuity of the gradient of the line length and line position distributions. Visual displays were made by joining two gradients in one texture pattern. At the edge (where the gradients interfaced) the distributions were continuous, so that only the change in gradients could be observed. The two texture patterns used were as follows:

The first texture pattern was produced by simulating the image on the retina occuring when a person sees a receeding surface met by a wall. One gradient was the null gradient, that is, the distributions of length and position were uniform. The second gradient was that of a non-vertical plane surface. To determine the resultant distribution on the retina image it was necessary only to compute the projection of a uniform distribution on a plane onto a spherical surface.

The second set of texture patterns was constructed arbitrarily using "reasonable" analytic gradients. The functions are of the form

$$f(y) = c(1-b)^{m/2}$$

where c is a constant

b is a uniformly distributed random variable over (-.5, +.5)

An extensive search of the psycho-physical literature was undertaken to determine what was the best experimental methodology. Under consideration were the following methods: paired comparison, multiple comparison, rank order and absolute value. In the paired comparison methods, two texture gradients at a time are presented to each subject, and the subject must choose which one has the most convincing edge. In the multiple comparison method three or more texture gradients are presented at one time, and the subject must choose which one has the

most convincing edge. In the rank order method, all the texture gradients are presented at one time and the subject must order the gradients from the one with the most convincing edge to the least convincing edge. In the absolute value method, the subject is presented with one texture gradient at a time, and he must assign some integer between 0 and 12 for each one; 12 indicates no edge and 0 indicates an absolutely sharp edge.

The absolute value method was chosen because it allows an average numerical quantity to be calculated for each texture gradient; from the numerical quantity the gradients cannot only be rank ordered but the distance from one gradient to the next may be estimated. The other methods assume nothing and only allow a rank ordering to be made. The disadvantage of the absolute value method is that it assumes the subject will unconsciously use a ratio scale to assign numbers (the number assigned to a texture gradient which has an edge twice as convincing as another, will be assigned a number which is twice as great as the other).

The computer programs were written to generate the texture gradients. Difficulty, however, was experienced in plotting the lines. The plotter was broken for days and weeks at a time; it was working less than fifty per cent of the time. By the middle of August a satisfactory model for generation of the texture gradients was found and plots had been made.

There was enough time to set up and do the first experiment before Dr. Epstein left the University.

Presently, line texture displays are being prepared with various line orientations. Plans include the production of textures which have basic elements which enclose larger areas than short lines do. We are also investigating the possibility of using a line printer to generate the textural displays.

PROGRAMS USED IN OPTIMIZING

Matrix Inversion

1. The first of the programs dealing with matrix inversion is a subroutine called GINV. This program calculates the generalized, or

pseudo-inverse of a rectangular matrix A which may be singular or non-singular. The psuedo inverse of A can be defined as follows: Given the matrix A of order N x M, the generalized inverse is the matrix A^- of order M x N which satisfies the equation

$$AA^-A = A. \quad (1)$$

2. The second of these routines dealing with matrix inversion is used to increase the accuracy of the inverse of a non-singular, square matrix. Given the matrix A and its estimated inverse B, subroutine ACCINC calculates a new inverse B* whose accuracy is increased by an arbitrary degree specified by an input parameter, EPS. The success of ACCINC requires that one condition be fulfilled. This condition is described in the equation below.

$$||I - AB|| \leq 1 \quad (2)$$

where I is the identity matrix.

The calculation process of GINV requires that the inverse of a non-singular square matrix be found, and consequently the user may desire a higher degree of accuracy than is normally provided by many standard inversion routines. Therefore subroutine ACCINC can be incorporated into GINV by exercising one of the user's options of GINV.

Eigenvalues and Eigenvectors

1. Subroutine BISECT was written to calculate the eigenvalues of a symmetric tridiagonal matrix by the method of bisection. The original program was written by W. Borth, R. S. Martin, and J. H. Wilkinson in ALGOL and represents one of the fastest and most recent variations of the bisection method. It was converted to FORTRAN IV and put in subroutine form. Later it was combined with the following two routines to form a package to calculate eigenvalues and eigenvectors.

2. Subroutine TRIDI was derived after testing many existing routines which found the tridiagonalized form of a symmetric matrix. TRIDI embodies the desirable characteristics of all of these routines including efficiency in calculation, increased accuracy and minimum storage require-

ments. As mentioned before, this was included in the eigenvalue-eigenvector package.

3. The last of these programs was developed in much the same way as TRIDI. Subroutine VECTOR is used to calculate the eigenvectors of the matrix and incorporates the best characteristics of the many routines that were tested.

Optimal Search Techniques

1. The first of the programs dealing with optimal search techniques applies itself to the one-dimensional allocation problem. The routine uses dynamic programming to maximize the non-linear function,

$$R(X_1, X_2, \ldots, X_n) = g_1(X_1) + g_2(X_2) + \ldots + g_n(X_n) \tag{3}$$

where g_i is the i^{th} activity function and X_i is the allocation to that activity. This is solved over all those points in a region

$$X_i \geq 0 \quad i = 1, 2, \ldots, N \tag{4}$$

which also satisfy the constraint

$$\sum_{i=1}^{N} X_i \leq XMAX \tag{5}$$

where XMAX is the total resource.

Since the solution of this is done in an incremental fashion, the g_i's need not be continuously defined between 0 and XMAX. Rather they need only to be defined for a finite set of points each separated from the next by a delta defined by

$$DELTA = XMAX/NINT \tag{6}$$

where NINT is the number of intervals into which the range between 0 and XMAX is divided into. Both XMAX and NINT are input variables to subroutine DYNMC.

2. If we are interested in maximizing the sum of a set of N activities which are functions of M-variables (M = 2, 3, ...), we wish to

solve an M-dimensional allocation problem. Similar to the previous problem, we wish to maximize the non-linear function,

$$R(X_1^1, X_2^1, \ldots, X_N^1; X_1^2, X_2^2, \ldots, X_N^2; \ldots; X_1^M, X_2^M, \ldots, X_N^M) = \sum_{i=1}^{N} g_i(X_i^1, X_i^2, \ldots, X_i^M) \quad (7)$$

where the superscript indicates the dimension number in an M-dimensional space. This is subject to the conditions

$$\sum_{i=1}^{N} X_i^j \leq XMAX^j \; X_i^j \geq 0 \quad i = 1, \ldots, N; \; j = 1, \ldots, M \quad (8)$$

For a two dimensional problem, (7) becomes the following:

$$R(X_1, X_2, \ldots, X_N; Y_1, Y_2, \ldots, Y_N) = \sum_{i=1}^{N} g_i(X_i Y_i) \quad (9)$$

in which the superscript notation has been dropped. By keeping the X allocation vector constant, (9) reduces to the same one-dimensional allocation problem as described previously.

$$R(Y_1, Y_2, \ldots, Y_N) = \sum_{i=1}^{N} g_i(X_i, Y_i) \quad (10)$$

Therefore if we supply an initial guess of the X allocation vector, an approximate solution of the Y allocation vector can be obtained by using the first program described in this section. Further by using the Y solution as the constant vector, an approximate solution of the X allocation vector can now be found. Repeating this procedure until the solutions remain unchanged for two successive approximations, a maximum of R is obtained. However, this may not be the absolute maximum of R but only a relative maximum. Finding one of the absolute maximums may be highly dependent on the initial guess because of the nature of the activities. Therefore, more than one attempt should be made in finding the absolute maximum each time using a different initial guess.

To apply this method of successive approximations to the more general case of m-dimensions, m-1 dimensions need to remain constant to reduce it to the one-dimensional allocation problem. Therefore, m-1 initial guess vectors should be suppled to start the calculation process.

The two subroutines that were developed to handle this problem were called SUCESN and DYNMCN where SUCESN controls the successive approximation methods and DYNMCN solves the one-dimensional allocation problem.

3. Subroutine STEEP was written to solve for the minimum of a unimodal function of N variables in a bounded region by the method of steepest descent. If the function is represented by

$$g(X_1, X_2, \ldots, X_N) \tag{11}$$

subject to the conditions

$$d_i \leq X_i \leq b_i \quad i = 1, 2, \ldots, N \tag{12}$$

then subroutine STEEP will solve for the true minimum of g after being supplied with an initial guess of this minimum.

The first step of the solution is to find the gradient vector at the initial point. Next a search is made in a direction opposite to the gradient vector to find a minimum between the initial point and the nearest boundary. This is accomplished by using a Fibonacci search procedure. When the minimum is found, then this can be used as the new initial point and the above steps can be repeated to find a new minimum. This continues until the minimum remains unchanged for two successive searches which means that the true minimum has been found.

BLANK PAGE

Appendix F

THE BAYESIAN APPROACH TO IDENTIFICATION OF A REMOTELY SENSED ENVIRONMENT

R. M. Haralick

THE BAYESIAN APPROACH TO IDENTIFICATION OF A REMOTELY SENSED ENVIRONMENT

Using remote sensors we can make measurements of an environment. The set of measurements made will be called the data set. Our job is to examine the data set in order to identify what the environment is made up of: our problem is how should we do it? In what follows we describe the Bayesian decision approach with a deterministic decision rule.

We assume that distinct boundaries enclose a limited environment, which is made up of small-area patches, one next to the other. The identification of the environment consists of identifying each small-area patch within one category of a given set of categories. We assume that such an identification is sensible and possible.

In order to make any identification we must have knowledge concerning which kind of measurements are typical measurements of the categories we wish to identify. This knowledge is succinctly contained in a classification, which is a mapping, associating with each measurement the category to which it is most typical — given a specific decision criterion. Therefore, if we are to identify measurements in a data set we must have a classification.

How do we obtain a classification? We perform an information gathering experiment. From the population of all environments, we sample one or a few in which it is possible to identify many small-area patches within each category of interest. The proportion of occurrence of each category in the sampled environment(s) does not have to be representative of the average probability of occurrence of each category in the entire environmental population. However, if we have no information regarding the average probability of occurrence of each categ y in the environmental population, then we would want to choose the sampled environment(s) so that the proportion of occurrence of each category in the sampled environment(s) is an unbiased estimate of the average probability of occurrence of each category in the environmental population. In either case, the small-area patches within each of the sampled environment(s) do have to be representative of the categories with which they are identified.

With each of our sensors, we measure each small-area patch in the chosen environments. From photo-interpretation or field studies, the environments are examined first hand, and an identification of each small-area patch is made. The sequence of such identifications is called the "ground truth identification" or simply "ground truth." It is from the data set (the sequence of measurements) and the ground truth (the sequence of identifications) that we can find a Bayes classification.

At this point we must introduce some mathematical notation. Let $C = \{c_i\}_{i=1}^{K}$ be the set of K given categories; c_i is the symbol used for the i^{th} category. We suppose, for convenience, that each sensor produces only one number for each measurement it makes of a small-area patch. We suppose further, that the j^{th} sensor must produce a number belonging to its range set $L_j = \{l_{j1}, l_{j2}, \ldots, l_{jN_j}\}$. This supposition is fully in accord with reality, since the output of any sensor is always equivalent to a pointer-reading on a dial. Pointer-readings can never be discerned precisely, and are thus discerned approximately to third, or fourth, or,...,N^{th} place accuracy.

Measurement space M is the set of all measurements which are possible to make with the set of S sensors. M is conveniently described as the cartesan product of the range sets; $M = L_1 \times L_2 \times \ldots \times L_S$. This is the set of measurements which contain for elements, all the possible numbers produced by sensor one, combined with all the possible numbers produced by sensor two,..., combined with all the possible numbers produced by sensor S. For convenience we number the measurements in M; $M = \{m_n\}_{n=1}^{N}$, where N is the total number of elements in measurement space. Finally we must provide a goodness criterion; thus, we introduce a gain function g. $g(c_i, c_j)$ is our economic gain if we identify a measurement as belonging within the i^{th} category when that measurement was made of a small-area patch actually belonging within the j^{th} category.

We have already mentioned that a classification is a mapping or rule which associates with each measurement m_n in M, the category c_i to which it is most typical — according to some decision criterion. Our decision criterion is economic; "most typical to" translates to, "that association by which we, on the average, gain the most economically." Therefore, according to our decision criterion, we can judge each possible classification. That classification which enables us to gain the most, on the average, is the classification which is best; it is that classification which we wish to find.

Let us now examine how the average gain may be calculated. Let f be a classification mapping. f is a function whose domain is the set M, and whose range is the set C; f: $M \rightarrow C$. For each element $m_n \in M$ the function associates one and only one category $c_i \in C$. We define the characteristic function h_f for f as follows: for every $m_n \in M$, $c_i \in C$,

$$\left.\begin{array}{l} h_f(c_i, m_n) = 1 \text{ if and only if } f(m_n) = c_i \\ \qquad\qquad\quad 0 \text{ otherwise} \end{array}\right\} .$$

In other words $h_f(c_i, m_n)$ is 1 if and only if the classification f identifies the measurement m_n as belonging within the category c_i. The average gain A for the classification f is easily seen to be:

$$A(f) = \sum_{i=1}^{K} \sum_{k=1}^{K} \sum_{n=1}^{N} g(c_k, c_i) h_f(c_k, m_n) P(m_n | c_i) P(c_i)$$

where $P(m_n | c_i)$ is the conditional probability that the measurement m_n will be made of a small-area patch given that the patch belongs within category c_i, $P(c_i)$ is the probability that any small-area patch of the environments in the population belongs within category c_i, and $g(c_k, c_i)$ is the amount gained if a patch which actually belongs within category c_i is identified within category c_k.

Of the four terms in the summation, $g(c_k, c_i)$ is specified as part of the identification goodness criteria, $h_f(c_k, m_n)$ is defined from the classification f, $P(m_n|c_i)$ will be determined from the data gathered in the experiment, and $P(c_i)$ is an additional a priori probability which we will have to specify. Let us now examine in detail how the conditional probabilities are determined from the experimental data.

The data set is a sequence D of R measurements;

$$D = \langle m_{r_1}, m_{r_2}, \ldots, m_{r_R} \rangle .$$

The ground truth corresponding to sequence D is a sequence T of R not necessarily different category identifications; $T = \langle c_{r_1}, c_{r_2}, \ldots, c_{r_R} \rangle$. Let # be the counting measure. #(D) is the number of elements in the sequence D; thus, #(D) = R. A sequence is really a function whose domain is the set of integers I. The data set D is then a function which associates with each integer, a measurement; D: I → M. The ground truth T is also a function and it associates with each integer a category; T: I → C. D(7), for example, is then just the seventh element in the sequence D; $D(7) = m_{r_7}$. $D^{-1}(m)$ is the set of all integers i for which D(i) = m. The statistic $\hat{P}(m_n|c_i)$ estimating $P(m_n|c_i)$ is defined as

$$\left.\begin{aligned} \hat{P}(m_n|c_i) &= \frac{\#(D^{-1}(m_n) \cap T^{-1}(c_i))}{\#(T^{-1}(c_i))} \quad \text{when } \#(T^{-1}(c_i)) \neq 0 \\ &= 0 \text{ otherwise} \end{aligned}\right\} .$$

$\hat{P}(m_n|c_i)$ is the number of integers which are associated with the measurement m_n in the sequence D and with the category c_i in the sequence T, divided by the number of integers associated with the category c_i in sequence T. Stated simply, $\hat{P}(m_n|c_i)$ is just the number of times the measurement m_n was made of a small-area patch belonging within category c_i, divided by the number of times a small-area patch belonged within the category c_i.

The a priori probabilities $P(c_i)$ can either be estimated from the sampled data set (if this data set is representative of the population) or from our foreknowledge of the population of environments. If we can assume that the few environments we have chosen to sample for our experiment are representative of the population, then

$$\hat{P}(c_i) = \frac{\#(T^{-1}(c_i))}{R}$$

is a reaonable estimate. If we cannot make such an assumption and we believe that a small-area patch is just as likely to belong within one category as within another, then $\hat{P}(c_i) = 1/K$ is a reasonable estimate.

From the estimates $\hat{P}(m_n|c_i)$ and $\hat{P}(c_i)$ we may estimate the average gain $\hat{A}$ for any classification f. As before let h_f be the characteristic function for f.

$$\left.\begin{array}{l} h_f(c_k, m_n) = 1 \text{ if and only if } f(m_n) = c_i \\ \qquad\qquad = 0 \text{ otherwise} \end{array}\right\} .$$

$$\hat{A}(f) = \sum_{i=1}^{K} \sum_{k=1}^{K} \sum_{n=1}^{N} g(c_k, c_i) h_f(c_k, m_n) \hat{P}(m_n|c_i) \hat{P}(c_i) .$$

We seek the Bayes classification f* which maximizes $\hat{A}$. f* is easily defined. For each measurement m_n and for any classification f, there will be one and only one category c_j such that $h_f(c_j, m_n) = 1$. Consider the amount $\hat{a}(c_j, m_n)$ gained due to the identification of measurement m_n as belonging within category c_j.

$$\hat{a}(c_j, m_n) = \sum_{i=1}^{K} g(c_j, c_i) \hat{P}(m_n|c_i) \hat{P}(c_i)$$

The maximum $\hat{A}(f)$ is certainly achieved if for each measurement m_n, $f(m_n) = c_j$ where c_j maximizes $\hat{a}(c_j, m_n)$. Therefore we just have to compute $\hat{a}(c_j, m_n)$ for $j = 1, 2, \ldots, K$ to determine which category, c_j, maximizes it. Then we define $f^*(m_n) = c_j$.

In this manner we can define how to best identify each measurement which actually occurred in the data sequence D. However, there may be many measurements in measurement space M which did not occur in the data sequence. How should these measurements be identified in the classification? Since we have no data or statistics for these measurements it seems that we have no way to deal with them! Here we must draw upon our knowledge of the structure of reality. We know that in any environment, if a measurement m is made of a small-area patch belonging within category c_i, then it is likely to make measurements $m + \delta$ for other small-area patches which also belong within category c_i. If a measurement m is typical of category c_i, then for small δ, $m + \delta$ is also typical of category c_i. Similar or close measurements are usually associated with similar or the same categories. Thus in the classification we can identify a measurement m, which did not occur in the data sequence, with the category associated with m', its nearest neighbor.

The part of the classification f^* which was defined by means of the statistics generated by the experiment is called a Bayes Classification and hence the name "Bayesian approach." The part of the classification which is not Bayesian is said to be defined by a nearest neighbor search.

Acknowledgement: This work was supported by Project Themis (USAETL Contract DAAK02-68-C-0089, ARPA order No. 1079).

BLANK PAGE

Appendix G

IDECS* SYSTEM DEVELOPMENT

G. Kelly and G. Dalke

*Acronym for Image Discrimination, Enhancement and Combination Sampling System.

APPENDIX G

IDECS* SYSTEM DEVELOPMENT

G. Kelly, G. Dalke

Introduction

The IDECS System consists of real-time and near real-time image processing equipment. The individual devices in the IDECS System are designed primarily for versatility of operation and interconnection to allow evaluation of different image processing techniques. The basic capabilities of the IDECS System have been added under various research contracts with the principal contributions as follows:

1. Real-time video processing devices, color matrixing, and initial research were supported primarily under NASA contract #17-004-003.
2. A six image synchronous flying spot scanner system and general purpose real-time decision logic with color coding capabilities (the spectrance selector) are being supported under USAETL contract # DAAK02-67-C-0435.
3. Improved operator control, digital interface and the capabilities for automatic control card processing are being supported under project Themis.

The final configuration of the IDECS System as it is now envisaged is shown in Figure 1. The subsystems which are being supported by Project Themis are indicated by asterisks and are described individually in the text. The function of each subsystem is the same as that presented in the semiannual report; however, the status of each is different.

I. ANALOG-TO-DIGITAL CONVERSION SUBSYSTEM

A. Function. The function of this subsystem is to convert analog

*Acronym for Image Discrimination, Enhancement and Combination System.

signals from the scanning densitometer of any of the flying-spot scanners into digital information. Each analog value is converted to a binary number variable between six and twelve binary digits and then stored in one or two 6-bit words on magnetic tape. This subsystem is also to have sufficient flexibility so that several channels can be multiplexed together. This would allow the repetitive sampling of each flying-spot scanner in a sequence.

B. Status. The analog to digital converter and the magnetic tape unit have been received; however, there was considerably delay because the magnetic tape unit had to be returned to the factory for repairs. The design for the high speed mode has been completed and the printed circuit boards are being constructed. The design for the increment mode is nearing completion. The total interface circuitry for the analog to digital conversion should be finished shortly after the cabinet enclosure arrives which will be about thirty days after the money for the next fiscal year is received. A block diagram of this subsystem is shown in Figure 2.

II. DIGITAL-TO-ANALOG SUBSYSTEM

A. Function. The function of this subsystem is to convert digital information from a digital magnetic tape, a small computer, or other digital information sources into an analog voltage. Initially this subsystem will be able to convert two binary numbers of ten bits each into two analog voltages suitable for input into a CRT display.

B. Status. The two required digital-to-analog modules have been ordered and received. Some necessary control circuits have been designed and implemented; however, there still is a considerable amount of design remaining to be completed. The block diagram for this subsystem is shown in Figure 3.

III. DISPLAY INTERFACE SUBSYSTEM

A. Function. The function of this subsystem is to enter data at a slow rate into the disk memory and then display this information at video rates onto the color display unit or any black-and-white monitor. Also

the subsystem will eventually have the capability of being used for data storage in a small computer.

B. Status. The disk memory has been received; however, some of the previous design objectives had to be altered in order to obtain suitable reliability in the video storage unit. A tentative design for the signal conditioning circuits between the disk memory and the video display has been completed; however, there is still considerable design work remaining on the control circuitry. This subsystem is shown in Figure 4.

IV. SMALL COMPUTER INTERFACE SUBSYSTEM

A. Function. The purpose of this subsystem is to provide a computer interface so that data may be processed and various control functions performed in "real time" or near "real time."

B. Status. The effort on this subsystem will be started when the necessary funds for a small computer are obtained.

V. SCANNING DENSITOMETER

A. Function. To process an image on a digital computer, it is required that the image information be changed to an analog signal. This can be done by using a scanning densitometer which consists of a rotating and translating glass drum with a photomultiplier tube inside. The image is placed around the glass drum. A light source placed above the drum shines through the image into the photomultiplier tube. The output of the photomultiplier is an analog signal proportional to the grey scale of the image. The translation of the image and the spot size are set so that 20 line pairs/mm are produced.

B. Status. The basic unit has been designed and built; however, there is currently some difficulty with a photo-diode which will be replaced as soon as funds become available.

VI. MASTER VIDEO CONTROL

A. Function. To evaluate the functions and subsystems individually

and combinationally, it is necessary that the IDECS system have the capability to connect and disconnect any device. This is the function of the video control. By switching the video control, various combinations of input and processing devices are presented at the cutput devices. The IDECS block diagram (Figure 1) shows the input, processing, and output devices that are connected to the video control.

B. Status. The video control has been designed, constructed and connected into the system.

VII. POSITION AND SIZE DEVICES

A. Function. In order to combine and process more than one image, it is necessary that the images be geometrically congruenced. This can be accomplished by controlling the raster on the flying spot scanning units. The position and size devices control this raster.

The positioning device will translate and rotate the raster, causing the image on the display to move horizontally, vertically, and angularly. The size device will expand or contract the raster; therefore, the size of the image on the display is controlled horizontally and vertically. The position and size devices are shown in Figure 5.

This device can accomadate the following corrections for a 8 x 10 cm. image field:

1. Vertical position: $\pm$ 3 cm.
2. Horizontal position: $\pm$ 5 cm.
3. Vertical size: 3 : 1
4. Horizontal size: 3 : 1
5. Rotation: $\pm$ 15°

B. Status. Both the position and size devices have been implemented for all six flying spot scanning units.

VIII. SYNCHRONIZATION DEVICE

A. Function. For the information on the input and output devices to correspond, it is essential that these devices scan in unison. The synchronization device accomplishes this by sending pulses to the horizontal input of the sweep circuits at a rate of 15,750 Hz and to the vertical input of the

sweep circuits at a rate of 60 Hz. The synchronization device is shown in Figure 5. This device is crystal controlled to a frequency accu acy of .003 %.

B. Status. A synchronization generator is in operation to match the flying spot scanning units to the displays.

IX. COLOR DISPLAY

A. Function. The color display is used to convert video signals proportional to gray scale on photographs or radar images into a color which varies in intensity and hue.

B. Status. The color display is operational.

X. TEXTURE GENERATOR

A. Function. The texture generator produces an electronic equivalent of zip-a-tone patterns. This allows multiple categories to be coded in gray levels and patterns rather than color.

B. Status. Although, no funding has been made available to build the texture generator, initial design and feasibility studies have been completed with in-house funds.

XI. TEXTURE FILTER

A. Function. The texture filter is used to discriminate image filters on the basis of image textures rather than image gray levels.

B. Status. Feasibility and design for the texture filters are complete from in-house funds. A prototype model is being constructed and tested under a NASA contract.*

Acknowledgement: This work was supported by Project Themis (USAETL Contract DAAK02-68-C-0089, ARPA order No. 1079).

---

* NASA Contract No. NAS-97175

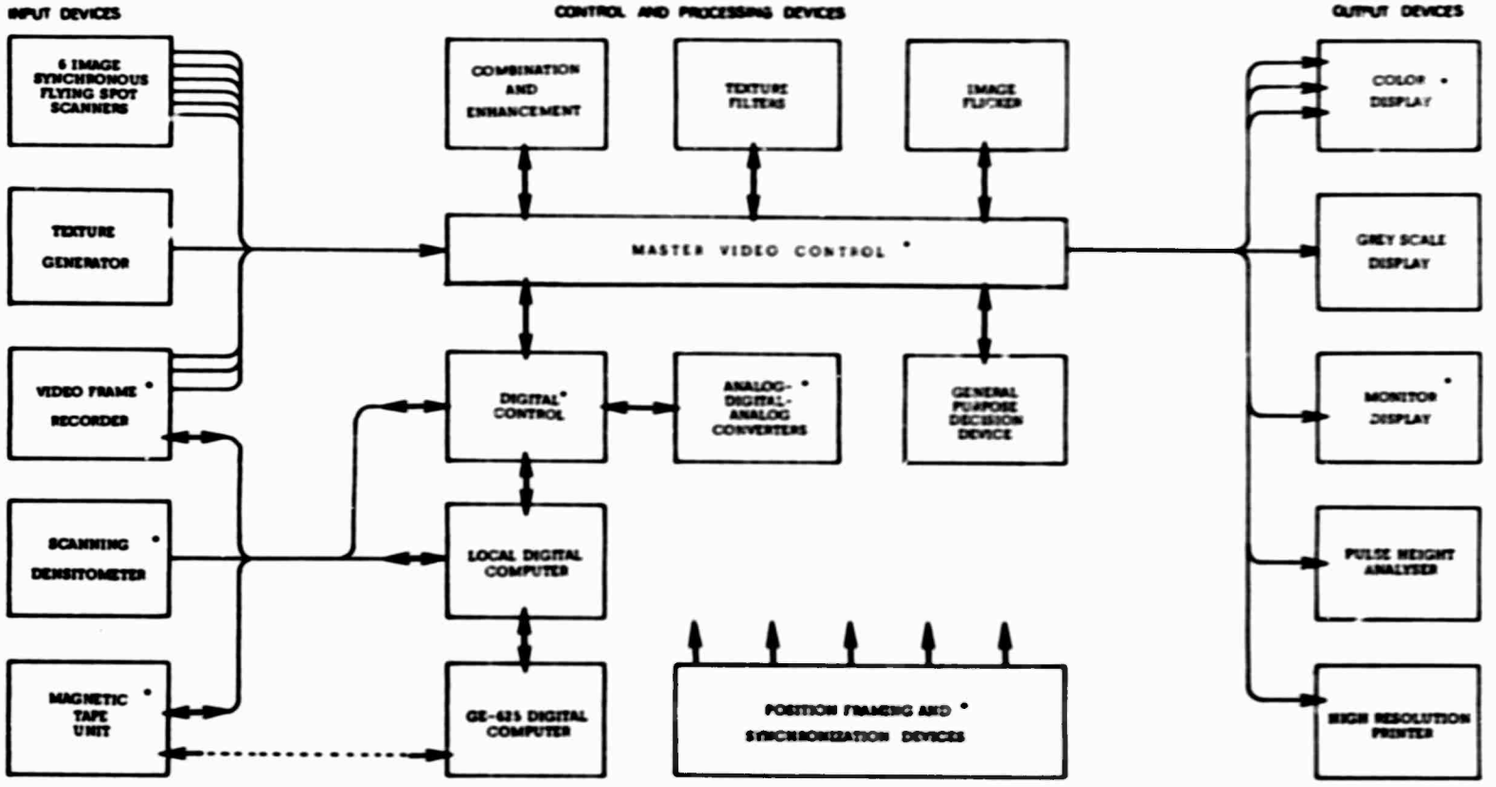

FIGURE 1 **IDECS SYSTEM DIAGRAM**

* EQUIPMENT SPONSORED BY PROJECT THEMIS

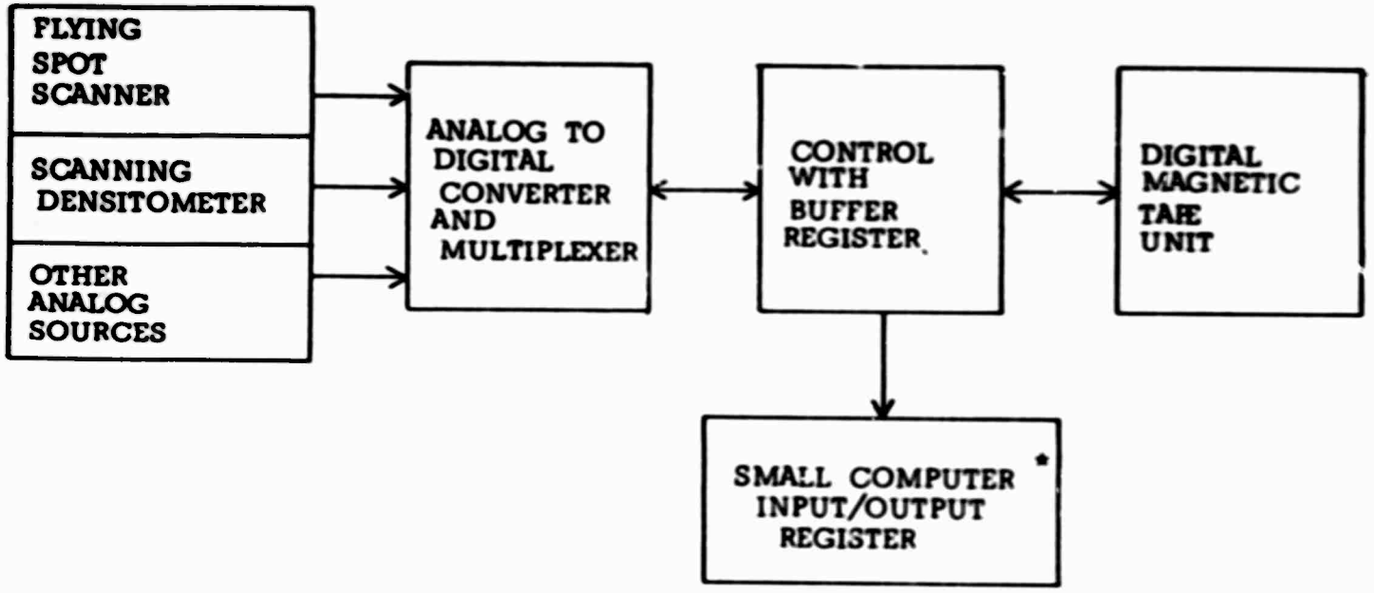

Figure 2. ANALOG TO DIGITAL CONVERSION SUBSYSTEM

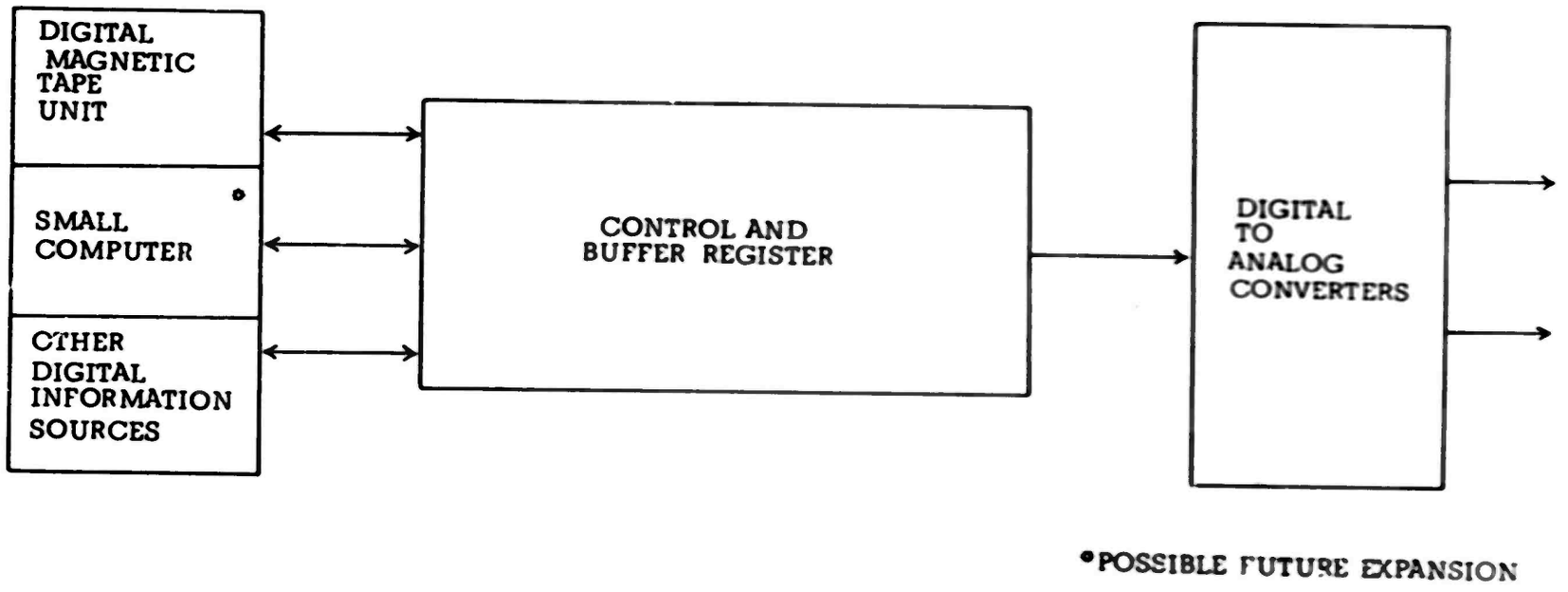

Figure 3. DIGITAL TO ANALOG CONVERSION SUBSYSTEM

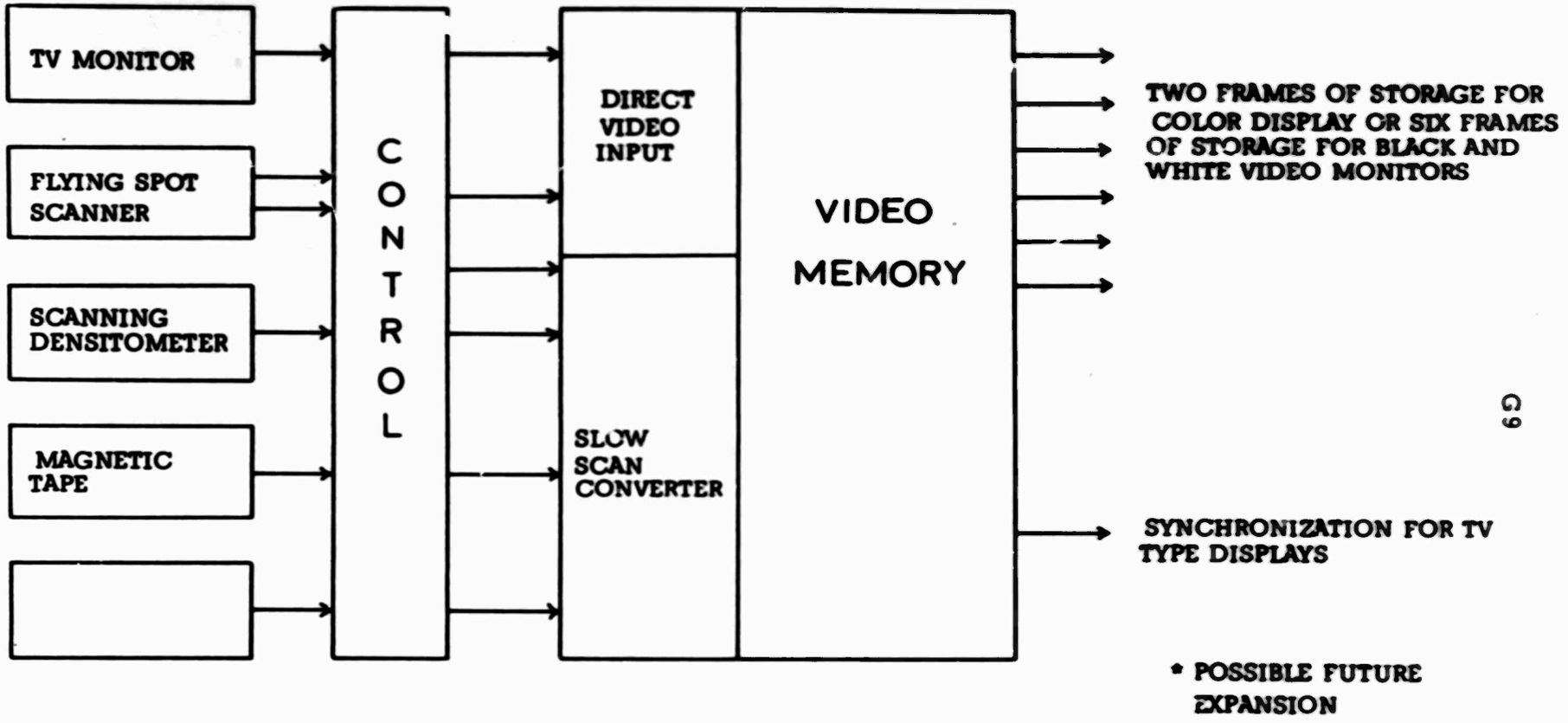

Figure 4. VIDEO STORAGE SUBSYSTEM FOR IDECS

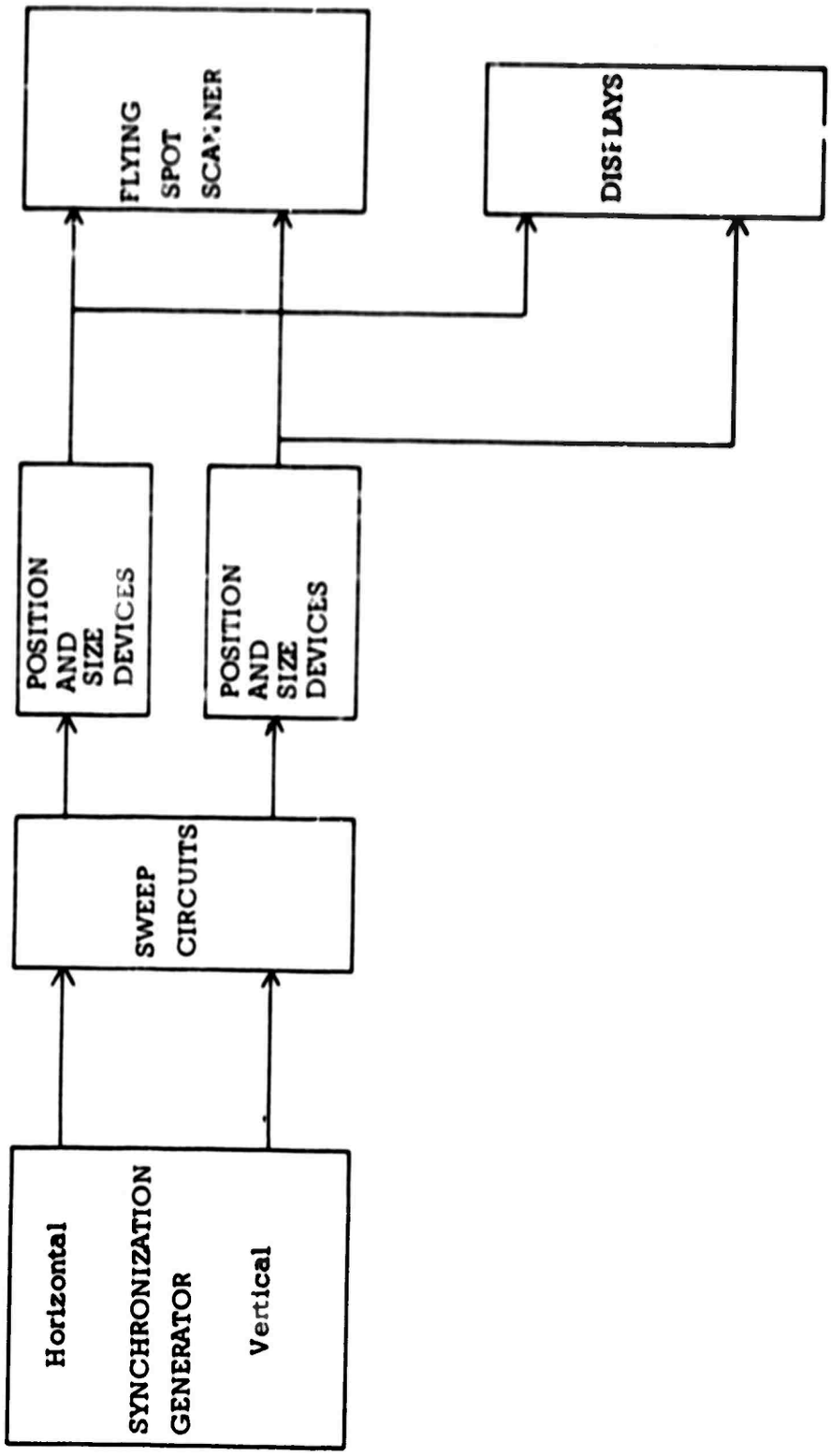

Figure 5. POSITION, SIZE, AND SYNCHRONIZATION DEVICES

BLANK PAGE

APPENDIX H

CRES BIBLIOGRAPHY

TECHNICAL REPORTS

CRES Technical Report 61-1 "Fresnel Zone Processing of Synthetic Aperture Radar Data," M. Buchanan, June 1965. Supported by NASA Contract NSR 17-004-003.

CRES Technical Report 61-2 "Plane Wave Scattering from a Rough Surface with Correlated Large and Small Scale Orders of Roughness," H. S. Hayre and D. E. Kaufman, May 1965. Supported by NASA Contract NSR 17-004-003.

CRES Technical Report 61-3 "Some Applications of Radar Return Data to the Study of Terrestrial and Oceanic Phenomena," W. J. Pierson, B. B. Scheps, D. S. Simonett, March 1965. Presented at the Third Goddard Memorial Symposium on Scientific Experiments for Manned Orbital Flights, Washington, D. C., March 1965, Published in Vol. 4, Scientific Experiments for Manned Orbital Flight, American Astronautical Society, p. 87-137. Supported by NASA Contract NSR 17-004-003.

CRES Technical Report 61-4 "Spacecraft Radar as a Means for Studying the Antarctic," D. S. Simonett, D. A. Brown, September 1965. Presented to VII Congress International Quaternary Assoc., Boulder, Colorado, September 1965. Published in the Proceedings. Supported by NASA Contract NSR 17-004-003.

CRES Technical Report 61-5 "Remote Sensing from Spacecraft as a Tool for Investigating Arctic Environments," D. S. Simonett, S. A. Morain, September 1965. Presented to VII Congress International Quaternary Assoc., Boulder, Colorado, September 1965, Published in the Proceedings. Supported by NASA Contract NSR 17-004-003.

CRES Technical Report 61-6 "Imaging Radars on Spacecraft as a Tool for Studying the Earth," R. D. Ellermeier, D. S. Simonett, November 1965. Presented at the International Symposium on Electromagnetic Sensing of the Earth from Satellites, Miami Beach, Florida, November 22-24, 1965. Published in the Proceedings, p. L1-L20. Supported by NASA Contract NSR 17-004-003.

CRES Technical Report 61-7 "Radar as a Remote Sensor," R. K. Moore, January 1966. Supported by NASA Contract NSR 17-004-003.

CRES Technical Report 61-8 "Use of Orbital Radars for Geoscience Investigations," J. W. Rouse, Jr., W. P. Waite, R. L. Walters, January 1966. Presented at the Third Space Congress Meeting, Cocoa Beach, Florida, March 1965. Published in the Proceedings, p. 77-94. Supported by NASA Contract NSR 17-004-003.

CRES Technical Report 61-9 "Vegetation Analysis with Radar Imagery," S. A. Morain, D. S. Simonett, April 1966. Presented at the Fourth Symposium on Remote Sensing of the Environment, University of Michigan, Ann Arbor, Michigan, April 1965. Published in the Proceedings, p. 605-622. Supported by NASA Contract NSR 17-004-003.

CRES Technical Report 61-10 "Some Empirical and Theoretical Interpretations of Multiple Polarization Radar Data," R. D. Ellermeier, A. K. Fung, D. S. Simonett, April 1966. Presented at Fourth Symposium on Remote Sensing of the Environment, University of Michigan, Ann Arbor, Michigan, April 1966. Published in the Proceedings, p. 657-670. Supported by NASA Contract NSR 17-004-003.

CRES Technical Report 61-11 "Radar Scatterometry--An Active Remote Sensing Tool," R. K. Moore, April 1966. Presented at Fourth Symposium on Remote Sensing of the Environment, University of Michigan, Ann Arbor, Michigan, April 1966. Published in the Proceedings, p. 339-375. Supported by NASA Contract NSR 17-004-003.

CRES Technical Report 61-12 "Present and Future Needs of Remote Sensing in Geography," D. S. Simonett, April 1966. Presented at Fourth Symposium on Remote Sensing of the Environment, University of Michigan, Ann Arbor, Michigan, April 1966. Published in the Proceedings, p. 37-49. Supported by NASA Contract NSR 17-004-003.

CRES Technical Report 61-13 "The Geological Value of Simultaneously Produced Like- and Cross-Polarized Radar Imagery," L. F. Dellwig, R. K. Moore, July 1966. Published in Journal of Geophysical Research, vol. 71, no. 4, July 15, 1966, p. 3597-3601. Supported by NASA Contract NSR 17-004-003.

CRES Technical Report 61-14 "The Potential of Low Resolution Radar Imagery in Regional Geologic Studies," L. F. Dellwig, J. N. Kirk, R. L. Walters, July 1966. Published in Journal of Geophysical Research, Letters, vol. 71, no. 20, October 15, 1966, p. 4995-4998. Supported by NASA Contract NSR 17-004-003.

CRES Technical Report 61-16 "Automatic Processing of Multi-Spectral Images," G. W. Dalke, September 1966. Supported by NASA Contract NSR 17-004-003.

CRES Technical Report 61-17 "Identification of Remote Objects by Means of Scatterometry Data and Application to Pisgah Crater," G. W. Dalke, February 1967. Supported by NASA Contract NSR 17-004-003.

CRES Technical Report 61-18 "Use of Radar for Mapping Information-Gathering in Cloudy Environments," D. S. Simonett, S. A. Morain (being completed). Supported by NASA Contracts NSR 17-004-003 and NAS 9-7175.

CRES Technical Report 61-19 "The Use of Multi-Parameter Radar Imagery for the Discrimination of Terrain Characteristics," R. D. Ellermeier, D. S. Simonett, L. F. Dellwig. Presented at IEEE International Convention, New York, March 1967. Published in the 1967 IEEE International Convention Record, Part 2, p. 128-135. Supported by NASA Contract NSR 17-004-003 and NASA Grant NsG-298.

CRES Technical Report 61-20 "Evaluation of Multiple Polarized Radar Imagery for the Detection of Selected Cultural Features," A. Lewis. (Classified Report). Supported by NASA Contracts NSR 17-004-003 and NAS 9-7175.

CRES Technical Report 61-21 "The Potential of Radar as a Remote Sensor in Agriculture: 1. A Study with K-Band Imagery in Western Kansas," D. S. Simonett, J. E. Eagleman, A. B. Erhart, D. C. Rhodes and D. E. Schwarz, March 1967. Supported by NASA Contract NSR 17-004-003 and NASA Grant NsG-298.

CRES Technical Report 61-22 "Field Studies on Vegetation at Horsefly Mountain, Oregon and its Relation to Radar Imagery," S. A. Morain, January 1967. Supported by NASA Contract NSR 17-004-003 and NASA Grant NsG-298.

CRES Technical Report 61-23 "K-Band Radar in Vegetation Mapping," S. A. Morain and D. S. Simonett. Presented at the Annual Convention of the American Society of Photogrammetry, Washington, D. C., March 1967. Published in Photogrammetric Engineering, vol. 33, no. 7, July 1967, p. 730-740. Supported by NASA Contract NSR 17-004-003 and NASA Grant NsG-298.

CRES Technical Report 61-24 "Geologic Evaluation by Radar of NASA Sedimentary Test Site," H. C. MacDonald, P. A. Brennan, and L. F. Dellwig. Published in IEEE Transactions on Geoscience Electronics, vol. GE-5, no. 3, December 1967, p. 72-78. Supported by NASA Contract NSR 17-004-003 and NASA Grant NsG-298.

CRES Technical Report 61-25 "Investigation of Cross-Polarized Radar on Volcanic Rocks," E. Gillerman, February 1967. Supported by NASA Contract NSR 17-004-003.

CRES Technical Report 61-26 Deleted

CRES Technical Report 61-27 "Application of Color-Combined Multiple-Polarization Radar Images to Geoscience Problems," D. S. Simonett, December 1966. Presented at the Colloquium on Classification Procedures: Computer Applications in the Earth Sciences, Kansas Geological Survey, Lawrence, Kansas, December 1966. Published as Computer Contribution 7, State Geological Survey, University of Kansas, Lawrence, Kansas, December 1966, p. 19-24. Supported by NASA Contract NSR 17-004-003.

CRES Technical Report 61-28 "Implementation of Pattern Recognition Techniques as Applied to Geoscience Interpretation," G. W. Dalke, December 1966. Presented as the Colloquium on Classification Procedures: Computer Applications in the Earth Sciences, Kansas Geological Survey, Lawrence, Kansas, December 1966. Published as Computer Contribution 7, State Geological Survey, University of Kansas, Lawrence, Kansas, December 1966, p. 24-29. Supported by NASA Contract NSR 17-004-003.

CRES Technical Report 61-29 "Orbital Remote Sensors--Data Processing for Geoscience Investigations," G. W. Dalke and J. W. Rouse, Jr. Presented at the American Astronautical Society Symposium, Huntsville, Alabama, June 1967. Published in the Transactions, vol. II, p. MM-23-1 to MM-23-20. Supported by NASA Contract NSR 17-004-003.

CRES Technical Report 61-30 "Radar Bibliography for Geosciences," R. L. Walters. (March 1968). Supported by NASA Contract NSR 17-004-003, NASA Grant NsG-298, USGS Contract 14-08-0001-10848, and NASA Contract NAS 9-7175.

CRES Technical Report 61-31 "An Evaluation of Radar Imagery as a Tool for Drainage Basin Analysis," R. M. McCoy, August 1967. Supported by NASA Contract NSR 17-004-003, NASA Grant NsG-298, and NASA Contract NAS 9-7175.

CRES Technical Report 61-32 "Potential Research and Earth Resource Studies with Orbiting Radars: Results of Recent Studies," R. K. Moore and D. S. Simonett. Presented at the 4th Annual Meeting of the American Institute of Aeronautics and Astronautics (AIAA), Anaheim, California, October 23-27, 1967. Published as AIAA Paper no 67-767, 21 pp. Supported by NASA Contract NSR 17-004-003, NASA Contract NAS 9-7175, USGS Contract 14-08-0001-10848, NAVOCEANO Contract N62305-67-C-0044, and NSF Grant GK-1153.

CRES Technical Report 118-1 "A Medial Transformation of Two-Dimensional Data with Applications to Data Compression and Noise Reduction," P. Youngberg, August 1967. Supported by NASA Contract NAS 9-7175.

CRES Technical Report 118-2 "Analysis of Scatterometry Data from Pisgah Crater," J. Lundien, August 1967. Supported by NASA Contract NAS 9-7175.

CRES Technical Report 118-3 "Scatterometer Data Analysis Techniques," H. Masenthin (July 1967). Supported by NASA Contracts NSR 17-004-003 and NAS 9-7175.

CRES Technical Report 118-4 "Pattern Recognition Ideas," R. Haralick (being completed). Supported by NASA Contract NAS 9-7175.

CRES Technical Report 118-5 "Adaptive Pattern Recognition by Similarity Set Construction," R. Haralick, October 1967. Supported by NASA Contracts NSR 17-004-003 and NAS 9-7175.

CRES Technical Report 118-6 "A Survey of Some Pattern Recognition Techniques," Jess O. Betlack (being completed). Supported by NASA Contract NAS 9-7175.

CRES Technical Report 118-7 "The Influence of Radar Look-Direction on the Recording of Geologic Lineament Patterns," J. Kirk, L. Dellwig and L. Jefferis (being completed). Supported by NASA Contract NAS 9-7175.

CRES Technical Report 118-8 "Possible Calderas and Major Lineaments Defined by SLAR, St. Francois Mountains, Missouri," E. Gillerman, October 1968. Supported by NASA Contract NAS 9-7175.

CRES Technical Report 118-9 "Radar Lineament Analysis of the Grand Canyon Area, Northern Arizona," L. H. Jefferis, October 1968. Supported by NASA Contract No. NAS 9-7175.

TECHNICAL MEMORANDA

CRES Technical Memorandum 61-2 "Multi-Frequency Acoustical Simulation System," M. Buchanan, September 1964. Supported by NASA Contract NSR 17-004-003.

CRES Technical Memorandum 61-3 "A Method of Analyzing NRL Flight Radar Return," J. W. Rouse, Jr., September 1964. Supported by NASA Contract NSR 17-004-003.

CRES Technical Memorandum 61-4 "Color Theory," G. W. Dalke, October 1964. Supported by NASA Contract NSR 17-004-003.

CRES Technical Memorandum 61-5 " Initial Design Considerations for the Multi-Color Display," G. W. Dalke, J. E. Rathke, J. W. Rouse, Jr., December 1964. Supported by NASA Contract NSR 17-004-003.

CRES Technical Memorandum 61-6 "Establishment of the Criteria for Determining the Pulse Repetition Frequency, the Beam Length, Beam Width and Pulse Length on the Ground," J. Butler, October 1964. Supported by NASA Contract NSR 17-004-003.

CRES Technical Memorandum 61-8 "Synthetic Aperture Power Requirements," R. K. Moore, J. Butler, November 1964. Supported by NASA Contract NSR 17-004-003.

CRES Technical Memorandum 61-9 "Satellite Altimeter Using Two Antennas," J. Butler, R. K. Moore, March 1965. Supported by NASA Contract NSR 17-004-003.

CRES Technical Memorandum 61-11 "Possible Lunar Analogs for Use by the Waterways Experiment Station, Vicksburg, Mississippi," D. A. Brown, December 1964. Supported by NASA Contract NSR 17-004-003.

CRES Technical Memorandum 61-12 "Considerations for Proposed NRL Modification to Add Synthetic Aperture Imaging Capability," J. W. Rouse, Jr., January 1965. Supported by NASA Contract NSR 17-004-003.

CRES Technical Memorandum 61-13 "Synthetic Aperture Antenna," J. W. Rouse, Jr., May 1965. Supported by NASA Contract NSR 17-004-003.

CRES Technical Memorandum 61-14 "Calculation of Tristimulus Coefficients for the CRES Multicolor Display," G. W. Dalke, May 1965. Supported by NASA Contract NSR 17-004-003.

CRES Technical Memorandum 61-15 "Modifications Made on Photovolt 520-A Densitometer," M. Buchanan, May 1965. Supported by NASA Contract NSR 17-004-003.

CRES Technical Memorandum 61-16 "Unfocused Synthetic Aperture Antenna Radar Power Requirements," J. W. Rouse, Jr., June 1965. Supported by NASA Contract NSR 17-004-003.

CRES Technical Memorandum 61-17 "Theory of Synthetic Aperture," M. Buchanan, June 1965. Supported by NASA Contract NSR 17-004-003.

CRES Technical Memorandum 61-18 "Remote Sensor Studies of the Pisgah Crater Area, California: A Preliminary Report," L. F. Dellwig, M. E. Bickford, N. Kirk, R. Walters, December 1965. Supported by NASA Contract NSR 17-004-003.

CRES Technical Memorandum 61-19 "Technique for Producing a Pseudo Three-Dimensional Effect with Monoscopic Radar Imagery," L. F. Dellwig, H. C. MacDonald, J. N. Kirk, December 1965. Supported by NASA Contract NSR 17-004-003.

CRES Technical Memorandum 61-21 "Reduction of Like-Images to Space Correlated Data Lists," G. W. Dalke, M. O. Vichellich, May 1966. Supported by NASA Contract NSR 17-004-003.

CRES Technical Memorandum 61-22 "The [3 x 3] Matrix Unit," F. Welter, May 1966. Supported by NASA Contract NSR 17-004-003.

CRES Technical Memorandum 61-23 "Pattern Recognition Problem," R. M. Haralick, June 1966. Supported by NASA Contract NSR 17-004-003.

CRES Technical Memorandum 61-24 "Photographic Color Combination Procedures and Equipment Available at CRES," D. Egbert, June 1966. Supported by NASA Contract NSR 17-004-003.

CRES Technical Memorandum 61-25 "Radar Bibliography for Geoscientists," R. L. Walters, June 1966. Supported by NASA Contract NSR 17-004-003.

CRES Technical Memorandum 61-26 "Radar Linears not Related to Geology," H. D. MacDonald, E. Gillerman, L. F. Dellwig, J. N. Kirk, July 1966. Supported by NASA Contract NSR 17-004-003.

CRES Technical Memorandum 61-27 "Radar Fundamentals," J. W. Rouse, Jr., W. P. Waite (being completed). Supported by NASA Contract NSR 17-004-003.

CRES Technical Memorandum 61-28 "Image Reproduction with Color Television Receiver," R. L. Knuckey, July 1966. Supported by NASA Contract NSR 17-004-003.

CRES Technical Memorandum 61-30 (Deleted)

CRES Technical Memorandum 61-31 "Automatic Acuteness Measurements for Multiple Images," G. W. Dalke, August 1966. Supported by NASA Contract NSR 17-004-003.

CRES Technical Memorandum 61-32 "Automatic Measurement and Reduction of Drainage Basin Data," G. W. Dalke, August 1966. Supported by NASA Contract NSR 17-004-003.

CRES Technical Memorandum 61-33 "Automatic Measurements of Texture and Detection of Lines in a Flying-Spot Scanner System," G. W. Dalke, August 1966. Supported by NASA Contract NSR 17-004-003.

CRES Technical Memorandum 61-34 (Deleted)

CRES Technical Memorandum 61-35 "Pattern Recognition and Similarity," R. M. Haralick, August 1966. Supported by NASA Contract NSR 17-004-003.

CRES Technical Memorandum 61-36 "Design System for Flying-Spot Scanner," J. E. Rathke, August 1966. Supported by NASA Contract NSR 17-004-003.

CRES Technical Memorandum 61-37 "The CRES Data Handling System," J. E. Rathke, August 1966. Supported by NASA Contract NSR 17-004-003.

CRES Technical Memorandum 61-38 "Photomultiplier, Compensated Video Amplifier and Video Amplifier Circuits," J. E. Rathke, September 1966. Supported by NASA Contract NSR 17-004-003.

CRES Technical Memorandum 61-39 "The 3-Channel Flying-Spot Scanner," J. E. Rathke, August 1966. Supported by NASA Contract NSR 17-004-003.

CRES Technical Memorandum 61-40 "The Tri-Color Display Unit," J. E. Rathke, September 1966. Supported by NASA Contract NSR 17-004-003.

CRES Technical Memorandum 61-41 (Deleted)

CRES Technical Memorandum 61-42 "Multi-Color Presentation of Images with Edge Enhancement," R. L. Knuckey, October 1966. Supported by NASA Contract NSR 17-004-003.

CRES Technical Memorandum 61-43 "Synthetic-Aperture Signal Film Quantity Calculations," J. W. Rouse, Jr., October 1966. Supported by NASA Contract NSR 17-004-003.

CRES Technical Memorandum 61-44 "An Analog to Digital to Paper Tape Converter," J. Betlack, April 1966. Supported by NASA Contract NSR 17-004-003.

CRES Technical Memorandum 61-45 "Terrain Discrimination by Radar Image Polarization Comparison," R. K. Moore, L. F. Dellwig, October 1966. Published in Proceedings IEEE, vol. 54, no. 9, September 1966, p. 1213-1214. Supported by NASA Contract NSR 17-004-003.

CRES Technical Memorandum 61-46 "Analog to Digital Converter for Low Frequency Sampling," R. Field, April 1967. Supported by NASA Contract NSR 17-004-003.

CRES Technical Memorandum 61-47 "Evaluation of Geoscience Information as a Function of Radar Resolution," R. McCoy (Classified-internal distribution only). Supported by NASA Contract NSR 17-004-003.

CRES Technical Memorandum 61-48 "Electronic Processing for Synthetic Aperture Array Radar," R. K. Moore, J. W. Rouse, Jr., Published in Proceedings IEEE, vol. 55, no. 2, February 1967, p. 233-234. Supported by NASA Contract NSR 17-004-003.

CRES Technical Memorandum 61-49 (Deleted)

CRES Technical Memorandum 61-50 "Radar Imagery, a New Tool for the Geologist," J. W. Kirk, R. L. Walters. Published in The Compass of Sigma Gamma Epsilon, vol. 43, no. 2, January 1966, p. 85-93. Supported by NASA Contract NSR 17-004-003.

CRES Technical Memorandum 61-51 Not assigned.

CRES Technical Memorandum 61-52 Not assigned.

CRES Technical Memorandum 61-53 Not assigned.

CRES Technical Memorandum 61-54 "Use of the Numerical Taxonomy System," R. Haralick, July 1967. Supported by NASA Contracts NSR 17-004-003 and NAS 9-7175.

CRES Technical Memorandum 61-55 "LGP-30 Autocorrelation Program," P. Youngberg, July 1967. Supported by NASA Contracts NSR 17-004-003 and NAS 9-7175.

CRES Technical Memorandum 61-56 "IBM Paper Tape Punch Program for the LGP-30 Computer," P. Youngberg, August 1967. Supported by NASA Contracts NSR 17-004-003 and NAS 9-7175.

CRES Technical Memorandum 61-57 "Analog to Digital to Paper Tape Data Printer for the LGP-30 Computer," P. Youngberg, August 1967. Supported by NASA Contracts NSR 17-004-003 and NAS 9-7175.

TECHNICAL MEMORANDA

CRES Technical Memorandum 117-1 "National Aeronautics and Space Administration Earth Resources Survey Program 90-Day Mission Analysis Report, NASA/MSC Mission 77, Site 76, Garden City, Kansas," J. Ratzlaff, October 1968. Supported by U.S.G.S. Contract No. 14-08-0001-10848.

CRES Technical Memorandum 118-1 "Pattern Recognition of Multi-Spectral Photographs Using a Conditional Probability Method," R. Haralick, September 1967. Supported by NASA Contract NAS 9-7175.

CRES Technical Memorandum 118-2 "Line Driving Amplifier," J. Bryant, November 1967. Supported by NASA Contract NAS 9-7175.

CRES Technical Memorandum 118-3 "Synthetic Aperture Radar Acoustic Simulator," L. Fromme, December 1967. Supported by NASA Contract NAS 9-7175.

CRES Technical Memorandum 118-4 "Preliminary Mission Analysis Report; NASA/MSC Mission No. 47, Site 93, Pt. Barrow, Alaska," J. Rouse, Jr., October, 1967. Supported by NASA Contract NAS 9-7175.

CRES Technical Memorandum 118-5 "Preliminary Report on Radar Lineaments in the Bosto Mountains of Arkansas," J. Kirk and R. Walters. Published in The Compass of Sigma Gamma Epsilon, vol. 45, no. 2, January 1968, p. 122-127. Supported by NASA Contract NSR 17-004-003 and NASA Grant NsG-298.

CRES Technical Memorandum 118-6 "On the Feasibility of Imaging Radar for Small Spacecraft," J. Rouse, Jr., (being completed). Supported by NASA Contract NAS 9-7175.

CRES Technical Memorandum 118-7 "Use of the Radar Scatterometer in Aircraft and Spacecraft Resources Programs," R. K. Moore, October 1968. Supported by NASA Contract NAS 9-7175.

CRES Technical Memorandum 118-8 "National Aeronautics and Space Administration Earth Resources Survey Program 90-Day Mission Analysis Report, NASA/MSC Mission 70, Site 166, Iceland," W. P. Waite and R. L. Walters, August 12, 1968. Supported by NASA Contract No. NAS 9-7175 and Naval Oceanographic Contract N62306-67C-0044.

CRES Technical Memorandum 118-9 "National Aeronautics and Space Administration Earth Resources Survey Program 90-Day Mission Analysis Report, NASA/MSC Mission 74, Site 76, Garden City, Kansas," D. H. Berger, 17 September 1968. Supported by NASA Contract NAS 9-7175 and U.S.G.S. Contract 14-08-0001-10848.

CRES Technical Memorandum 118-10 "National Aeronautics and Space Administration Earth Resrouces Survey Program 90-Day Mission Analysis Report, NASA/MSC Mission 74, Site 85, Lawrence, Kansas," R. L. Walters, September 1968. Supported by NASA Contract NAS 9-7175 and U.S.G.S. Contract No. 14-08-0001-10848.

CRES Technical Memorandum 118-11 "National Aeronautics and Space Administration Earth Resources Survey Program 90-Day Mission Analysis Report, NASA/MSC Mission 74, Site 85, Lawrence, Kansas," R. L. Walters, September 1968. Supported by NASA Contract No. NAS 9-7175 and U.S.G.S. Contract No. 14-08-0001-10848.

CRES Technical Memorandum 118-12 "National Aeronautics and Space Administration Earth Resrouces Survey Program 90-Day Mission Analysis Report, NASA/MSC Mission 54, Site 85, Lawrence, Kansas," W. G. Brooner and R. L. Walters, (in preparation). Supported by NASA Contract No. NAS 9-7175 and U.S.G.S. Contract No. 14-08-0001-10848.

TECHNICAL MEMORANDA

CRES Technical Memorandum 112-1 "Acoustic Scattering from Surfaces with Controlled Wave Spectra: Part I," R. Knuckey, March 1967. Supported by NAVOCEANO Contract No. NOO N62306-67-C-0044.

CRES Technical Memorandum 112-2 "Acoustic Scattering from Surfaces with Controlled Wave Spectra: Part II," R. Knuckey, June 1967. Supported by NAVOCEANO Contract No. NOO N62306-67-C-0044.

CRES Technical Memorandum 112-3 "Range Error Statistics for Split-Gate Altimeter: Part I, Square Law Detection," H. Lee, October 1967. Supported by NAVOCEANO Contract No. NOO N62306-67-C-0044.

CRES Technical Memorandum 112-4 "Range Error Statistics for Split-Gate Altimeter: Part II, Linear Detection," H. Lee, October 1967. Supported by NAVOCEANO Contract No. NOO N62306-67-C-0044.

CRES Technical Memorandum 112-5 "The Accuracy of the Correlated Split Gate Altimeter," H. L. Lee, October 1968. Supported by NAVOCEANO Contract No. NOO N62306-67-C-0044.

TECHNICAL MEMORANDA

CRES Technical Memorandum 121-1 "Ice Type Identification by Radar; Earth Resources Survey Program, Mission Analysis Report, NASA/MSC Mission 47," J. Rouse, Jr., February 1968. Supported by AINA Contract No. ONR-394.

TECHNICAL REPORTS

CRES Technical Report 121-1 "Ice Type Identification by Radar," J. Rouse, Jr., February 1968. Supported by AINA Contract No. ONR-394.

CRES Technical Report 121-2 "Arctic Ice Thickness Measurement by Radar," J. Rouse, Jr., March 1968. Supported by AINA Contract No. ONR-394.

CRES Technical Report 121-3 "Arctic Ice Thickness Measurement by Radar," J. Rouse, Jr., September 1968. Supported by AINA Contract No. ONR-394.

TECHNICAL MEMORANDA

CRES Technical Memorandum 137-1 "Orbit Considerations for Radar Imagery of Arctic Sea Ice," R. Gerchberg, March 1968. Supported by NOL Contract No. NOO N62306-67-C-0044.

CRES Technical Memorandum 137-2 "Unfocused Synthetic Aperture Radar: Basic System Requirements," R. Gerchberg, March 1968. Supported by NOL Contract No. NOO N62306-67-C-0044.

TECHNICAL REPORTS AND OTHER PUBLICATIONS

CRES Technical Report 48-1 "Exact Solution to the Scattering of Waves From a Rough Surface," A. K. Fung, June 1964. Supported by NSF Grant GP-2259 and NASA Grant NsG-298.

CRES Technical Report 48-3 "Scattering Theories and Radar Return," A. K. Fung, May 1965. Supported by NSF Grant GP-2259 and NASA Grant NsG-298.

CRES Technical Report 48-4 "The Omnidirectional Scattering of Acoustic Waves from Rough Surfaces with Application to Electromagnetic Scattering," B. E. Parkins, June 1965. Supported by NSF Grant GP-2259 and NASA Grant NsG-298.

CRES Technical Report 48-5 "Scattering and Depolarization of Electromagnetic Waves by Rough Surfaces," A. K. Fung, November 1965. Supported by NSF Grant GP-2259 and NASA Grant NsG-298.

CRES Technical Report 48-6 "Frequency Dependence of Waves Scattered from Rough Surfaces," A. K. Fung, December 1965. Supported by NSF Grant GP-2259 and NASA Grant NsG-298.

CRES Technical Report 48-7 "Literature Survey on Scattering from Layered Media," T. Leovaris, July 1966. Supported by NSF Grant GP-2259 and NASA Grant NsG-298.

CRES Technical Report 48-8 "Polarized and Depolarized Powers Returned from a Dielectric Rough Surface," A. K. Fung, July 1966. Supported by NSF Grant GP-2259 and NASA Grant NsG-298.

CRES Technical Report 48-9 "Omnidirectional Measurements of Acoustic Waves Scattered from a Known Rough Surface at Various Angles of Incidence," W. D. Boles, August 1966. Supported by NSF Grant GP-2259 and NASA Grant NsG-298.

CRES Technical Report 48-10 "Theory of Radar Scatter from Rough Surfaces, Bistatic and Monostatic with Application to Lunar Radar Return," A. K. Fung, March 1964. Published in Journal of Geophysical Research, vol. 69, no. 6, March 1964, p. 1063-1073. Supported by NSF Grant GP-2259 and NASA Grant NsG-298.

CRES Technical Report 48-11 "Effects of Structure Size on Moon and Earth Radar Returns at Various Angles," A. K. Fung and R. K. Moore, March 1964. Published in Journal of Geophysical Research, vol. 69, no. 6, March 1964, p. 1075-1081. Supported by NSF Grant GP-2259 and NASA Grant NsG-298.

CRES Technical Report 48-12 "Notes on Backscattering and Depolarization by Gently Undulating Surfaces," A. K. Fung, R. K. Moore and B. E. Parkins, March 1965. Published in Journal of Geophysical Research, vol. 70, no.6, March 1965, p. 1559-1562. Supported by NSF Grant GP-2259 and NASA Grant NsG-298.

CRES Technical Report 48-13 "Scattering and Depolarization of EM Waves from a Rough Surface," A. K. Fung, March 1966. Published in Proceedings IEEE Letters, vol. 54, no. 3, March 1966, p. 395-396. Supported by NSF Grant GP-2259 and NASA Grant NsG-298.

CRES Technical Report 48-14 "The Correlation Function in Kirchhoff's Method of Solution of Scattering of Waves from Statistically Rough Surfaces," A. K. Fung and R. K. Moore, June 1966. Published in Journal of Geophysical Research, vol. 71, no. 12, June 1966, p. 2939-2943. Supported by NSF Grant GP-2259 and NASA Grant NsG-298.

CRES Technical Report 48-15 "On Depolarization of Electromagnetic Waves Backscattered from a Rough Surface," A. K. Fung, July 1966. Published in Planetary Space Science, vol. 14, July 1966, p. 563-568. Supported by NSF Grant GP-2259 and NASA Grant NsG-298.

CRES Technical Report 48-16 "Vector Scatter Theory Applied to Moon and Venus Radar Return," A. K. Fung, July 1966. Published in Proceedings IEEE, vol. 54, no. 7, July 1966, p. 996-998. Supported by NSF Grant GP-2259 and NASA Grant NsG-298.

CRES Technical Report 48-17 "Frequency Dependence and Surface Roughness," A. K. Fung, October 1966. Published in Proceedings IEEE, vol. 54, no. 10, October 1966. p. 1482-1483. Supported by NSF Grant GP-2259 and NASA Grant NsG-298.

CRES Technical Report 60 N-1 "Radar Astronomy Usage" R. K. Moore, April 1966. Published in IEEE Spectrum Correspondence, vol. 3, no. 4, April 1966, p. 156-159. Supported by NSF Grant GP-2259 and NASA Grant NsG-298.

CRES Technical Report 37-1 "A Study of Earth Radar Returns from Alouette Satellite," R. C. Chia, H. H. Doemland, and R. K. Moore, April 1967. Supported by NASA Grant NsG-477.

CRES Technical Report 105-1 "Rough Surface Scattering and its Application to Earth and Moon Radar Returns," A. K. Fung, January 1967. Supported by NSF Grant GK-1153.

CRES Technical Report 105-2 "Scattering and Depolarization of Electromagnetic Waves by a Horizontally Weakly Inhomogeneous Medium," A. K. Fung, May 1967. Supported by NSF Grant GK-1153.

CRES Technical Report 105-3 "Scattering of Electromagnetic Waves from a Slightly Rough Dielectric Layer," A. K. Fung, May 1967. Presented at Spring URSI Meeting, May 22-25, 1967, Ottawa, Ontario, Canada. Supported by NSF Grant GK-875.

CRES Technical Report 105-4 "Wave Propagation Across an Irregular Interface Between a Homogeneous and an Inhomogeneous Medium," A. K. Fung and C. M. Tu, July 1967. Supported by NSF Grant GK-1153.

CRES Technical Report 105-5 "Transducer Design," T. Leovaris, N. Boles, and A. Fung, March 1968. Supported by NSF Grant GK-875 and GK-1153.

Fung, A. K., "Theory of Radar Scatter from Rough Surfaces, Bistatic and Monostatic, with Application to Lunar Radar Return," Journal of Geophysical Research, vol. 69, no. 6, March 16, 1964, p. 1063-1073. Supported by NSF Grant GP-2259 and NASA Grant NsG-298.

Fung, A. K. and R. K. Moore, "Effects of Structure Size on Moon and Earth Radar Returns at Various Angles," Journal of Geophysical Research, vol. 69, no. 6, March 15, 1964, p. 1075-1081. Supported by NSF GP-2259 and NASA Grant NsG-298.

Chia, R. C., A. K. Fung and R. K. Moore, "High Frequency Backscatter from the Earth Measured at 1000 km Altitude," Proceedings IEEE Letters, vol. 52, no. 11, November 1964, p. 1384-1385. Supported by NASA Grant NsG-477.

Fung, A. K., R. K. Moore, and B. E. Parkins, "Notes on Backscattering and Depolarization by Gently Undulating Surfaces," Journal of Geophysical Research, vol. 70, no. 6, March 15, 1965, p. 1559-1562. Supported by NSF Grant GP-2259 and NASA Grant NsG-298.

Chia, R. C., A. K. Fung and R. K. Moore, "High Frequency Backscatter from the Earth Measured at 1000 km Altitude," Radio Science, Journal of Research NBS/USNC-URSI, vol. 69D, no. 4, April 1965, p. 641-649. Supported by NASA Grant NsG-477.

Fung, A. K., "Scattering and Depolarization of EM Waves from a Rough Surface," Proceedings IEEE Letters, vol. 54, no. 3, March 1966, p. 395-396. Supported by NSF Grant GP-2259 and NASA Grant NsG-298.

Fung, A. K., "On Depolarization of Electromagnetic Waves Backscattered from a Rough Surface," Planetary Space Science, vol. 14, July 1966, p. 563-568. Supported by NSF Grant GP-2259 and NASA Grant NsG-298.

Fung, A. K. and R. K. Moore, "The Correlation Function in Kirchhoff's Method of Solution of Scattering of Waves from Statistically Rough Surfaces," Journal of Geophysical Research, vol. 71, no. 12, July 15, 1966. Supported by NSF Grant GP-2259 and NASA Grant NsG-298.

Fung, A. K., "Vector Scatter Theory Applied to Moon and Venus Radar Return," Proceedings IEEE, vol. 54, no. 7, July 1966, p. 996-998. Supported by NSF Grant GP-2259 and NASA Grant NsG-298.

Moore, R. K. and B. E. Parkins, "Omnidirectional Scattering of Acoustic Surfaces of Known Statistics," Journal of the Acoustical Society of America, vol. 40, no. 1, July 1966, p. 17-175. Supported by NSF Grant GP-2259 and NASA Grant NsG-298.

Fung, A. K., "Frequency Dependence and Surface Roughness," Proceedings IEEE, vol. 54, no. 10, October 1966, p. 1482-1483. Supported by NSF Grant GP-2259 and NASA Grant NsG-298.

Fung, A. K. and C. M. Tu "Reflection of Electromagnetic Waves from a Two-Dimensionally Inhomogeneous Medium," Presented at Southwestern IEEE Conference (SWIEEECO), April 19-21, 1967, Dallas, Texas. Published in the SWIEEECO Record, IEEE Catalog No. F-72, p. 12-4-2 to 12-4-7. Supported by NSF Grant GK-1153.

Fung, A. K. "A Note on the Wiener-Khintchine Theorem for Autocorrelation," Proceedings IEEE Letters, vol. 55, no. 4, April 1967, p. 594-595. Supported by NSF Grant GK-1153.

Fung, A. K. and P. Beckmann "Surface Current of a Locally Flat Conductor and Depolarized Backscatter," Proceedings IEEE, vol. 55, no. 7, July 1967, p. 1235. Supported by NSF Grant GK-1153.

Parkins, B. E., "Omnidirectional Scattering of Acoustic Waves by Rough, Imperfectly Reflecting Surfaces," Journal of the Acoustical Society of America, vol. 51, no. 1, July 1967, p. 126-134. Supported by NSF Grant GP-2259 and NASA Grant NsG-298.

Fung, A. K. "Theory of Cross-Polarized Power Returned from a Random Surface," Applied Science Research, vol. 18, August 1967, p. 50-60. Supported by NSF Grant GP-2259 and NASA Grant NsG-298.

Fung, A. K. "Comments on Electromagnetic Scattering from Rough Finitely Conducting Surfaces," Radio Science, Journal of Research NBS/USNC-URSI, vol. 2, no. 12, December 1967, p. 1525. Supported by NSF Grant GK-1153.

Fung, A. K. "Character of Wave Depolarization by a Perfectly Conducting Rough Surface and its Application to Earth and Moon Experiments," Planetary Space Science, vol. 15, 1967, p. 1337-1347. Supported by NSF Grant GK-1153.

Fung, A. K. "Mechanisms of Polarized and Depolarized Scattering from a Rough Dielectric Surface," Journal of the Franklin Institute, vol 285, no. 2, February 1968, p. 125-133. Supported by NSF Grant GK-875 and GK-1153.

Fung, A. K. "Backscattering of Waves by Composite Rough Surfaces," Presented at Spring URSI Meeting, Washington, D. C., April 9-12, 1968. Supported by NSF Grant GK-875 and GK-1153.

Moore, R. K., A. Zachs and R. C. Chia "Radar Scattering from the Ocean--Theory, Simulation and Experiment," Presented at Spring URSI Meeting, Washington, D. C., April 9-12, 1968. Supported by NSF Grant GK-1153.

TECHNICAL REPORTS

CRES Report 122-1 "Multi-Image Correlation Systems Study for MGI Study Plan," G. Dalke, July 1967. Supported by USAETL Contract No. DAAK02-67-C-0435.

CRES Report 122-2 "Multi-Image Correlation Systems Study for MGI, Phase I Technical Report," G. Dalke, December 1967. Supported by USAETL Contract No. DAAK02-67-C-0435.

CRES Report 122-3 "Multi-Image Correlation Systems Study for MGI, Phase II Technical Report," G. Dalke, June 1968. Supported by USAETL Contract No. DAAK02-67-C-0435.

TECHNICAL REPORTS

CRES Technical Report 133-1 "Project THEMIS: A Center for Remote Sensing Study Plan (U)," R. D. Ellermeier, January 1968. Supported by THEMIS Contract No. DAAK02-68-C-0089.

CRES Technical Report 133-2 "Project THEMIS: A Center for Remote Sensing Semi-Annual Technical Report (U)," R. D. Ellermeier, April 1968. Supported by THEMIS Contract No. DAAK02-68-C-0089.

CRES Technical Report 133-3 "Adaptive Pattern Recognition of Agriculture in Western Kansas by Using a Predictive Model in Construction of Similarity Sets," R. M. Haralick, March 1968. Supported by THEMIS Contract No. DAAK02-68-C-0089.

CRES Technical Report 133-4 "The Frequency Dependence of Backscatter from Rough Surfaces," Ph.D. Dissertation, August 1968. Supported by THEMIS Contract No. DAAK02-68-C-0089.

CRES Technical Report 133-5 "Interim Technical Progress Report, Second Semi-Annual Technical Report, Project THEMIS: A Center for Remote Sensing," R. D. Ellermeier, October 1968. Supported by THEMIS Contract No. DAAK02-68-C-0089.

TECHNICAL MEMORANDA

CRES Technical Memorandum 133-1-1 "Antenna and Power Otuput Considerations for the Polypanchromatic Radar," W. Waite, January 1968. Supported by THEMIS Contract No. DAAK02-68-C-0089.

CRES Technical Memorandum 133-1-2 "System and Component Considerations for the Polypanchromatic Radar," P. D. Shaw, October 1968. Supported by THEMIS Contract No. DAAK02-68-C-0089.

CRES Technical Memorandum 133-1-3 "A Digital System to Control Sampling Measurements for a Polypanchromatic Radar," Its'hak Dinstein, October 1968. Supported by THEMIS Contract No. DAAK02-68-C-0089.

CRES Technical Memorandum 133-2 "Broad Spectrum Backscatter Acoustic System," J. W. Rouse, Jr., March 1968. Supported by THEMIS Contract No. DAAK02-68-C-0089 and NASA Contract NAS 9-7175.

CRES Technical Memorandum 133-3 "IDECS System Development," G. Kelly and G. Dalke, March 1968. Supported by THEMIS Contract No. DAAK02-68-C-0089.

CRES Technical Memorandum 133-4 "Observations on the Geomorphology of Part of the Wasatch Range, Utah," R. Peterson, March 1968. Supported by THEMIS Contract No. DAAK02-68-C-0089 and NASA Contract NAS 9-7175.

CRES Technical Memorandum 133-5 "A Statistical and Conditional Probability Study of Crop Discrimination Using Radar Images," R. Haralick, F. Caspall, R. Moore and D. Simonett. Presented at IEEE International Convention, March 18-21, 1968, New York. To be published in the Convention Record. Supported by THEMIS Contract No. DAAK02-68-C-0089, U.S.G.S. Contract No. 14-08-0001-10848 and NASA Contract NAS 9-7175.

TECHNICAL REPORTS

CRES Technical Report 152-1 "Narrative Report for Geoscience Overlays, Darien Province, Panama," Dellwig, L. F., A. J. Lewis and H. C. MacDonald, October 1968. Supported by USAETL Contract No. DAAK02-68-M-6993.

TECHNICAL MEMORANDA

CRES Technical Memorandum 156-1 "Availability of Construction Materials in the Mekong Delta," L. F. Dellwig, E. Gillerman, and L. H. Jefferis, August 1968. Supported by USAETL Contract No. DAAK02-69-M-0255.

OTHER PUBLICATIONS

Moore, R. K. and W. J. Pierson, "Measuring Sea State and Estimating Surface Winds from a Polar Orbiting Satellite," Presented at the International Symposium on Electromagnetic Sensing of the Earth from Satellites, Miami Beach, Florida, November 22-24, 1965. Published in the Proceedings, p. R1-R28. Supported by NASA Contract NSR 17-004-003.

Moore, R. K. and D. S. Simonett. Contribution to several chapters in the National Academy of Science-National Research Council Publication entitled Multi-Spectral Sensing of Agricultural Resources. The contributions summarize the present status of knowledge of radar as a remote sensor in agriculture. (To be published). Supported by NASA Contract NSR 17-004-003, NASA Grant NsG-298, NASA Contract NAS 9-7175, and USGS Contract 14-08-0001-10848.

Moore R. K. and D. S. Simonett, "Radar Remote Sensing in Biology," Bioscience, vol. 17, no. 6, June 1967, p. 384-394. Supported by NASA Contract NSR 17-004-003.

Rouse, J. W., Jr. "Preliminary Mission Analysis Report, NASA/MSC Mission No. 47, Site 93, Pt. Barrow, Alaska, "October 1967. Supported by NASA Contract NAS 9-7175.

Moore, R. K. and A. W. Biggs, "Research in Radar Scatterometry and Altimetry," Presented at the Ninth Meeting of the Ad Hoc Spacecraft Oceanography Advisory Group, Texas A & M University, College Station, Texas, January 23-24, 1968. Published in Technical Papers, pp. 1-17. Supported by NAVOCEANO Contract NOO N62306-67-C-0044.

Dellwig, L. F., H. C. MacDonald, and J. N. Kirk, "The Potential of Radar in Geologic Exploration, Presented at the Fifth Symposium on Remote Sensing of Environment, University of Michigan, Ann Arbor, Michigan, April 16-18, 1968. Published in the Proceedings, pp. 747-764. Supported by NASA Contract No. NAS 9-7175.

Schwarz, D. and F. Caspall, "The Use of Radar in the Discrimination and Identification of Agricultural Land Use," Presented at the Fifth Symposium on Remote Sensing of Environment, University of Michigan, Ann Arbor, Michigan, April 16-18, 1968. Published in the Proceedings, pp. 233-248. Supported by U.S.G.S. Contract No. 14-08-0001-10848.

OTHER PUBLICATIONS (CONT'D.)

Simonett, D. S., "Land Evaluation Studies with Remote Sensors in the Infrared and Radar Regions," Presented at the Land Evaluation Symposium, a joint CSIRO-UNESCO symposium, Canberra, Australia, August 26-31, 1968. Published in Land Evaluation, pp. 349-366. Supported by U.S.G.S. Contract No. 14-08-0001-10848.

Simonett, D. S., "Potential of Radar Remote Sensors as Tools in Reconnaissance Geomorphic, Vegetation and Soil Mapping," Presented at the 9th Congress, International Soil Science Society, August 1968. Published in Proceedings. Supported by U.S.G.S. Contract No. 14-08-0001-10848.

RECENT OR PENDING PAPERS

Dellwig. L. F., "What's New in Radar for the Geologist," Presented to the Highway Research Board of the National Research Council, January 19, 1968, Washington, D. C. Supported by NASA Contracts NSR 17-004-003 and NAS 9-7175 and NASA Grant No. NsG-298.

STANDARD DISTRIBUTION LIST

Project "THEMIS" Center for Remote Sensing

ARPA Order # 1079

Contract # DAAK02-68-C-0089

Unclassified
Security Classification

DOCUMENT CONTROL DATA - R & D

(Security classification of title, body of abstract and indexing annotation must be entered when the overall report is classified)

1. ORIGINATING ACTIVITY (Corporate author) Center for Research, Inc. University of Kansas	2a. REPORT SECURITY CLASSIFICATION Unclassified 2b. GROUP

3. REPORT TITLE

Interim Technical Progress Report, Project Themis: A Center for Remote Sensing

4. DESCRIPTIVE NOTES (Type of report and inclusive dates)
Second Semi Annual Technical Report, April 1968 to October 1968

5. AUTHOR(S) (First name, middle initial, last name)

Compiled by R. D. Ellermeier

6. REPORT DATE October 1968	7a. TOTAL NO. OF PAGES 193	7b. NO. OF REFS
8a. CONTRACT OR GRANT NO. DAAK02-68-C-0089 ARPA Order No. 1079 b. c. d.	9a. ORIGINATOR'S REPORT NUMBER(S) 133-6 9b. OTHER REPORT NO(S) (Any other numbers that may be assigned this report)	

10. DISTRIBUTION STATEMENT

See attached Distribution List.

11. SUPPLEMENTARY NOTES Funded by DOD Project Themis under ARPA Order No. 1079	12. SPONSORING MILITARY ACTIVITY Monitoring U. S. Army Engineer Topographic Labs. Geographic Information Systems Branch Geographic System Division Ft. Belvoir, Virginia

13. ABSTRACT

This report summarizes the technical progress under the subject contract on a broad interdisciplinary effort for the improvement of user utility of remotely sensed data. This effort involves theoretical work, sensor development, processing and display, and data analysis for specific user application. A number of technical reports and memoranda describing work underway are attached.

DD FORM 1 NOV 68 1473 REPLACES DD FORM 1473, 1 JAN 64, WHICH IS OBSOLETE FOR ARMY USE.

Unclassified
Security Classification